UNIVERSIDADE DA BEIRA INTERIOR
Faculdade de Engenharia

Development of an Opposed Piston Geared Hypocycloid Engine

Alexandre José Rosa Nunes

Dissertação para obtenção do Grau de Mestre em
Engenharia Aeronáutica
(ciclo de estudos integrado)

Orientador: Prof. Doutor Francisco Miguel Ribeiro Proença Brojo

Covilhã, Outubro de 2017

Dedication

This work is dedicated to my mother who always supported me unconditionally in all my endeavours, to my sister who always pushed me to be a better brother and a better man and to my father whose critical thinking and engineering prowess in all his projects were my role model and gave me the tools to become who I am today.

"What we usually consider as impossible are simply engineering problems… there's no law of physics preventing them."
Michio Kaku

"Simplicity is the ultimate sophistication."
Leonardo Da Vinci

"There's only one way to do thing. The right way."
José Nunes (my father)

Resumo

O motor convencional biela-manivela domina a indústria com escassas alternativas a conseguirem terem sucesso comercial. Em aplicações aeronáuticas onde o balanceamento do motor é crítico para reduzir as vibrações induzidas, motores com a configuração 'boxer' foram desenvolvidos para minimizar este problema. O crescente custo de combustível e preocupação com as emissões de gases poluentes levou a um aumento no interesse por motores alternativos onde os ambos os motores de pistões opostos e engrenagem hipocicloidal apresentam algumas vantagens sobre os motores de biela-manivela convencionais.

Neste estudo é feita uma comparação entre dois motores de pistões opostos, o primeiro com um conjunto biela-manivela e o segundo com engrenagem hipocicloidal, seguido de uma proposta de desenho de um motor de pistões opostos hipocicloidal para ser usado em aplicações aeronáuticas.

Verificou-se que o desempenho do motor com engrenagem hipocicloidal foi semelhante ao do motor com biela-manivela em todas as características de desempenho consideradas neste estudo, mesmo excluindo as perdas mecânicas por fricção entre o pistão e o cilindro. Assim, se considerarmos a potencial redução nas perdas por fricção, o motor com engrenagem hipocicloidal deverá alcançar uma eficiência superior.

Verificou-se também que o desenvolvimento de um motor é uma tarefa complexa que normalmente é feita com base na experiência e relações empíricas sendo necessário muito trabalho experimental para melhor desenvolver e caracterizar o desempenho do motor. Apesar disso, neste estudo não foi feito qualquer trabalho experimental.

Palavras-chave

Motor de Combustão Interna (ICE), Motor de Pistões Opostos (OPE), Motor Biela-Manivela (SCE), Motor com Engrenagem Hipocicloidal (GHE), Quatro-Tempos (4S), Ignição por Faísca (SI), Ciclo de Otto

Abstract

The conventional slider crank engine has dominated the industry with very few alternative configurations having commercial success. In aircraft applications where engine balancing is critical to reduce vibrations, boxer engines have been developed to reduce this issue. The rising cost of fuel and awareness of pollutant emissions has led to an increased interest in alternative designs where both opposed piston and geared hypocycloid engines present some advantages over the conventional slider crank engine.

In this study, a comparison between an opposed piston slider crank and geared hypocycloid engine was made followed by the design of a proposed opposed piston geared hypocycloid engine to be used in aircraft applications.

It was found that the performance of the geared hypocycloid engine was similar to that of the slider crank engine in all performance characteristics considered in this study, even when excluding the mechanical losses due to friction of the piston head against the cylinder. Therefore, when considering the potential reduced losses due to friction, the geared hypocycloid engine should achieve higher efficiency.

It was also found that the design of an engine is a complex task that is usually done from experience and empirical relations with a lot of practical work needing to be done to better design and describe an engine's performance. However, this study did not include any practical testing.

Keywords

Internal Combustion Engine (ICE), Opposed Piston Engine (OPE), Slider Crank Engine (SCE), Geared Hypocycloid Engine (GHE), Four-Stroke (4S), Spark Ignition (SI), Otto Cycle

Table of Contents

List of Figures

List of Tables

List of Abbreviations and Symbols

Abbreviation or Symbol	Nomenclature	Units
a	Acceleration	m/s^2
h_a	Addendum	mm
x	Addendum Modification Factor	
AFR	Air/Fuel Ratio	
AFR_{stoich}	Air/Fuel Stoichiometric Ratio	
ß	Angle Between Connecting Rod and Axis of the Cylinder	º
θ_{start}	Angle at Start of Combustion	º
EVC	Angle at Exhaust Valve Close	º
EVO	Angle at Exhaust Valve Open	º
IVC	Angle at Intake Valve Close	º
IVO	Angle at Intake Valve Open	º
σ_{FP}	Allowable Bending Stress	MPa
σ_b	Allowable Bending Stress for Crankpin	MPa
σ_{HP}	Allowable Contact Stress	MPa
σ_t	Allowable Bending (Tensile) Stress	MPa
$C_{reboring}$	Allowance for Reboring	mm
σ_S	Allowable Shear Stress	MPa
σ_f	Allowable Tensile Strength	MPa
σ_{bolt}	Allowable Tensile Stress for Material of Bolts	MPa
N	Angular Velocity	rpm
ω	Angular Velocity	rad/s
$\overline{T}q$	Average Torque	N.m
A	Area	m^2
t_2	Axial Thickness of Piston Ring	mm
j	Backlash	mm
B	Bore	m
R_{BHS}	Bore/half-stroke Ratio	
R_{BS}	Bore/stroke Ratio	
BDC	Bottom Dead Centre	
HB	Brinell Hardness	
c	Clearance	mm
V_c	Clearance Volume	m^3
η_c	Combustion Efficiency	
η_{cmax}	Combustion Maximum Efficiency	
CI	Compression Ignition	
CR	Compression Ratio	
a_{Nu}	Constant for Nusselt Number	
a_{weibe}	Constant for Weibe Function	
m_{weibe}	Constant for Weibe Function	
C_h	Convection Heat Transfer	$W/(m^2.K)$
C_k	Conduction Heat Transfer	W/(m.K)

θ	Crank Angle	°
r	Crank Radius	m
h_d	Dedendum	mm
ρ	Density	kg/m^3
d_{bolt}	Diameter of Bolts	mm
$d_{crankpin}$	Diameter of Crankpin	mm
d_r	Diameter of Piston Rod	mm
d_{shaft}	Diameter of Output Shaft	mm
b	Distance	m
d_{BDC}	Distance Between both pistons at BDC	mm
d_{TDC}	Distance Between both pistons at TDC	mm
d_{force}	Distance Between Centre of Bearing and Force Applied at Crankshaft	mm
$d_{bearing}$	Distance Between Centre of Bearings	mm
d_{centre}	Distance Centre	mm
C_{mf}	Distribution Factor	
K_V	Dynamic Factor	mm
$\Delta\theta$	Duration of Combustion	°
η	Efficiency	
Z_E	Elastic Coefficient	$(N/mm^2)^{0.5}$
E	Elastic Modulus	Pa
FW	Face Width	mm
r_t	Fillet Radius	mm
F	Force	N
F_t	Force Applied to the Piston	N
F_i	Force of Inertia	N
F_p	Force of Pressure	N
4S	Four-Stroke	
η_{fuel}	Fuel Conversion Efficiency	
QHV	Fuel Heat Power	J/kg
GHE	Geared Hypocycloid Engine	
b_{groove}	Groove Depth for Piston Ring	mm
C_H	Hardness Ratio Factor	
Q	Heat	J
C_p	Heat Capacity at Constant Pressure	J/(kg.K)
C_v	Heat Capacity at Constant Volume	J/(kg.K)
H	Heat Flowing Through the Piston Head	J
Q_R	Heat Released from Combustion	J
Q_L	Heat Lost to Heat	J
Q_{vap}	Heat Lost to Vaporize Fuel	J
L_{rod}	Height of Piston Rod	mm
L_{piston}	Height of Piston Head	mm
HPSTC	Highest Point of Single Tooth Contact	
R	Ideal Gas Constant	J/(kg.K)
ICE	Internal Combustion Engine	
ID_{cap}	Internal Diameter of Piston Rod Cap	mm
U	Internal Energy	J
h_{vap}	Latent Heat of Vaporization	J/kg

C_{mc}	Lead Correction Factor	
$l_{crankpin}$	Length of the Crankpin	mm
$L_{cylinder}$	Length of the Cylinder	mm
Y_N	Life Factor	
Z_N	Life Factor	
K_m	Load Distribution Factor	
m	Mass	kg
x_b	Mass Fraction of Fuel Burn	
$\dot{m}$	Mass Flow	kg/s
dm	Mass Flow Increment	kg
η_{cmax}	Maximum Combustion Efficiency	
$F_{bearing}$	Maximum Force Applied at the Main Bearing	N
t_3	Maximum Thickness of Piston Barrel	mm
mep	Mean Effective Pressure	Pa
$\bar{S}_p$	Mean Piston Velocity	m/s
C_e	Mesh Alignment Correction Factor	
C_{ma}	Mesh Alignment Factor	
t_4	Minimum Thickness of Piston Barrel	mm
M	Momentum	N.m
m_n	Normal Module	mm
n_{bolt}	Number of Bolts	
n_R	Number of Revolutions	
n_{rings}	Number of Rings	
Nu	Nusselt Number	
OPE	Opposed Piston Engine	
OPGHE	Opposed Piston Geared Hypocycloid Engine	
OPSCE	Opposed Piston Slider Crank Engine	
K_O	Overload Factor	
σ_c	Permissible Hoop Stress	MPa
C_{pf}	Pinion Proportion Factor	
C_{pm}	Pinion Proportion Modifier	
a_{piston}	Piston Acceleration	m/s^2
A_{piston}	Piston Area	m^2
S_{piston}	Piston Position	m
v_{piston}	Piston Velocity	m/s
d_{pitch}	Pitch diameter	mm
v_t	Pitch-line Velocity	m/s
I	Pitting Resistance Factor	
v	Poisson's Ratio	
C_{heat}	Portion of Heat Released during Combustion that Flows through the Piston Head	
P	Power	W
p	Pressure	Pa
Φ	Pressure Angle	°
p_w	Pressure of Gas on the Cylinder Wall	MPa
t_1	Radial Thickness of Piston Ring	mm
C_r	Radiation Heat Transfer	$W/(m^2K^4)$
λ	Relative Air/Fuel Ratio	

K_R	Reliability Factor	
Re	Reynolds Number	
K_B	Rim Thickness Factor	
HR15N	Rockwell 15-N Hardness Scale	
l	Rod Length	m
SF	Safety Factor	
SH	Safety Factor	
K_S	Size Factor	
SCE	Slider Crank Engine	
SI	Spark Ignition	
sfc	Specific Fuel Consumption	g/kWh
γ	Specific Heat Capacity	J/(kg.K)
S	Stroke	m
C_f	Surface Condition Factor	
F_{gt}	Tangential Gear Tooth Load	N
T	Temperature	K
T_C	Temperature at Centre of Piston Head	K
T_E	Temperature at Edge of Piston Head	K
K_T	Temperature Factor	
η_t	Thermal Efficiency	
t	Thickness	mm
$t_{crankweb}$	Thickness of Crankweb	mm
t_{cw}	Thickness of Cylinder Wall	mm
t_H	Thickness of Piston Head	mm
dt	Time interval	s
J	Tooth Bending Geometry Factor	
TDC	Top Dead Centre	
Tq	Torque	N.m
θ_{total}	Total Cycle Angle	°
Av	Transmission Accuracy Level	
C_{mt}	Transverse Load Distribution Factor	
UHS	Ultrahigh-Strength	
μ	Viscosity	kg/(s.m)
V	Volume	m^3
$V_{displaced}$	Volume Displaced by the piston	m^3
$V_{displacement}$	Volume of Displacement	m^3
h_t	Whole Depth	mm
WOT	Wide-Open-Throttle	
w	Width	mm
b_2	Width of Other Lands	mm
$w_{crankweb}$	Width of the Crankweb	mm
b1	Width of Top Land	mm
W	Work	J
σ_F	Working Bending Stress	MPa
σ_H	Working Contact Stress	MPa
h’	Working Depth	mm

Chapter 1

Introduction

Ever since the industrial revolution and the development of the steam engine, a huge technological advance took place. One of the main contributors is the engine, which can be described as a machine that converts chemical energy into mechanical energy [Heywood, 1988] and is essential to our industrialized civilization. In fact, our modern society would not be possible if not for engines in general, but also for aircraft with traffic growing each year at a very fast rate. Powered-flight, as we know it, is only possible not only because of such technological advancements but also because engines evolved to such a degree that the power developed compared to their weight made them suitable for aircraft applications.

Aircraft are not only used for large commercial or military applications with interest in light aircraft increasing, whether it is for tourism, access to remote regions or even as a hobby. Therefore, more focus should be given to the development of one of the most, if not the most, critical component of an aircraft.

1.1 Motivation

With the rising cost of fuel and awareness of emissions, the technology used in conventional engines is approaching its limits. This means an ever-increasing cost of development for engines that meet the increasing rigorous requirements for fuel economy and emissions. Some attention must then be given to alternative configurations and technologies to meet such increasingly strict requirements.

Although some alternative engines and sources of energy exist, these cannot yet meet the requirements for applications in aviation and the cost for development and introduction of such new technologies in the aviation industry is prohibitive. Therefore, some focus must be given to alternative technologies and configurations that can be implemented successfully in a relatively short time with a cost of development and introduction in the aviation industry that can be supported by companies.

1.2 Scope of Work

This thesis focuses on the design of an engine that implements two different technologies in one engine. These are opposed piston configuration in a four-stroke spark-ignition configuration which has not seen much development, contrary to two-stroke diesel engines that have been quite popular in the first half of the 19th century and only recently have been given some attention again [Pirault, 2010]; and a geared hypocycloid mechanism which dates back to when the steam engine was introduced and has been given very little attention, despite its promising advantages over slider crank mechanisms.

1.3 Objectives

This thesis aims to propose an alternative engine configuration to be used in aircraft applications. A comparison between the designed opposed piston geared hypocycloid and slider crank engines is provided to understand the possible performance gains of one over the other. This was done by developing a model in MATLAB to compare both engines. Then, the parts were designed in CATIA V5 and assembled to more easily view the design. The study of heat dissipation via the heat fins, the valve system and consequent intake and exhaust processes are beyond the scope of this study.

1.4 Outline

To provide an easier reading of this work, this thesis was organized in six chapters as will be described next.

This first chapter gives the motivation behind this study. The approach considered is also explained and the objectives presented. Finally, the structure of this thesis is described.

The second chapter, designated State of the Art, considers the internal engine background and explains the work and thermodynamic cycles relevant for this study. The appropriate background referring to a more accurate simulation of the cycles is also presented. Next, some engine operating parameters are explained which will be included in the model. Finally, an overview of both slider crank and geared hypocycloid mechanisms is given followed by opposed piston engines and spur gears, both internal and external.

The third chapter focuses on the engine modelling with an initial parametric review of other engines being done as a starting point and to more closely model the combustion timings. It is followed by the definition of the initial parameters for the model ending with the results for the kinematics and dynamics of both engines.

The fourth chapter describes the design process for each component of the engine proposed in this study and shows the respective CATIA parts. Initially, the materials selected are explained and its properties presented with two steel alloys and three aluminium alloys having been selected. Then, the piston and rod design is explained, followed by the cylinder, gearset, crankshaft, output and support shaft where the balancing of the engine is taken into account, ending with considerations for the belt drive, bearings selected and crankcases. At the end, the final design is presented.

The fifth chapter presents the results obtained from the model for the performance of each engine and a comparison is made. The average torque, power, specific fuel consumption, mean effective pressure, fraction of fuel energy loss and thermal efficiency are considered for both engines. The power-to-weight ratio was also considered for the opposed piston considered in this study.

The sixth and final chapter presents the conclusions taken at the end of this study. It also suggests alternative materials that may have an impact on the engine performance as well as possible improvements ending with suggestions for future work.

Chapter 2

State of the Art

2.1 Internal Engine Background

An Internal Combustion Engine (ICE) is an engine where chemical energy is released and converted to mechanical energy through the combustion of a mixture of fuel and oxidizer, usually air. [Heywood, 1988] Contrary to external combustion engines, the combustion in ICE occurs inside the engine and so, the mixture of fuel and air and the burned products are the actual working fluids. The term 'Internal Combustion Engines' may be applied to reciprocating ICE or to open circuit gas turbines. However, the term 'reciprocating' is usually omitted and when the term ICE is used, it refers to reciprocating internal combustion engines, unless otherwise stated. [Stone, 1999]

There are two main types of ICE - spark ignition (SI) engines where a spark ignites the fuel and compression ignition (CI) engines where the fuel ignites spontaneously due to the rise in temperature and pressure during combustion. Other terms used to refer to SI engines are petrol, gasoline or Otto engines while CI engines may also be referred to as Diesel engines.

2.2 Work Cycle

During each crankshaft revolution of an ICE there are two piston strokes, and so there are two main operating cycles in which both engines may be designed to operate – two- or four- stroke.

The four-stroke cycle can be described, with reference to figure 2.1, by: [Stone, 1999]

1. *The induction stroke*. The inlet valve opens, and a charge of air is drawn in as the piston travels down the cylinder. For SI engines, usually fuel pre-mixed with air is drawn in while CI engines only draw in air.
2. *The compression stroke*. Both the inlet and exhaust valves and the charge is compressed as the piston travels up the cylinder. As the piston approaches top dead centre (TDC), ignition occurs. In SI engines, this usually occurs with a spark while CI engines, fuel is injected instead and auto-ignites.
3. *The expansion, power or working stroke*. Combustion occurs which raises the pressure and temperature and forces the piston down the cylinder. At the end of this stroke, as the piston approaches bottom dead centre (BDC) the exhaust valve opens.

4. *The exhaust stroke*. The exhaust valve remains open, the burned gases are expelled as the piston travels up the cylinder, and the exhaust valve is closed at the end of this stroke.

The four-stroke cycle may sometimes be summarized as 'suck, squeeze, bang and blow'. To provide energy for the other three strokes, some of the power from the expansion stroke is stored in a flywheel. [Stone, 1999]

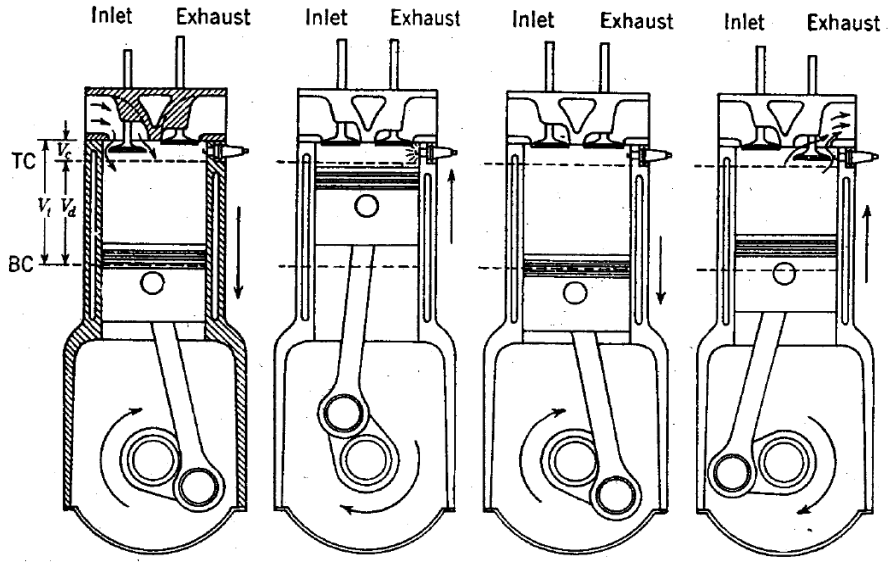

Figure 2.1. The four-stroke cycle. From left to right: induction stroke, compression stroke, expansion stroke, exhaust stroke. [Heywood, 1988]

The two-stroke cycle eliminates both the induction and exhaust strokes and can be described, with reference to figure 2.2, by: [Stone, 1999]

1. *The compression stroke*. Similar to the four-stroke cycle, a charge is compressed as the piston travels up the cylinder. As the piston approaches TDC, ignition occurs. Simultaneously, a charge is drawn in through a spring loaded non-return inlet valve by the underside of the piston.
2. *The power stroke*. Similar to the four-stroke cycle, combustion occurs which raises the pressure and temperature and forces the piston down the cylinder. Simultaneously, the charge in the crankcase is compressed by the downward motion of the piston. The exhaust port is uncovered and blowdown occurs as the piston approaches the end of its stroke. When at BDC, the piston uncovers the transfer port and the charge compressed in the crankcase expands into the cylinder.

When comparing two- and four-stroke engines of similar sizes operating at a specific speed, the former will produce more power than the latter because it has twice as many power strokes per unit time. However, the two-stroke engine will likely have lower efficiency than the four-stroke engine because ensuring efficient induction and exhaust processes is an issue. This is more evident for SI engines as the pressure inside the crankcase may be below atmospheric pressure at part throttle operation, with a rich air/fuel mixture becoming necessary for all conditions and, therefore, low efficiency. [Stone, 1999]

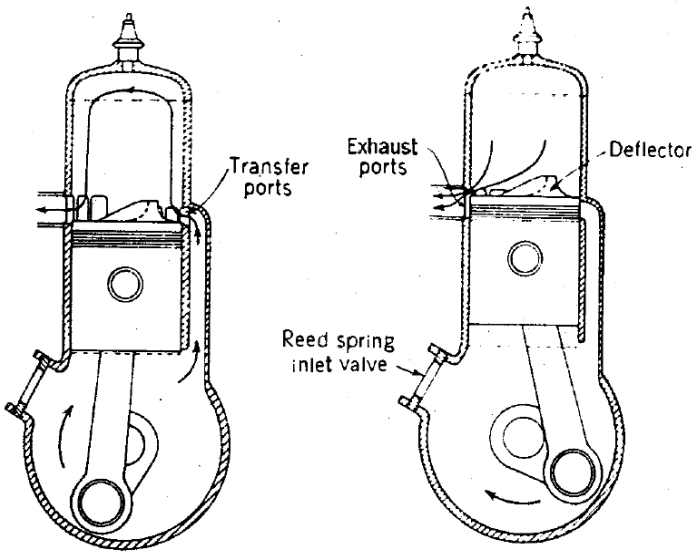

Figure 2.2. The two-stroke cycle. From left to right: compression stroke, expansion stroke. [Heywood, 1988]

2.3 Thermodynamic Cycle

There are several thermodynamic cycles on which an engine can operate. However, in this study only the Otto Cycle will be considered.

2.3.1 Ideal Otto Cycle

The thermodynamic cycle on which four-stroke SI engines operate is often referred to as the Otto cycle. Theoretically, the ideal Otto cycle assumes for each stroke of the cycle that [Blair, 1999]:

a) The compression stroke begins at BDC and is an isentropic, i.e., adiabatic, process.
b) All heat release (combustion) takes place at constant volume at TDC.
c) The expansion stroke begins at TDC and is an isentropic, i.e., adiabatic, process.
d) A heat rejection process (exhaust) occurs at constant volume at BDC.

Both compression and expansion processes are considered to be isentropic and adiabatic (ideal conditions) where the working fluid is air. Those processes can be calculated as: [Blair, 1999]

$$pV^{\gamma} = constant \tag{2.1}$$

The exponent (γ) is the ratio between heat capacity at constant pressure (C_p) and heat capacity at constant volume (C_v), and assumes a value for air of 1.4, as:

$$\gamma = \frac{C_p}{C_v} \tag{2.2}$$

The thermal efficiency (η_t) of the cycle is given by:

$$\eta_t = 1 - \frac{1}{CR^{\gamma-1}} \tag{2.3}$$

where CR is the compression ratio of the engine and will be discussed later. The thermal efficiency may be defined as the ratio between the work produced per cycle and the heat available as input per cycle [Blair, 1999]. It can be observed that the thermal efficiency depends on the compression ratio and not the temperatures in the cycle and with increasing compresson ratio there's increasing thermal efficiency.

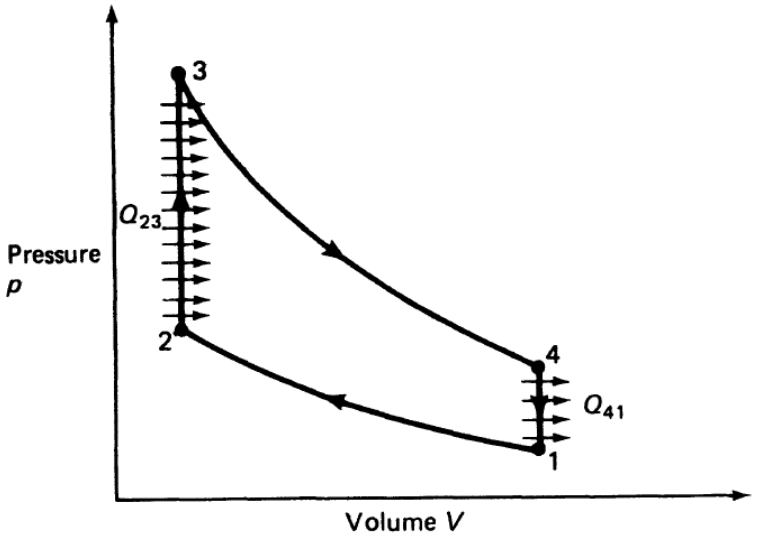

Figure 2.3. Ideal air standard Otto cycle. [Stone, 1999]

2.3.1.1 Thermodynamic Navigation around the Ideal Otto Cycle

Referring to figure 2.3, the cycle commences at BDC, at point 1. The mass of air (m_1) in the cylinder is then given by: [Blair, 1999]

$$m_1 = \frac{p_1 V_1}{R T_1} \tag{2.4}$$

And the mass of air trapped in the cylinder (m_{air}), by:

$$m_{air} = \frac{p_1 V_{displaced}}{R T_1} \tag{2.5}$$

Where $V_{displaced}$ is the volume displaced by the piston and R is the ideal gas constant. The mass of fuel trapped (m_{fuel}) is then found by:

$$m_{fuel} = \frac{m_{air}}{AFR} \tag{2.6}$$

Where AFR is the air/fuel ratio and will be described later. The heat transfer at TDC is equivalent to the heat energy in the fuel:

$$Q_2^3 = \eta_C m_{fuel} QHV \tag{2.7}$$

Where η_c is the combustion efficiency and QHV is the lower heating value of the fuel.

Process 1-2, Adiabatic and Isentropic Compression [Blair, 1999]

The pressure (p_2) and temperature (T_2) at the end of compression is given, respectively, by:

$$p_2 = p_1 \left(\frac{V_2}{V_1}\right)^{-\gamma} \tag{2.8}$$

$$T_2 = T_1 \left(\frac{V_2}{V_1}\right)^{1-\gamma} \tag{2.9}$$

The work and the change of internal energy done during compression is, respectively, negative and positive, and given by:

$$W_1^2 = -m_1 C_v (T_2 - T_1) \tag{2.10}$$

$$U_2 - U_1 = m_1 C_v (T_2 - T_1) \tag{2.11}$$

Process 2-3, Constant Volume Combustion [Blair, 1999]

Applying the first law of thermodynamics to the combustion process:

$$Q_2^3 = U_3 - U_2 + W_2^3 = m_1 C_v (T_3 - T_2) + 0 \tag{2.12}$$

Solving for T_3:

$$T_3 = T_2 + \frac{Q_2^3}{m_1 C_v} \tag{2.13}$$

Using the state equation and solving for p_3:

$$p_3 = p_2 \frac{V_2}{V_3} \frac{T_3}{T_2} = p_2 \frac{T_3}{T_2} \tag{2.14}$$

The change of internal energy during the process from 2-3 is given by:

$$U_3 - U_2 = Q_2^3 \tag{2.15}$$

Process 3-4, Adiabatic and Isentropic Expansion [Blair, 1999]

The pressure (p_4) and temperature (T_4) at end of expansion, after process 3-4 is given by:

$$p_4 = p_3 \left(\frac{V_4}{V_3}\right)^{-\gamma} = CR^{-\gamma} \tag{2.16}$$

$$T_4 = T_3 \left(\frac{V_4}{V_3}\right)^{1-\gamma} = CR^{1-\gamma} \tag{2.17}$$

The work and the change of internal energy done during expansion is, respectively, positive and negative, and given by:

$$W_3^4 = -m_1 C_v (T_4 - T_3) \tag{2.18}$$

$$U_4 - U_3 = m_1 C_v (T_4 - T_3) \tag{2.19}$$

Process 4-1, Cycle completion by constant volume heat rejection [Blair, 1999]

From the first law of thermodynamics:

$$Q_4^1 = U_1 - U_4 + W_4^1 = m_1 C_v (T_1 - T_4) + 0 \tag{2.20}$$

$$U_1 - U_4 = Q_4^1 = m_1 C_v (T_1 - T_4) \tag{2.21}$$

2.3.1.2 Otto Cycle in a Closed System

For design purposes, the ideal Otto cycle is quite inaccurate. For this reason, the first step to more accurately predict the operation of the engine is to introduce a combustion process that relates the burning of fuel with respect to time. The next step in view of improving accuracy is introducing heat transfer loss into the simulation of the ideal Otto cycle, making it no longer an ideal cycle though. This heat transfer loss no longer considers the processes to be ideal (isentropic and adiabatic). Finally, another step is to consider friction and pumping losses that occur in the engine cycle. [Blair, 1999] However, this last step will not be included in this model.

The engines were modelled as a closed system, which means that the mass within the system is constant, i.e., the volume, pressure and temperature may change but the mass does not. It also considers all the gas within the cylinder when all valves or apertures to the cylinder are closed and assumes that piston rings make a perfect gas seal with the cylinder walls. A typical situation is illustrated in figure 2.4 where the piston moves from position 1 to position 2 and a compression process occurs, with the volume decreasing from V_1 to V_2 and the pressure increasing from p_1 to p_2. For this compression process to occur, the piston must expend work. The data on pressure and volume are graphed in figure 2.4. An expansion process would have occurred if the piston had been descending instead. [Blair, 1999]

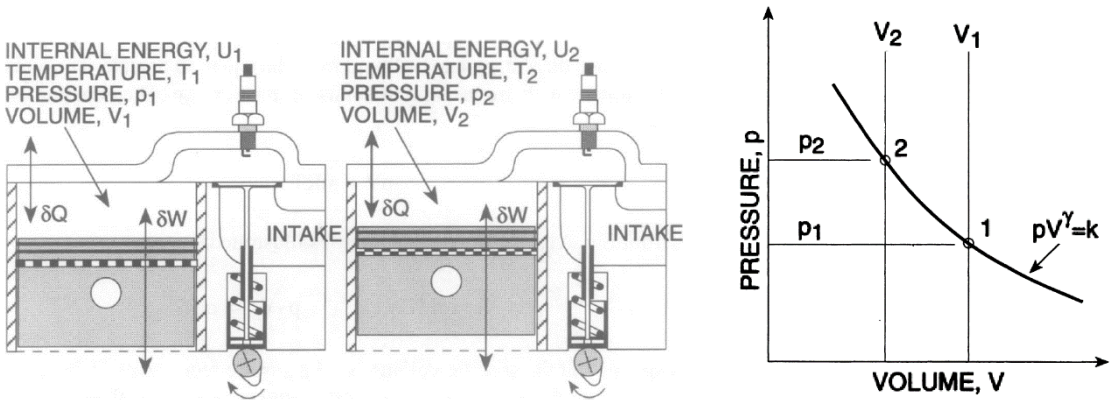

Figure 2.4 – Closed system process in a four-stroke engine (left) and p-V changes for a closed system process (right). *[Adapted from Blair, 1999]*

If a gas experiences a work process (δW) within a closed system, it is observed as a change of volume (dV) at pressure (p), and can be evaluated by: [Blair, 1999]

$$\delta W = pdV \tag{2.22}$$

Applying the first law of thermodynamics for a closed system, it is possible to relate any work change (δW) to any change of heat transfer (δQ) and internal energy (dU) as:

$$\delta Q = dU + \delta W \tag{2.23}$$

If specific to unit of mass, heat transfer (δq), work (δw) and internal energy (du) may be defined, respectively, as:

$$\delta q = \frac{\delta Q}{m} \tag{2.24}$$

$$du = \frac{dU}{m} \tag{2.25}$$

$$\delta w = \frac{\delta W}{m} \tag{2.26}$$

Eq. 2.24 can then be divided across the mass (m) to obtain a specific formulation for the first law of thermodynamics:

$$\delta q = du + \delta w \tag{2.27}$$

2.3.3 Heat Release Model

The combustion process may be described thermodynamically as a heat addition process to a closed system. It occurs in a chamber of varying volume, the minimum value of which is the clearance volume, V_c. [Blair, 1999]

In single-zone models, a mass fraction burn curve is usually considered to predict the heat release, and is often referred to as a Weibe function. This function represents the fraction of chemical energy released from the fuel burn as a function of crank angle. It varies with an s-curve from 0% at the start of the combustion to 100% burned at the end of combustion. This s-curve, as represented in figure 2.5, is described as: [Kuo, 1996]

$$\chi_b = 1 - exp\left[-a_{weibe}\left(\frac{\theta - \theta_0}{\Delta\theta}\right)^{m_{weibe}+1}\right] \tag{2.28}$$

Where θ_0 is the angle considered for the start of combustion (about equal to the angle of spark firing), $\Delta\theta$ is angle for which the combustion occurs and the constants a_{weibe} and m_{weibe} are determined experimentally, with real burn fraction curves having been fitted by the Weibe function with a_{weibe}=5 and m_{weibe}=2 [Kuo, 1996 and Heywood, 1988].

The heat release can then be calculated as: [Blair, 1999]

$$\delta Q = \eta_c(\chi_b - \chi_{b0})m_{fuel}.QHV \tag{2.29}$$

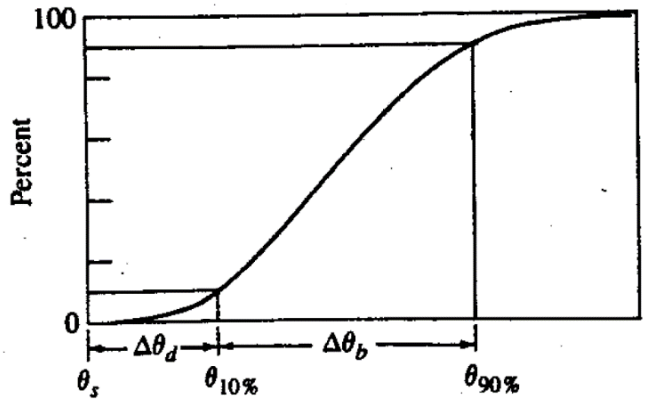

Figure 2.5. Definition of flame-development angle ($\Delta\theta_d$) and rapid-burning angle (θ_b) on mass fraction burned versus crank angle curve. [*Adapted from Heywood, 1988]*

2.3.4 Heat Transfer Model

One of the indispensable issues in studying ICE is heat transfer because decisive parameters of operation such as temperature and pressure inside the cylinder are influenced by it. There are three heat transfer mechanisms: conduction, convection and radiation [Spitsov, 2013].

The heat transfer included in this model was the Annand model, which is referred as being the most effective and accurate method for calculating heat transfer from the cylinder during the closed cycle for SI engine. [Blair, 1999]

Annand's heat transfer theory proposes an expression for the Nusselt number (Nu) which leads to a conventional derivation for the convection heat transfer (C_h). Therefore, to relate the Reynolds and Nusselt numbers, Annand recommends the following expression:

$$Nu = a_{Nu} Re^{0.7} \tag{2.30}$$

With a_{Nu}=0.26 or a_{Nu}=0.49 for 2-stroke and 4-stroke engines, respectively. The Reynolds number is calculated by:

$$Re = \frac{\rho_{cyl} \bar{S}_p B}{\mu_{cyl}} \tag{2.31}$$

Where B is the cylinder bore. The values of density (ρ_{cyl}), mean piston velocity ($\bar{S}_p$) and viscosity (μ_{cyl}) can be calculated:

$$\rho_{cyl} = \frac{p_{cyl}}{R_{cyl} T_{cyl}} \tag{2.32}$$

$$\overline{S}_p = \frac{2SN}{60} \tag{2.33}$$

$$\mu_{cyl} = 7.457\text{x}10^{-6} + 4.1547\text{x}10^{-8} T - 7.4793\text{x}10^{-12} T^2 \tag{2.34}$$

Now, the convection heat transfer (C_h) can be extracted from the Nusselt number:

$$C_h = \frac{C_k Nu}{B} \tag{2.35}$$

The parameter Ck is the thermal conductivity of the cylinder gas. It may be assumed to be identical with that of air at the instantaneous cylinder temperature (T_{cy}) and calculated as:

$$C_k = 6.1944\text{x}10^{-3} + 7.3814\text{x}10^{-5} T - 1.2491\text{x}10^{-8} T^2 \tag{2.36}$$

The value of the cylinder wall (T_{wall}) is the average temperature of the cylinder wall, and may be assumed to be 350K. [Stone, 1999]

Annand also considers the radiation heat transfer (C_r) to be:

$$C_r = 4.25\text{x}10^{-9}\left(\frac{{T_{cyl}}^4 - {T_{wall}}^4}{T_{cyl} - T_{wall}}\right) \tag{2.37}$$

The heat transfer (δQ_L) can be inferred over a crankshaft angle interval ($d\theta$) and a time interval (dt) for the mean value of that transmitted to the total surface area exposed to the cylinder gases, with:

$$dt = \frac{d\theta}{360}\frac{60}{N} \tag{2.38}$$

Then:

$$\delta Q_L = (C_h + C_r)\big(T_{cyl} - T_{wall}\big)A_{cyl}dt \tag{2.39}$$

Where the surface area of the cylinder (A_{cyl}) is:

$$A_{cyl} = A_{cylinder\ liner} + A_{piston\ crown} + A_{cylinder\ head} \tag{2.40}$$

It should be noted that opposed piston engines don't have a cylinder head and, therefore, the heat loss is reduced and thermal efficiency is increased.

2.3.5 Fuel Vaporization Model

During the closed cycle, fuel vaporization occurs. For SI engines, this normally occurs during compression and prior to combustion. With θ_{vap} being the crankshaft interval between IVC and the ignition point, and assuming that fuel vaporization occurs linearly during this interval, the rate at which the fuel vaporizes with respect to crank angle ($\dot{m}_{vap}$) is given by: [Blair, 1999]

$$\dot{m}_{vap} = \frac{m_{fuel}}{\theta_{vap}} \tag{2.41}$$

Therefore, the loss of heat from the cylinder (δQ_{vap}) for any given crankshaft interval ($d\theta$) may be calculated by:

$$\delta Q_{vap} = \dot{m}_{vap} h_{vap} d\theta \tag{2.42}$$

The model described before is only accurate for mixtures that are stoichiometric or richer. For leaner than stoichiometric mixtures, this model may not be accurate and another model based on CI engines should be applied, which is not covered in this study.

2.4 Engine Operating Parameters

When characterizing engine operation, some basic geometrical relationships and parameters are common and will be described next. To an engine user, the following factors are considered of importance [Heywood, 1988]:

1. The performance of the engine over its operating range;
2. The fuel consumption of the engine within this operating range and the cost of the required fuel;
3. The noise and air pollutant emissions of the engine within this operating range;
4. The engine's initial cost and its installation;
5. The engine's reliability and durability, its maintenance requirements, and how these affect engine availability and operating costs.

This study will only consider the performance and efficiency of both engines, though the remaining factors listed above may be equally important.

Engine performance is more precisely defined by the maximum power (or maximum torque) available at each speed within the useful engine operating range; and the range of speed and power over which engine operation is satisfactory. [Heywood, 1988]

2.4.1 Geometrical Properties of Reciprocating Engines

The basic geometry of a reciprocating engine may be defined by the compression ratio (CR), which is the ratio between the maximum and minimum cylinder volume; and the bore/stroke ratio (R_{BS}), which is the ratio between the cylinder bore and piston stroke: [Heywood, 1988]

$$CR = \frac{V_{displacement} + V_c}{V_c} \tag{2.43}$$

$$R_{BS} = \frac{B}{S} \tag{2.44}$$

For SI engines, these parameters have typical values of RC between 8 and 12 and R_{BS} in the range of 0.8 to 1.2 for small- and medium- sized engines, decreasing to about 0.5 for large slow-speed CI engines. [Heywood, 1988] The mean piston velocity is also an important characteristic and has already been described previously.

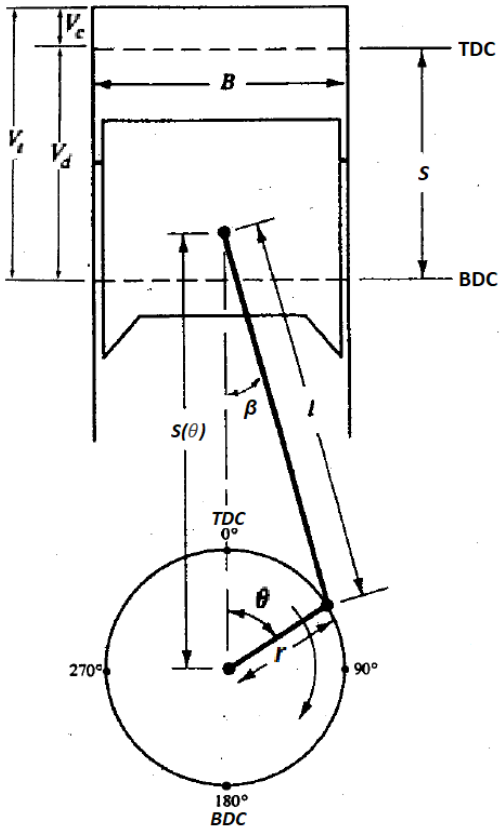

Figure 2.6. Geometry of slider crank engine. *[Adapted from Heywood, 1988]*

2.4.2 Brake Torque and Power

Torque may be defined as a force applied through a radius to produce a turning moment. It also can be defined as the tendency of a force to rotate an object around a pivot.

The torque (Tq) produced by an engine is, therefore, defined as:

$$Tq = F.b \tag{2.45}$$

Where F is the tangential force applied in relation to the crank radius and b is the distance between the centre of rotation and where the force is applied. Throughout the engine cycle, the torque is constantly varying depending on crank angle therefore, the power being developed is also constantly varying. However, if the torque is averaged for the whole cycle, then the power developed in kW (P_{kW}) can be calculated as:

$$P_{kW} = 2\pi \frac{N}{60} Tq = Tq.\omega \tag{2.46}$$

With ω as the angular velocity in rad/s. It can be converted to horsepower (P_{HP}) by:

$$P_{HP} = 1.34102209\, P_{kW} \tag{2.47}$$

It should be noted that torque is a measure of an engine's ability to do work and power is the rate at which work is done. [Heywood, 1988]

2.4.3 Indicated Work per Cycle

The work transfer of gas in the cylinder to the piston due to the pressure can be calculated with such pressure data. If a diagram of the cylinder pressure and volume throughout the engine cycle is plotted, as in figure 2.7, the area enclosed on the p-V diagram, obtained by integrating around the curve, will give the indicated work per cycle, per cylinder ($W_{c,i}$): [Heywood, 1988]

$$w_{c,i} = \oint p\, dV \tag{2.48}$$

As far as two-stroke cycle are concerned, Eq. 2.48 becomes simple to apply. However, the addition of inlet and exhaust strokes for the four-stroke cycle introduces some ambiguity and so two definitions of indicated output are commonly used. Gross indicated work per cycle ($W_{i,cg}$) is defined to be the work delivered to the piston over the compression and expansion strokes only, while net indicated work per cycle ($W_{i,cn}$) is defined to be the work delivered to the piston over the entire four-stroke cycle.

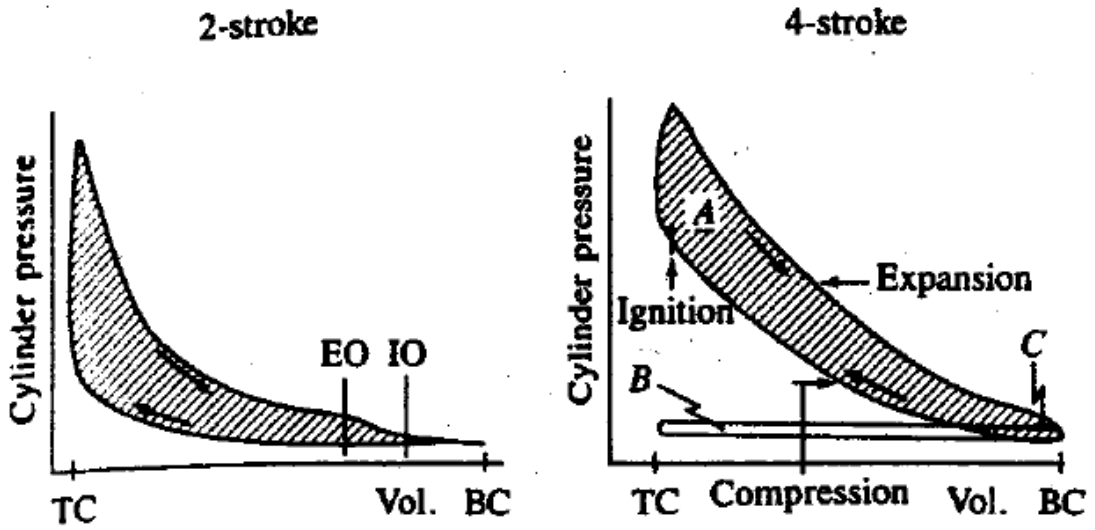

Figure 2.7. Example of a p-V diagram for a two-stroke engine (left) and a four-stroke engine (right). *[Adapted from Heywood, 1988]*

In this study only the gross indicated work per cycle will be considered since indicated quantities are used primarily to identify the impact of the compression, combustion and expansion processes on engine performance. [Heywood, 1988]

The indicated work per cycle and the power per cylinder are related:

$$P_i = \frac{W_{c,i} N}{n_R} \tag{2.49}$$

Where n_R represents the number of crank revolutions for each power stroke per cylinder and is equal to 2 and 1 for four-stroke and two-stroke cycles, respectively. This power is the indicated power, i.e., the rate of work transfer from the gas within the cylinder to the piston.

2.4.4 Mean Effective Pressure

Although torque is an important parameter to evaluate an engine's performance, it depends on engine size. Therefore, a more useful relative parameter to measure engine performance is obtained by dividing the work per cycle by the cylinder volume displaced per cycle, in dm^3. This parameter is defined as mean effective pressure (mep) and has units of force per unit area: [Heywood, 1988]

$$mep = \frac{P\, n_R}{V_{displaced} \frac{N}{60}} \tag{2.50}$$

Or, if expressed in terms of torque:

$$mep = \frac{6.28\, n_R Tq}{V_{displaced}} \tag{2.51}$$

The maximum mean effective pressure of good engine designs is well established and is basically constant over a wide range of engine sizes. Typical values for maximum mep, for naturally aspirated SI engines, are 850 kPa to 1050 kPa at the engine speed for maximum torque. At maximum rated power, bmep values are 10 ro 15 % lower. [Heywood, 1988]

2.4.5 Specific Fuel Consumption and Efficiency

When testing an engine, the fuel consumption is measured as a flow rate-mass per unit time ($\dot{m}_{fuel}$). However, it is more useful to measure how efficiently an engine is using the fuel supplied to produce work. This parameter is termed specific fuel consumption (sfc), and is the fuel flow rate per unit power output: [Heywood, 1988]

$$sfc = \frac{\dot{m}_{\text{fuel}}}{P_{kW}} \tag{2.52}$$

Typical best values of sfc for SI engines are about 75 μg/J=270 g/(kW.h). [Heywood, 1988]

However, the specific fuel consumption has units. A dimensionless parameter which relates the desired engine output (work per cycle or power) to the necessary input (fuel flow) would have more fundamental value. Therefore, it is commonly used the ratio of the work produced per cycle to the amount of fuel energy supplied per cycle that can be released in the combustion process, and is a measure of the engine's efficiency. The fuel energy supplied that can be released by combustion is given by the mass of fuel supplied to the engine per cycle times the heating value of the fuel (QHV) which defines its energy content.

This measure of an engine's efficiency (termed fuel conversion efficiency η_{fuel}) is given by:

$$\eta_{fuel} = \frac{W_c}{m_{fuel} QHV} = \frac{P}{m_{fuel} QHV} = \frac{1}{sfc.\, QHV} \tag{2.53}$$

2.4.6 Air/Fuel Ratio

Both the air and fuel mass flow rates ($\dot{m}_{air}$ and $\dot{m}_{fuel}$, respectively) are normally measured. The ratio between these flow rates is a useful parameter in defining engine operating conditions:

$$AFR = \frac{\dot{m}_{air}}{\dot{m}_{\text{fuel}}} \tag{2.54}$$

Conventional SI engines with gasoline as fuel normally operate with AFR between 12 and 18. The model developed in this study includes the possibility of running lean or rich mixtures and their effect in engine operating conditions. However, as seen before, for lean mixtures fuel vaporization should not be considered unless another model for describing it is adopted. As such, it was described the relative air/fuel ratio (λ) for SI engines, as:

$$\lambda = \frac{AFR}{AFR_{stoich}} \tag{2.55}$$

The combustion efficiency (η_c) of a gasoline type fuel can be expressed in terms of relative air/fuel ratio from measured data as: [Blair, 1999]

$$\eta_c = \eta_{cmax}(-1.6082 + 4.6509\lambda - 2.0764\lambda^2) \tag{2.56}$$

For values of λ between 0.75 and 1.2. The maximum value for η_{cmax} is typically 0.9 for SI engines using gasoline fuel. It should be noted that Eq. 2.56 maximizes at about 12% lean of stoichiometric. [Blair, 1999]

2.5 Slider Crank Engine

The slider crank internal combustion engine (ICE) drives numerous machines from generators and automobiles to boats and aircraft, being the most used nowadays in developed parts of the world. The slider crank mechanism is mainly used to convert the reciprocating motion of the piston into rotary motion of the output shaft.

Although many technological advancements have been made over the past 100 years as far as ICE are concerned, the fundamental slider crank based mechanism has remained essentially unchanged. Despite its success, this mechanism presents two shortcomings:

1. The angle between the connecting rod and the axis of the cylinder (ß) that occurs during an engine operation produces a force on the piston perpendicular to the axis of the cylinder, thus causing piston side load. This piston side load causes friction between the piston and the cylinder wall, with consequent reduced efficiency and additional heat that must be dissipated by the cooling system.
2. Balance is an issue due to the reciprocating motion of the piston and the complex motion of the connecting rod. Furthermore, the piston also describes a non-sinusoidal motion which causes a second order vibration and makes even more difficult to achieve engine balance.

2.5.1 Slider Crank Engine Kinematics

The crank engine kinematics such as instantaneous piston position (S_{piston}), piston velocity (v_{piston}) and piston acceleration (a_{piston}) can be described, referring to figure 2.6, as a function depending on crank angle (θ) as follows [Heywood, 1988]:

$$S_{piston}(\theta) = r\cos(\theta) + (l^2 - r^2\sin(\theta)^2)^{1/2} \tag{2.57}$$

Knowing that the instantaneous piston velocity is the derivative of the instantaneous piston position, with ω as the angular velocity in rad/s:

$$v_{piston}(\theta) = S'_{piston}(\theta) = \left[-r.\sin(\theta) - \frac{r^2\cos(\theta)\sin(\theta)}{(l^2 - r^2\sin(\theta)^2)^{1/2}}\right]\omega \tag{2.58}$$

Similarly, the instantaneous piston acceleration (a_{piston}) is the derivative of the instantaneous piston velocity, and it can be described as:

$$a_{piston}(\theta) = v'_{piston}(\theta) = \tag{2.59}$$

$$\left[-r.\cos(\theta) - \frac{r^2\cos(\theta)^2}{(l^2 - r^2\sin(\theta)^2)^{1/2}} + \frac{r^2\sin(\theta)^2}{(l^2 - r^2\sin(\theta)^2)^{1/2}} - \frac{r^4\cos(\theta)^2\sin(\theta)^2}{(l^2 - r^2\sin(\theta)^2)^{3/2}}\right]\omega^2$$

Finally, the chamber volume ($V_{chamber}$) can be described by:

$$V_{chamber}(\theta) = A_{piston}\big(l + r - S(\theta)\big) + V_c \tag{2.60}$$

Where Apiston is the piston crown area. The clearance volume (V_c), which is the combustion chamber volume at TDC, can be calculated by:

$$V_c = \frac{V_{displacement}}{CR - 1} \tag{2.61}$$

2.5.2 Slider Crank Engine Dynamics

Considering the engine dynamics previously described, some of the ICE dynamics may be described. Knowing that the force applied to the piston (F_t) is the sum of both the force of inertia (Fi) and force of pressure (Fp), it is described by:

$$F_t = F_i + F_p \tag{2.62}$$

With:

$$F_i = m_{piston}.a(\theta) \tag{2.63}$$

$$F_p = p.A_{piston} \tag{2.64}$$

Knowing the force that is applied to the piston, the instantaneous torque in respect to the crank angle (Tq(θ)) and the average torque over the cycle ($\bar{T}$q) can be calculated by:

$$Tq(\theta) = \frac{F_t}{\cos(\beta)}\, r.\sin(\theta + \beta) \tag{2.65}$$

$$\bar{T}q = \frac{\sum Tq(\theta)}{\theta_{total}} \tag{2.66}$$

The angle between the connecting rod and the axis of the cylinder () is given by:

$$\beta = \sin^{-1}\left(\frac{r\sin\theta}{l}\right) \tag{2.67}$$

As described previously, the power developed by the engine is given by Eqs. 2.46 and 2.47 and its efficiency by Eq. 2.53.

2.6 Geared Hypocycloid Engine

The first documented cardan geared mechanism dates back to the 15th century, named after Girolamo Cardano (1501 – 1576). However, such mechanisms may have been studied and developed much earlier, using the geometry of Elementa written by Euclid of Alexandria (325 - 265 BC) [Karhula, 2008].

The first engine to implement this mechanism dates back to 1802 with such engine having been developed and built for water pumping in 1805 by British steam engine manufacturer Matthew Murray. In 1875, the German mechanical engineer and professor Franz Releaux (1829 – 1905) presented the basis of both slider crank and cardan gear mechanisms, and is treated as the originator of the mechanism design. Throughout the 20th century, the cardan gear mechanism has not seen much development and adoption with the slider-crank mechanism being much more popular. Research of particular interest began in the mid 1970's with the work of Ishida who published a paper focusing on the inertial shaking forces and moments of a geared hypocycloid engine and compared with a slider crank engine. This was followed by another paper published in 1986 where a two-stroke cycle single cylinder reciprocating chainsaw utilizing an internal gear system was studied. Later in 1991, another paper was published which provided a list of proposed benefits and design equations for GHE as well as another version of the basic GHE was introduced, which was called the modified hypocycloid engine. In 1998, a team of researchers from Italy released work on the design and testing of a full crank 1255cc two-stroke hypocycloid engine. In 2001, a patent was filled by Mr. Randal Wiseman in a research effort to give a major focus into the cardan gear mechanism, more specifically, the geared hypocycloid mechanism, depicted in figure 2.8.

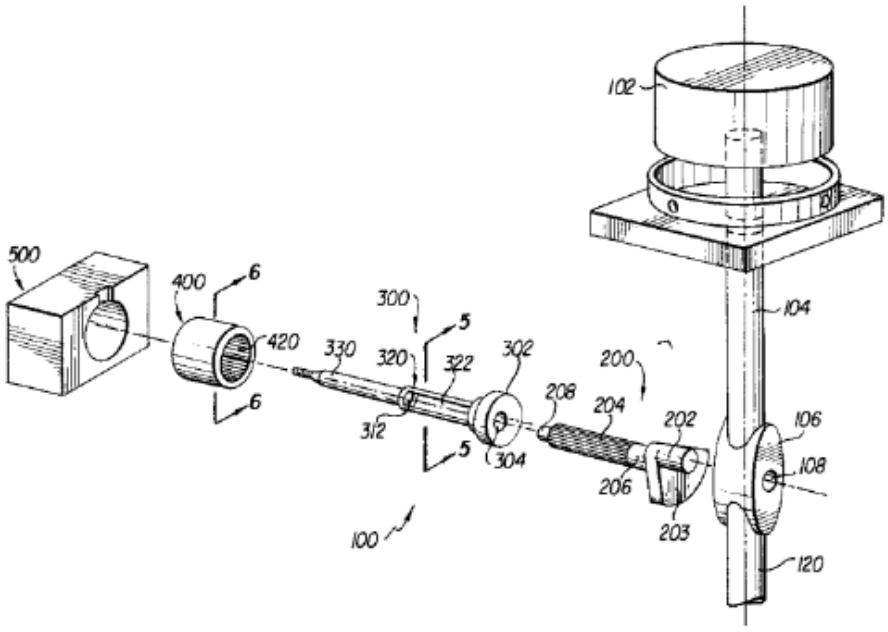

Figure 2.8. Sketch from Wiseman US Patent #6510831. *[Conner, 2011]*

One of the most recent comprehensive studies regarding GHE was published by Karhula in 2008, where extensive insight in comparing similar slider crank and cardan gear engines is provided. In 2011, Conner provided work with a focus on the balancing and development of a modified engine provided by Wiseman Technologies Inc. (WTI) and comparing its performance with an unmodified engine. Later in 2014, Ray also published some work continuing the development of the engine provided by WTI. In 2016, Azziz published a paper where an enhanced hypocycloid gear mechanism for internal combustion engine applications was proposed as a replacement for slider crank mechanisms to further improve engine performance.

The increasing awareness of emissions and fuel consumption has increased the interest in alternative engine designs, with GHE being one of the alternatives.

2.6.1 Hypocycloid Concept

The geared hypocycloid engine (GHE) takes advantage of the hypocycloid concept to convert the linear motion of the piston into rotary motion of the output shaft. A hypocycloid, by definition, is the curve traced by a fixed point (A) on the circumference of a small circle of radius R_a that rolls without slipping along the inside of a larger fixed circle or radius R_b, as shown in figure 2.9. [Azziz, 2016]

In the particular case of a circle ratio of 2:1, i.e., the diameter of the inner circle is half the diameter of the outer circle, any point in the inner circle draws a straight-line as it rolls around inside the outer circle. This allows a geared hypocycloid mechanism to be designed with a 2:1 gear ratio to convert the linear motion of the piston into rotary motion. This gives the engine some advantages, such as:

1. The piston will describe a sinusoidal motion which is important for engine balance.
2. Reduced or even non-existent piston side-load which leads to reduced friction and heat and better efficiency.
3. Piston and rod may be designed without piston skirt or pin wrist which reduces its mass and, therefore, the inertial forces that act upon the piston.

Very few engines have been built. Wiseman claims to have tested and compared two similar engines, one with a slider crank and the other with a geared hypocycloid mechanism and registered an improvement in fuel efficiency of 50.5% while producing the same power output. Conner, however, claims to have seen reduced power output and increased fuel consumption. [Conner, 2011]

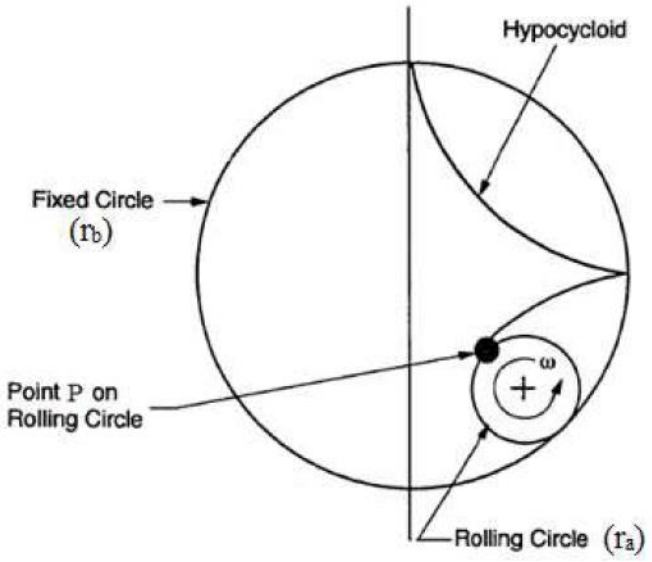

Figure 2.9. Hypocycloid concept. *[Adapted from Ray, 2014]*

2.6.2 Geared Hypocycloid Engine Kinematics

The GHE kinematics such as instantaneous piston position (S_{piston}), piston velocity (v_{piston}) and piston acceleration (a_{piston}) can be described, referring to figure 2.10, as a function depending on crank angle (θ), as follows [Azziz, 2016]:

$$S_{piston}(\theta) = 2r\cos(\theta) + l \tag{2.68}$$

Knowing that the instantaneous piston velocity is the derivative of the instantaneous piston position, with ω as the angular velocity in rad/s:

$$v_{piston}(\theta) = S'_{piston}(\theta) = [-2r\sin(\theta)]\omega \tag{2.69}$$

Similarly, the instantaneous piston acceleration (a_{piston}) is the derivative of the instantaneous piston velocity, and it can be described as:

$$a_{piston}(\theta) = v'_{piston}(\theta) = [-2r\cos(\theta)]\omega^2 \tag{2.70}$$

Finally, the chamber volume ($V_{chamber}$) can be described by:

$$V_{chamber}(\theta) = A_{piston}\big(l + 2r - S(\theta)\big) + V_c \tag{2.71}$$

Where Apiston is the piston crown area. The clearance volume (V_c), which is the combustion chamber volume at TDC, can be calculated by:

$$V_c = \frac{V_{displacement}}{CR - 1} \tag{2.72}$$

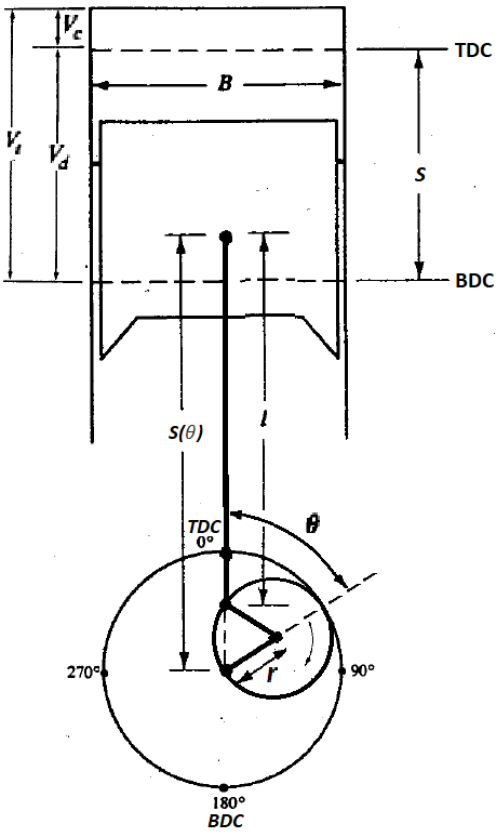

Figure 2.10. Geometry of geared hypocycloid engine. *[Adapted from Heywood, 1988]*

2.6.3 Geared Hypocycloid Engine Dynamics

Considering the engine dynamics previously described, some of the GHE dynamics may be described. Similar to ICE, the force applied to the piston (F_t) is the sum of both the force of inertia (Fi) and force of pressure (Fp), and can be calculated by Eqs. 2.63, 2.64 and 2.65.

Knowing the force that is applied to the piston, the instantaneous torque in respect to the crank angle (Tq(θ)) and the average torque over the cycle ($\overline{T}$q) can be calculated by:

$$Tq(\theta) = \frac{F_t}{\cos(\theta)}\, r.\sin(2\theta) \tag{2.73}$$

$$\bar{T}q = \frac{\sum Tq(\theta)}{\theta_{total}} \tag{2.74}$$

The tangential gear tooth load (F_{gt}) can be calculated by: [Azziz, 2016]

$$F_{gt} = F_t \sin(\theta) \tag{2.75}$$

As described previously, the power developed by the engine is given by Eqs. 2.46 and 2.47 and its efficiency by Eq. 2.53.

2.7 Opposed Piston Engine

The first public appearance of an opposed piston engine (OPE) was probably a two-stroke, gas-fuelled by Wittig in Germany in 1878, although in 1874 Gilles de Cologne had already built a single cylinder OPE in which one piston was connected to the crankshaft and the other was a free piston. In opposed piston engines, a pair of pistons operate in a single cylinder, which eliminates the need for cylinder heads. Although the concept of OP is applicable to both two- and four-stroke engines, most OP engines developed operate on two-stroke, CI cycles, probably for simplicity and because they were intended to achieve high thermal efficiency and high-power density. The history of OPE can be divided into three main periods – pre-1900, 1900-1945 and post 1945. [Pirault & Flint, 2010].

The pre-1900 period is characterized by the mention and introduction of many key features of the modern OP engine. The key advantages of OPE in comparison to their competitors during that time were simplicity, balance, absence of the then problematic cylinder head joint, relatively light mechanical loading of the crankshafts due to the possibility of large engines with low bore/stroke ratios (B/S), and the benefit in terms of mixing air with the fuel and turbulence generation because of the opposing retreating motion of the pistons. In this period, OPE greatly improved the efficiency of two-strokes, achieving values close to those of four-stroke engines.

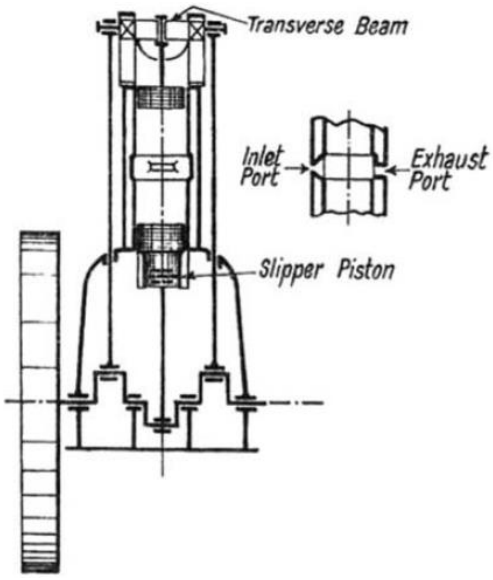

Figure 2.11. Wittig gas engine, 1878. *[Pirault & Flint, 2010]*

During the 1900-1945 period, many stationary and marine applications were developed with diesel fuel, despite a hiatus in new engine development during World War I, with this period being the formative period for this technology, with some limited volume applications by Junkers, CLM, Doxford and Sulzer. Some of the most famous engines are the OPE developed in Germany by Junkers which were mainly used in aviation and were two-stroke CI engines.

The post-1945 period has seen more production applications, although mainly in land and marine applications such as those from Doxford, Napier, Deltic, Fairbanks Morse or the complex military Leyland L60 and Rolls-Royce K60. Despite this, the most iconic OPE is probably the two-stroke CI engine Jumo 205E due to its power-to-weight ratio of 0.9 kW/kg and brake thermal efficiency of 40.6%.

In the aviation industry, there are very few commercial piston engine applications largely because of the high risk and liability present in aeronautical power units. Moreover, because most OPE are two-stroke CI engines which have a relatively lower power-to-weight ratio compared to SI engines. There have been many aeronautical diesel engines through the years but very few have been OPE. In fact, only since 2000 have some converted automotive four-cylinder four-stroke diesel OPE been used for this application. More recently, some emphasis has been given to OPE research though mainly, but not exclusively, for military applications. In view of further developing OPE to increase fuel economy and tackle engine emission issues, some engines were or are being recently developed such as the engines developed by Fairbanks Morse, Golle Motor AG, Pinnacle, Pattakon, Achates Power Inc., Ecomotor, Kharkiv Morozov Machine Building or Monolith Engine.

Fixed-wing light aircraft and helicopter are applications well suited for OPE because its advantages on power-to-weight ratio, power-to-bulk ratio, fuel efficiency, simplicity and safety. Despite future transport requirements forecasting a strong growth for both fixed- and rotary-wing aircraft requiring engines with 100-500 kW, a field not well suited to turbo-machinery in terms of cost and fuel efficiency, a safer route to develop new aviation engines before launching into the very sensitive aviation field is the unmanned aerial vehicles (UAV), powered gliders or the ultralight aircraft segments. [Pirault]. An increasingly important niche market are engines from 1-100 Kw to be applied in UAV operating as coast guard, highway surveillance and logistics. These engines are usually developed to drive a propeller, although a demand for electrical generation is increasing.

The OPE presents several advantages and disadvantages, compared to conventional four-stroke engines. Such advantages are high specific torque, power/weight and power/volume ratios, lower cooling rates which lead to smaller radiators for cooling, as high reliability and low maintenance requirements as well as superior engine balance. However, there are some disadvantages. The low reliability of the most prominent engines produced - the Junkers Jumo 205E, Leyland L60 and Napier Deltic, with reduced durability or high-cost maintenance. To be

fair, though, all these engines were under dimensioned for their application and their power density and power/volume ratio were so ahead of their time compared to other Diesel engines that it's surprising there weren't more issues. Their development periods were very short and their applications in large military vehicles, trains and aircraft had large public visibility. The most prominent issue, though, was the oil consumption, particularly in two-stroke CI engines, which led to high pollutant emissions.

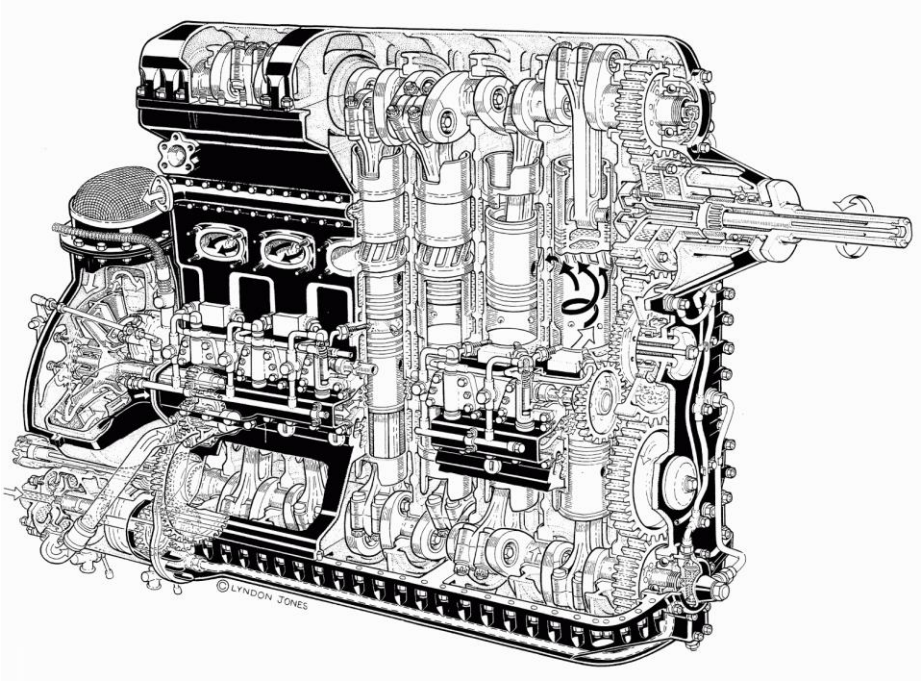

Figure 2.12. Cross-section through view of Jumo 205. *[Lyndon Jones, 1995]*

There are several possible configurations for OPE. These are crankless, single-crank where both the three-throw single-crank and the folded cranktrain are included, twin-crankshaft, multiple-crankshaft, rotary and barrel cam engine configurations, all of which are discussed by Pirault and Flint. For this study, a twin crankshaft configuration was chosen.

2.8 Spur Gear Background and Nomenclature

The term "gear" is defined as a machine element to transmit motion and power between rotating shafts by means of progressive engagement of projections called teeth. Gears can be seen as two cylinders rolling without slipping and thus, transmitting motion from one to the other. Although gears have been used for over 3000 years, the modern form of gearing technology has a history of only 100 years and are common elements in all machinery nowadays. In recent times, the gear design has become a highly complicated and comprehensive subject [Maitra, 1996] with gear design becoming a complicated art. [Radzevich, 2012]

Compared to other drives like belt, rope and chain drives, gears present as advantages an exact velocity ratio transmission, may be used to both transmit large power and for shafts with small centre distances, have high efficiency, reliable service and compact layout. As disadvantages, the requirement of special tools and equipment for their manufacture making them costlier than other drivers, possible vibrations and noise during operation if there's error in cutting teeth and the need of suitable lubricant and reliable method of applying it for gear drives to operate properly.

There are four main types of gears: spur, helical, bevel and worm gears. Spur gears have teeth parallel to the axis of rotation and are used to transmit motion from one shaft to another, parallel shaft. Of all types, spur gears are the simplest and will be the only type considered for this study. [Budynas & Nisbett, 2015]

Considering the fundamental law of gearing which states that the angular velocity ratio between the gears of a gearset must remain constant throughout the mesh, with the common normal to the tooth profiles, at all contact points within the mesh, always passing through a fixed point on the line centres. [Srivastava, 2006] There are many possible teeth profiles to be used such as the cycloidal profile which is still used in some watches and clocks however, only the involute tooth profile will be considered since it's by far the most commonly used, particularly in power transmission applications. Furthermore, involute teeth are used for power gearing instead of cycloidal teeth because they are easier to manufacture, small changes to centre distance don't affect the velocity ratio and are one of the strongest and most durable tooth profiles. The involute of a circle is exemplified in figure 2.13 and can be seen as a stretched string being unwrapped from a cylinder. The cylinders from which the strings are unwrapped are called bases circles and are smaller than the diameters of the original rolling circles which are called pitch circles.

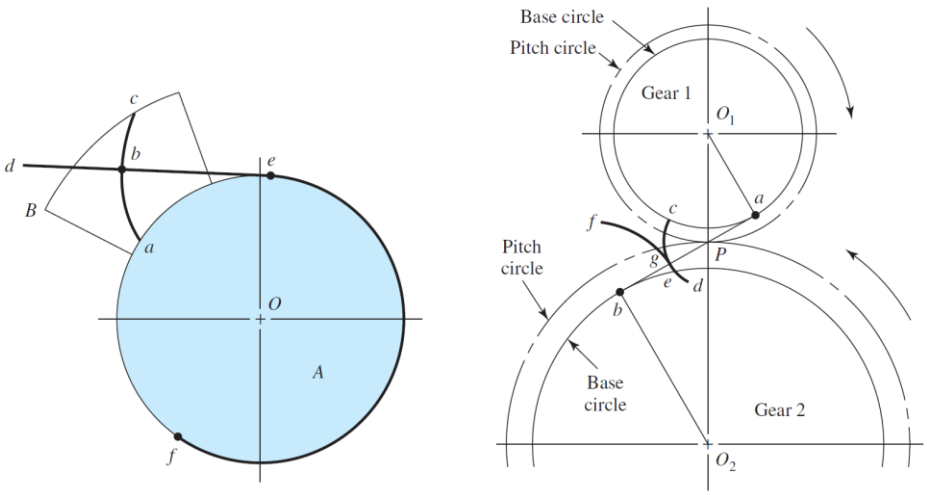

Figure 2.13. Generation of an involute (left) and involute action (right). *[Adapted from Budynas & Nisbett, 2015]*

2.8.1 Internal Gears

Hypocycloid gear mechanisms require an internal gear to mesh with an external gear. Internal gears have many applications, mostly in planetary gear systems. External and internal gears are very similar with the most obvious difference being if the teeth face outwards, the gear is called external gear, and if they face inwards, the gear is called an internal gear [Colbourne, 1987].

Compared to equivalent external gears, internal gears present several advantages: [Maitra, 2001 & Radzevich, 2012]

1. Because an internal gear with involute teeth have a concave instead of a convex shape, its base is thicker which makes the internal gear stronger.
2. Also, because an internal gear wraps around its mating pinion, the contact ratio is increased, load transfer from tooth to tooth is gradual and a natural guard is formed over the meshing teeth.
3. The increased contact ratio either increases the load that the system can take for the same surface stress and life, or decreases the surface stress for the same load which increases the life of gears.
4. The gradual load transfer from tooth to tooth and the reduced load on one tooth reduces the impact force at the beginning of tooth engagement therefore resulting in a quieter and smoother operation.
5. The sliding velocity along the profile is lower which increases efficiency and reduces wear.
6. Units composed of internal gears are more compact because they operate at a closer centre distance with its mating pinion.
7. When two parallel shafts need to rotate in the same direction, no idler gear needs to be used.

There are two types of interference that may occur in an internal gear drive. The first, known as undercut, occurs with the mating of the involute profile of one of the gears with the non-involute portion of the other and can be avoided by modifying the teeth to ensure that no contact occurs until the “interference point” is reached. The second type is known as fouling and only happens with internal gear drives. When the difference between the numbers of teeth of the mating gears is too small and no corrective measures are considered, fouling or tip interference may occur. This interference may be avoided by ensuring a minimum difference between the number of teeth of the pinion and internal gear.

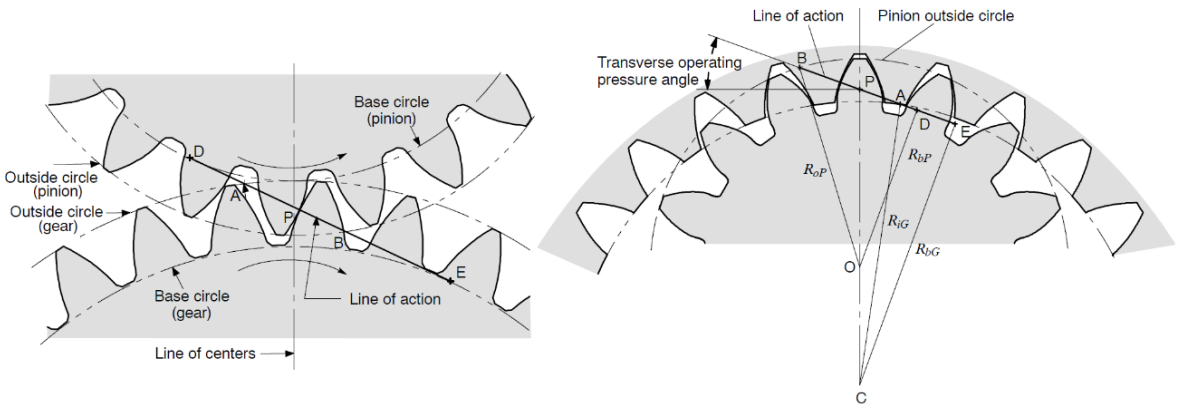

Figure 2.14. Meshing between external spur gear (left) and internal spur gear (right) with its pinion. *[Adapted from AGMA 917-B97]*

2.8.2 Spur Gear Basic Geometry

Because gear technology is such a comprehensive field of study, only a review of some basic terms and nomenclature regarding spur gear geometry in metric units will be given, with reference to figure 2.15. [Khurmi & Gupta, 2005 & Radzevich, 2012]

Pitch diameter (d_{pitch}). Diameter of an imaginary circle upon which all calculations are based. This circle, called pitch circle, can be seen as the circumference of an imaginary cylinder which rolls without slipping with another cylinder.

Module (m_n). Ratio of between the pitch diameter and the number of teeth.

Pressure angle (Φ). Angle between the common normal to two gear teeth at the point of contact and the common tangent at the pitch point.

Addendum (h_a). Radial height of a gear tooth from the pitch circle to the top of the tooth. The circle drawn is the addendum circle.

Dedendum (h_d). Radial height of a gear tooth from the pitch circle to the bottom of the tooth. The circle drawn is the dedendum circle.

Whole depth (h_t). Total radial height of a gear tooth and is equal to the sum of the addendum and dedendum.

Working depth (h'). Radial height from the addendum circle to the clearance circle of a gear and is equal to the sum of the addendum of the two meshing gears.

Clearance (c). Radial distance from the top of the tooth of one gear to the bottom of the of the tooth of the other meshing gear. The circle drawn is the clearance circle.

Backlash (j). Difference between the tooth space and the tooth thickness, measured on the pitch circle.

Face width (FW). Width of the gear tooth measured along its axis.

Fillet radius (r_t). Radius that connects the root circle to the profile of the tooth.

Distance Centre (d_{centre}). Distance between the centre of rotation of the mating gears.

It should be noted that, contrary to external gears, the addendum and dedendum circles of internal gears is to the inside and outside of the pitch circle, respectively.

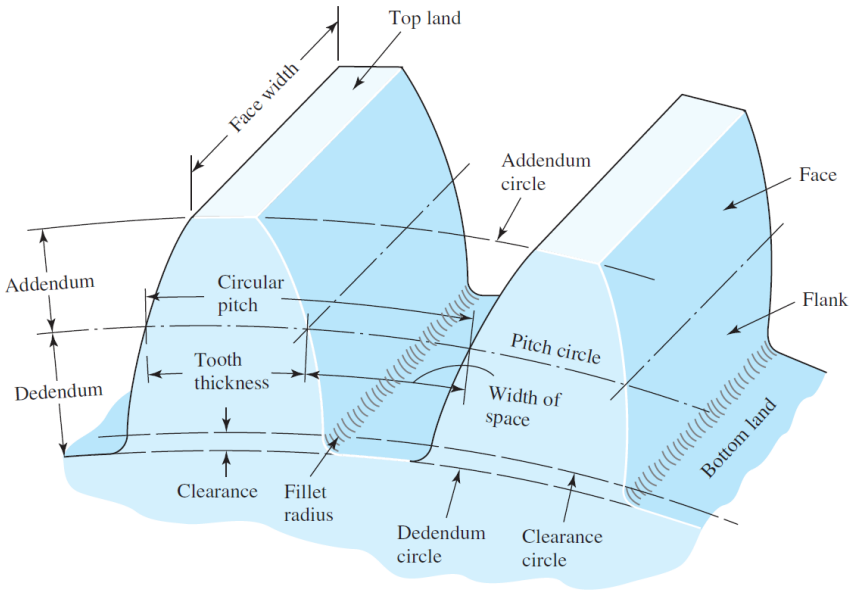

Figure 2.15. Basic geometry of a spur gear tooth. *[Budynas & Nisbett, 2015]*

2.8.3 Design Methods for Involute Spur Gears

To design a gear drive, one must calculate the stresses applied. There are several methods for calculating such stresses. For this study, it was considered the methods described in the standards published by the American Gear Manufacturers Association (AGMA) which is one of the most widely used standards.

The two stresses considered are the bending and the contact or pitting stresses. The pitting of gear teeth is considered to be a fatigue phenomenon. The aim of the pitting resistance formula is to determine a load rating at which progressive pitting of the teeth does not occur during

their design life. The bending strength of a gear teeth is a fatigue phenomenon related to the resistance to cracking at the tooth root fillet in external gears and at the critical section in internal gears. [AGMA 2001-D04]

2.8.3.1 Fundamental Bending Stress Formula

The bending strength of a gear tooth was first described by Wilfred Lewis in 1893. However, the formula only considered a static applied load and is not accurate enough for demanding applications. Thus, the fundamental formula for bending stress number presented by AGMA includes several correction factors to take into account many factors that affect the gear tooth bending strength and is given by: [AGMA 2101-C95 & AGMA 2001-D04]

$$\sigma_F = F_{gt} K_O K_V K_S \frac{1}{FW.m_n} \frac{K_m K_B}{J} \tag{2.76}$$

With σ_F as the working bending stress, F_t as the tangential load applied, K_O as the external application factor, K_V as the dynamic factor, K_S as the size factor, K_m as the load distribution factor, K_B as the external rim thickness factor and J as the tooth bending strength geometry factor.

2.8.3.2 Allowable Bending Stress

The working bending stress may be calculated by: [AGMA 2101-C95 & AGMA 2001-D04]

$$\sigma_F = \frac{\sigma_{FP} Y_N}{SF.K_T K_R} \tag{2.77}$$

With σ_{FP} as the allowable bending stress for a given material, Y_N as the life factor, K_T as the temperature factor, K_R as the reliability factor and SF as the safety factor.

2.8.3.3 Fundamental Contact Stress Formula

The contact stress formula is based on the Hertzian contact stresses between two cylinders and is given by: [AGMA 2101-C95 & AGMA 2001-D04]

$$\sigma_H = Z_E \sqrt{F_{gt} K_O K_V K_S \frac{K_m}{d_{pitch}.FW} \frac{C_f}{I}} \tag{2.78}$$

With σ_H as the working contact stress, Z_E as the elastic coefficient, C_f as the surface condition factor and I as the tooth pitting resistance geometry factor.

2.8.3.4 Allowable Contact Stress Formula

The working contact stress may be calculated by (based on AGMA 2101-C95 and AGMA 2001-D04):

$$\sigma_H = \frac{\sigma_{HP} Z_N C_H}{SH.K_T K_R} \tag{2.79}$$

With σ_{HP} as the allowable contact stress for a given material, Z_N as the life factor, C_H as the hardness ratio factor and SH as the safety factor.

Chapter 3

Engine Modelling

In this chapter, the model will be described and some operating parameters obtained to design some of the parts of the engine, with reference to Chapter 2. In order to design the engine, a computational model was developed that predicts the performance of both conventional slider-crank and geared hypocycloid engine without the need to conduct tests and to deduce the performance of parameters that can be difficult to measure in tests. This was achieved with MATLAB by firstly creating a model that allows a comparison between the performance of both engines in specific conditions. Later, a model was created that predicts the performance of both engines across all operating conditions as well as the dimensioning of several parts regarding the design intended. Empirical correlations are used for predicting processes such as heat transfer, start of combustion and burn rate. Even if a multi-dimensional model was available that predicted performance by solving the underlying physical phenomenon, its use may not be adequate since the computational requirements may be prohibitive and most engine design is derivative and evolutionary.

3.1 Engine Parametric Review

The opposed piston geared hypocycloid engine (OPGHE) designed in this study, with a twin crankshaft configuration, may be viewed as two conventional engines mounted opposite of each other with the cylinder heads removed, where the stroke of each engine equals the half-stroke of the OPE. Information regarding OPE is scarce and most of the engines developed are 2-stroke CI engines. Since the objective of this work is to design a 4-stroke SI engine, a selection of engines, mainly from the aeronautical industry, was made and their characteristics compared and is available in Annex A.1.

Because there's not much work available as far as OPGHE are concerned, and to compare to previous work [Gregório, 2017], a similar displacement of $2.86 \times 10^{-5}\ m^3$ (or 286 cc) was intended.

3.1.1 Bore x Stroke

The first step to start designing the engine was to choose the bore and stroke of the engine. It was observed that the bore/stroke ratio (R_{BS}) across the engines selected ranged from as low as 0.28 up to 1.650, mainly depending on the fuel, work cycle and type of engine.
When comparing OPE engines, the bore/half-stroke ratio (R_{BHS}) ranged from 0.571 to 1.0, averaging 0.723 for the engines reviewed. OPE tend to have lower R_{BS} which increase thermal efficiency through faster combustion and reduce fuel consumption [Qin, 2010]. However, it should be noted that all the OPE reviewed were 2-stroke CI engines.

When comparing conventional slider-crank engines (SCE), CI engines tend to have lower (R_{BHS}), typically from 0.9 to 1.0, while SI engines tend to have (R_{BHS}) typically from 1.0 to 1.65. Also, the work cycle in which the engines operate may influence this ratio, with 2-stroke engines having slightly lower R_{BS} than 4-stroke engines. In fact, from the engines reviewed, the R_{BS} of 2-stroke SI engines averaged 1.210 while 4-stroke SI engines averaged 1.251. However, some exceptions exist such as the 2-stroke SI model L275E engine from Limbach or the 4-stroke SI model O-145 engine from Lycoming which have a R_{BS} of 1.65 and 1.034 respectively.

After reviewing all the engines, and with the goal of designing an OPGHE with a R_{BHS} ratio similar to the R_{BS} of conventional engines for a closer comparison, a bore of 60 mm and a half-stroke of 52 mm was chosen for the OPGHE considered in this study, with a R_{BHS} of 1.154 (or a R_{BS} of 0.577) and a displacement of 2.9405×10^{-5} m^3 (or 294.05 cc).

It should be noted, however, that lower R_{BS} allow GHE, and conversely OPGHE, to have a more compact gearing system, as it will be discussed later.

3.1.2 Combustion Timings

Instead of assuming constant start and duration of combustion for the entire operating range, both were modelled empirically based on the known duration of combustion of two four-stroke SI engines in different speeds to improve the accuracy of the results. Thus, by taking into consideration the data collected in table A.2 in Annex, the duration of combustion ($\Delta\theta$) and start of combustion (θ_{start}) were modelled linearly as:

$$\theta_{start} = -0.0004\,N + 350.93 \tag{3.1}$$

$$\Delta\theta = 0.0027\,N + 30.663 \tag{3.2}$$

Table 3.1. Combustion data for two engines at different operating speeds.

N [rpm]	$\Delta\theta$ [deg]	θ_{start} [deg]	Description
1200	352	32	Naturally-aspirated, 4-valve Spark-ignition automotive engine with 500 cc of displacement. [Blair, 1999]
2400	348	41	
3600	350	39	
4800	349	44	
6000	346	44	
7600	349	51	Naturally-aspirated, Spark-ignition racing engine with 4500 cc of displacement. [Blair, 1999]
9200	347	56	

3.2 Initial Parameters

The model considered the working fluid to be a perfect gas and the conditions in which the engines operates to be those at sea level in the ISA Atmosphere. The fuel considered is gasoline aviation [Blair, 1999] and both engines are considered aspirated, so the pressure ratio is 1, which means that the intake pressure is equal to the ambient pressure. It is also considered that both engines run on a stoichiometric fuel-air mixture. The temperature of the cylinder wall can be assumed to be 350K [Stone, 1999]. Also, the intake and exhaust processes are taken as being done according to the ideal Otto cycle. Finally, the rod length was estimated and its influence on engine performance is negligible.

Therefore, the following parameters are considered:

Table 3.2. Initial Parameters for modelling.

Bore	0.060 m
Stroke	0.104 m
Compression Ratio	10
Rod length	0.090 m
Piston mass	0.250 kg
Piston Area	0.02827 m^2
Volume Swept or Displacement	2.9405×10^{-4} m^3
Clearance Volume	3.2673×10^{-5} m^3
Ambient Temperature	288.15 K
Ambient Pressure	101325 Pa
Intake Temperature	288.15 K
Pressure Ratio	1
Intake Pressure	101325 Pa
Gas Constant	287.04 J/(kg.K)
Heat Capacity Ratio	1.4
Specific Heat at Constant Volume	718 J/(kg.K)
Stoichiometric Air-Fuel Ratio	15.06
Relative Air/Fuel Ratio	1
Air-Fuel Ratio	15.06
Fuel Heat Power	43.5 MJ/kg
Latent heat of vaporization of gasoline aviation	400 kJ/kg
Intake Valve Open	0 deg
Intake Valve Close	180 deg
Exhaust Valve Open	540 deg
Exhaust Valve Close	720 deg
Maximum Rated Speed	8000 rpm
Cylinder Wall Temperature	350 K

3.3 Engine Kinematics

The next step was to model the kinematics of both the opposed piston slider-crank (OPSCE) and hypocycloid (OPGHE) engines, which was done with the equations described in Chapter 2 for both slider crank and geared hypocycloid engine kinematics.

Applying the values in table 3.2, the engines kinematics such as piston position, piston velocity, piston acceleration and chamber volume for both engines were obtained.

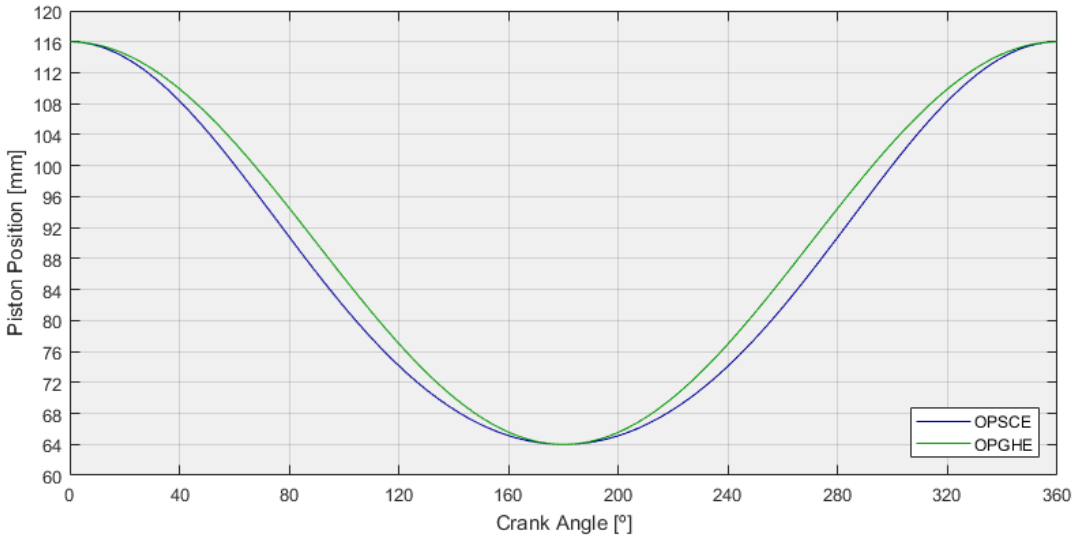

Figure 3.1. Piston position for the OPSCE and OPGHE models during a crank revolution.

From figure 3.1 it is clear the piston in an OPGHE stays close to the TDC for longer during the crank revolution compared to the OPSCE.

Figures 3.2 and 3.3 clearly show the sinusoidal movement of the piston in an OPGHE, as opposed to the OPSCE. The maximum values for the piston velocity is 22.7 m/s and 21.8 m/s for the OPSCE and OPGHE, respectively.

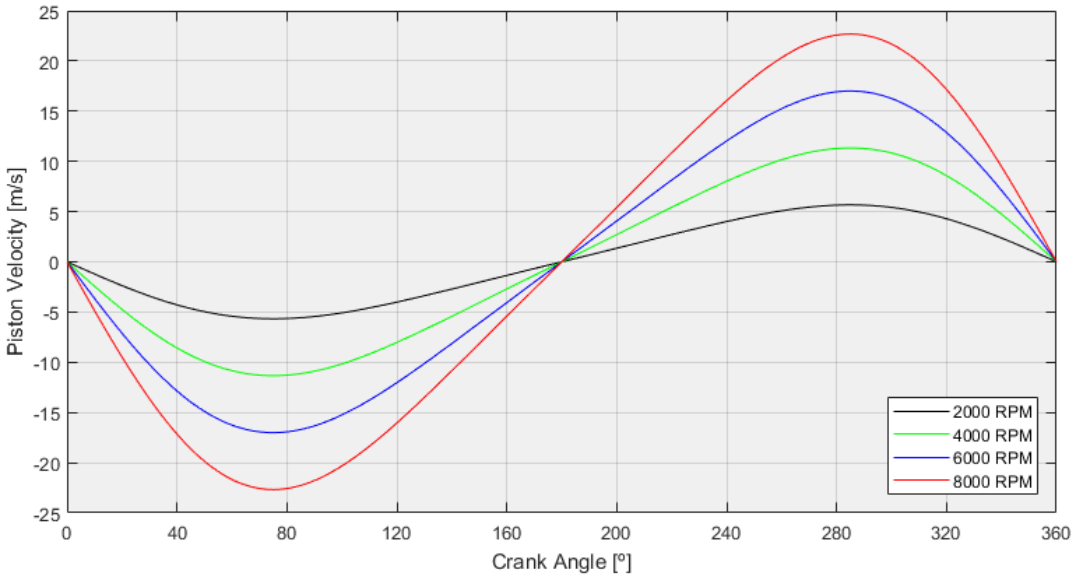

Figure 3.2. Piston velocity for the OPSCE model during a crank revolution.

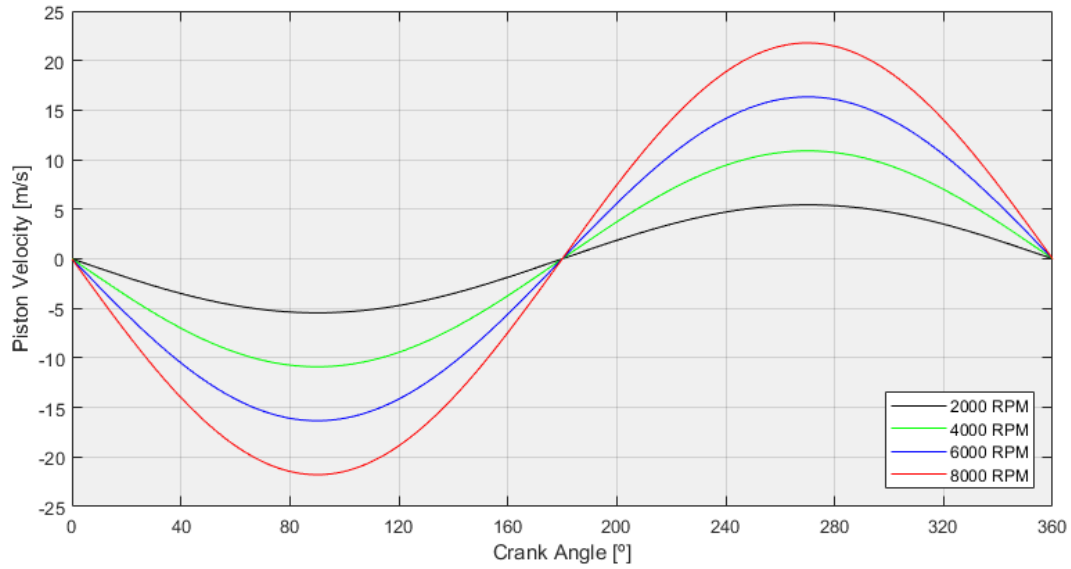

Figure 3.3. Piston velocity for the OPGHE model during a crank revolution.

Figures 3.4 and 3.5 also corroborate the sinusoidal movement of the piston in an OPGHE. The OPSCE has a maximum absolute piston acceleration of 23519.4 m/s^2 (which is equal to 2397.5 G's of acceleration), with the OPGHE having a lower maximum absolute piston acceleration with a value of 18247.8 m/s^2 (which is equal to 1860.1 G's of acceleration) for the same operating speed. Thus, the OPGHE will reduce the inertial forces by 22.4%.

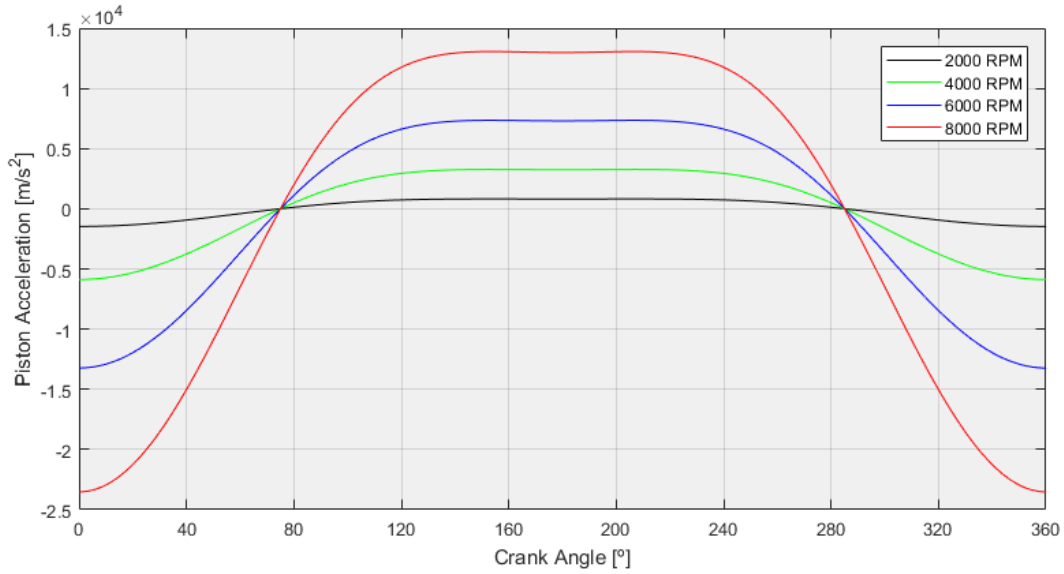

Figure 3.4. Piston acceleration for the OPSCE model during a crank revolution.

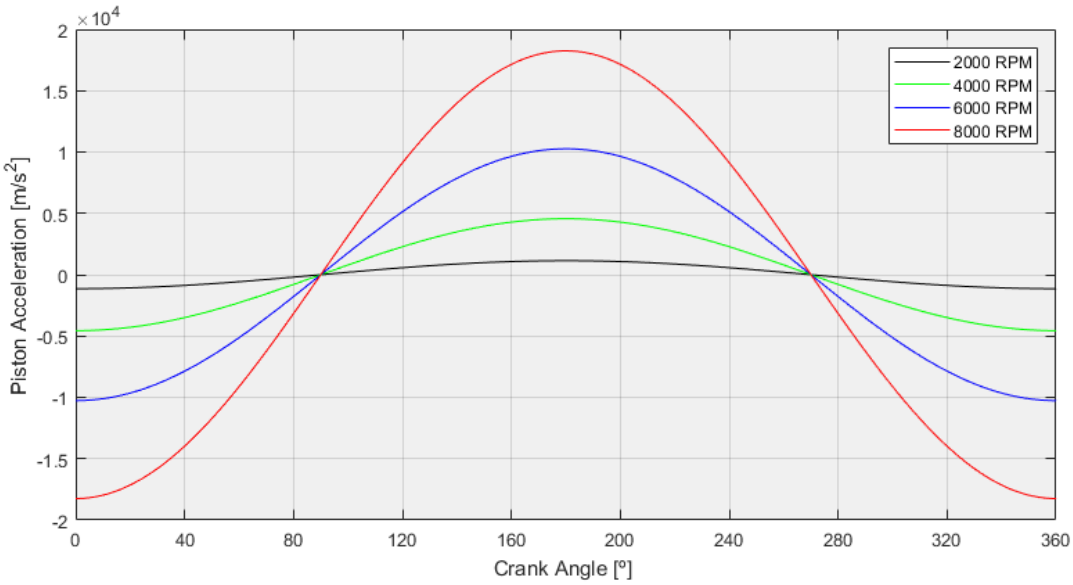

Figure 3.5. Piston acceleration for the OPGHE model during a crank revolution.

Figure 3.6 verifies that in an OPGHE, the piston stays close to the TDC for longer during the crank revolution. Because constant volume combustion is one of the most effective ways to increase the efficiency of ICE, [Azziz, 2016] this will bring the combustion process in an OPGHE closer to such condition.

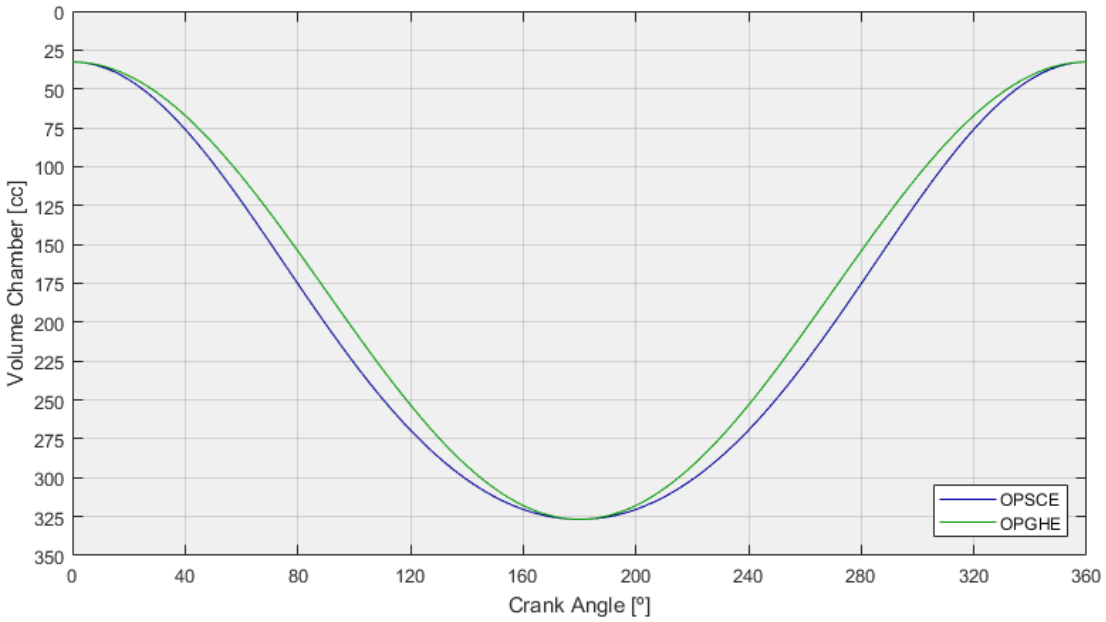

Figure 3.6. Volume chamber for the OPSCE and OPGHE models during a crank revolution.

3.4 Engine Dynamics

3.4.1 Closed Cycle Single-Zone Model

As previously seen, the ideal Otto cycle is not accurate enough for describing the operating cycle of both engines. Thus, a closed cycle model approach was considered with a single-zone model developed as a modelling technique to be used in this study. A single-zone engine model treats the cylinder as a solitary fluid or zone and is the simplest approach in engine modelling. In this model, the burnt and unburnt gases, residual gases and unburnt hydrocarbons within the cylinder are viewed as an ideal gas with uniform pressure. In fact, the ideal gas law is the basis for the single-zone engine model, and is defined as:

$$pV = mRT \tag{3.3}$$

With P as the pressure of an ideal gas, V as the volume of the gas, m is the mass of the gas, R is the gas constant and T is the mean gas temperature.

The closed cycle model within engine simulations was then used [Blair, 1999]. This approach uses all the theory discussed above in Chapter 2 on heat transfer, fuel vaporization, heat release rates and mass fraction burned behaviour and solves the First Law of Thermodynamics, which was extended to include fuel vaporization, at every step in a computation.

It is described as:

$$\delta Q_R - \delta Q_L - \delta Q_{vap} = \frac{P_2 V_2 - P_1 V_1}{\gamma - 1} + \frac{P_1 + P_2}{2}(V_2 - V_1) \tag{3.4}$$

Rearranging Eq. 3.4 and with Eq. 3.3, the new pressure P_2 and temperature T_2 for each phase of the closed cycle can be calculated by:

$$P_2 = \frac{2\left(\delta Q_R - \delta Q_L - \delta Q_{vap}\right) + P_1(G_6 V_1 - V_2)}{G_6 V_2 - V_1} \tag{3.5}$$

$$T_2 = \frac{P_2 V_2}{m_2 R} \tag{3.6}$$

With:

$$G_6 = \frac{\gamma+1}{\gamma-1} = 6 \text{ for air, where } \gamma = 1.4 \tag{3.7}$$

$$m_2 = m_1 + dm \tag{3.8}$$

Where G_6 is equal to 6 for air with a specific heat ratio (γ) of 1.4 and dm is the mass flow increment. [Blair, 1999] The following assumptions are made for the closed cycle model:

<u>During the compression in SI engines:</u>

$$\mathrm{dm} = \dot{m}_{vap} d\theta \tag{3.9}$$

$$\delta Q_{vap} = \dot{m}_{vap} h_{vap} d\theta \tag{3.10}$$

$$\delta Q_R = 0 \tag{3.11}$$

<u>During the combustion in SI engines:</u>

$$\mathrm{dm} = 0 \tag{3.12}$$

$$\delta Q_{vap} = 0 \tag{3.13}$$

$$\delta Q_R = \eta_c(\chi_b - \chi_{b0}) m_{fuel}.QHV \tag{3.14}$$

During expansion in SI engines:

$$\mathrm{dm} = 0 \tag{3.15}$$

$$\delta Q_{vap} = 0 \tag{3.16}$$

$$\delta Q_R = 0 \tag{3.17}$$

It should be noted that the closed cycle commences at IVC on the compression stroke, i.e., this model does not consider how the engine gets filled with air nor how it gets rid of the exhaust gas, nor any scavenging during the valve overlap period.

3.4.2 Slider Crank Engine Dynamics

To be able to compare the performance between the OPSCE and OPGHE, the dynamics of the OPSCE were modelled as described in Chapters 2 and Sub-Chapter 3.4.1.

It can be seen from Figure 3.7 that the maximum in-cylinder pressure tends to decrease with increasing operating speed. The maximum in-cylinder pressure is 9.188 MPa at 370 rpm. For reference, the maximum in-cylinder pressure at 2000 rpm is 8.707 MPa and 6.690 MPa at 8000 rpm.

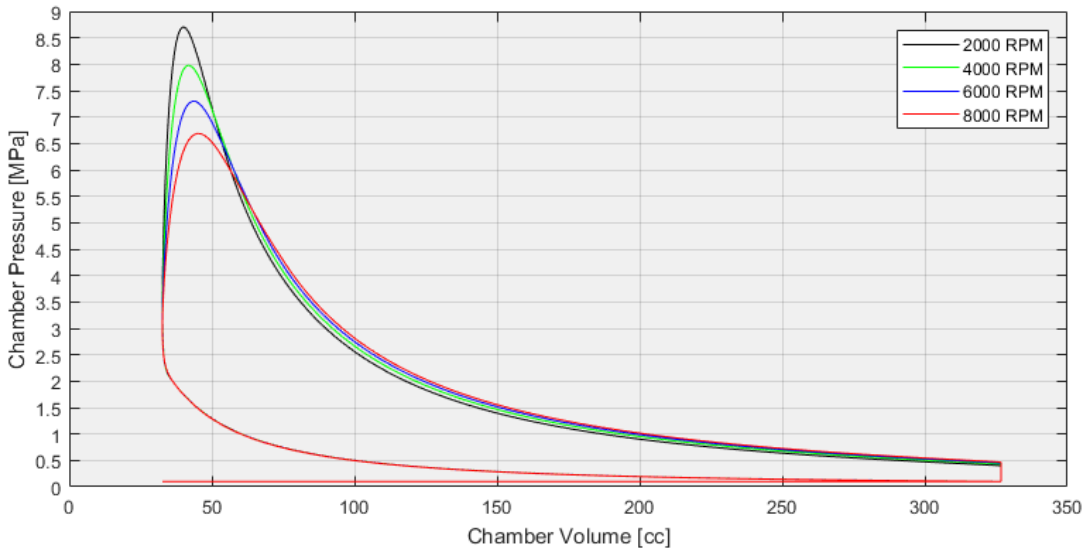

Figure 3.7. Pressure-volume (p-V) diagram for the OPSCE model at various operating speeds.

It is observed in figure 3.8 that the inertial and pressure forces tend to increase and decrease, with increasing operating speed, respectively, therefore decreasing the maximum total force applied to the piston. The maximum total force applied to the piston is 25967 N at 360 rpm. For reference, the maximum force applied to the piston at 2000 rpm is 24273 N and 13690 N at 8000 rpm.

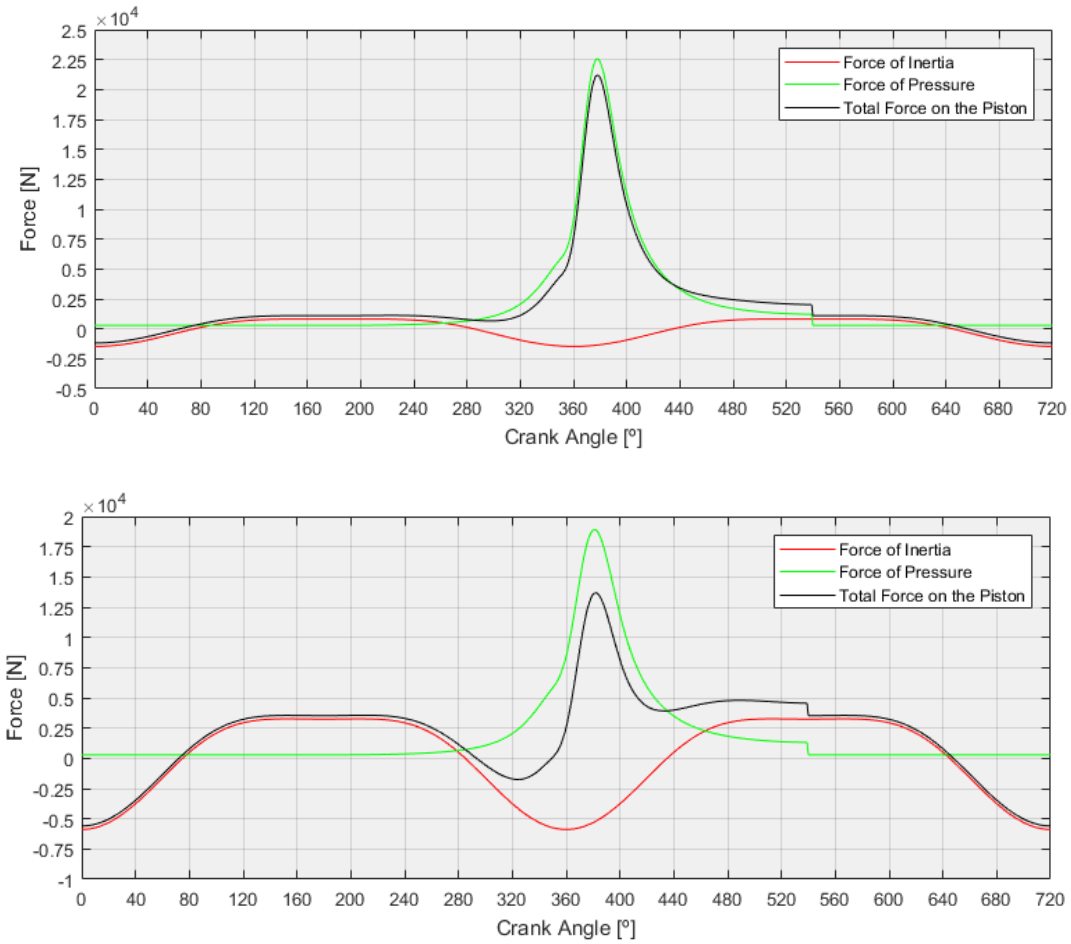

Figure 3.8. Forces applied to the piston for the OPSCE model during the cycle at 4000 rpm (top) and 8000 rpm (bottom).

Figure 3.9 shows that the maximum instantaneous torque output tends to decrease with increasing operating speed. The maximum instantaneous torque output is 276.255 N.m at 1550 rpm with an average torque of 35.904 N.m. For reference, the maximum instantaneous torque output at 2000 rpm is 275.731 N.m with an average of 36.284 N.m; and 195.075 N.m with an average of 36.908 N.m at 8000 rpm. It should be noted that the maximum average torque output is 37.138 N.m at 5400 rpm, with a maximum instantaneous torque output of 245.032 N.m.

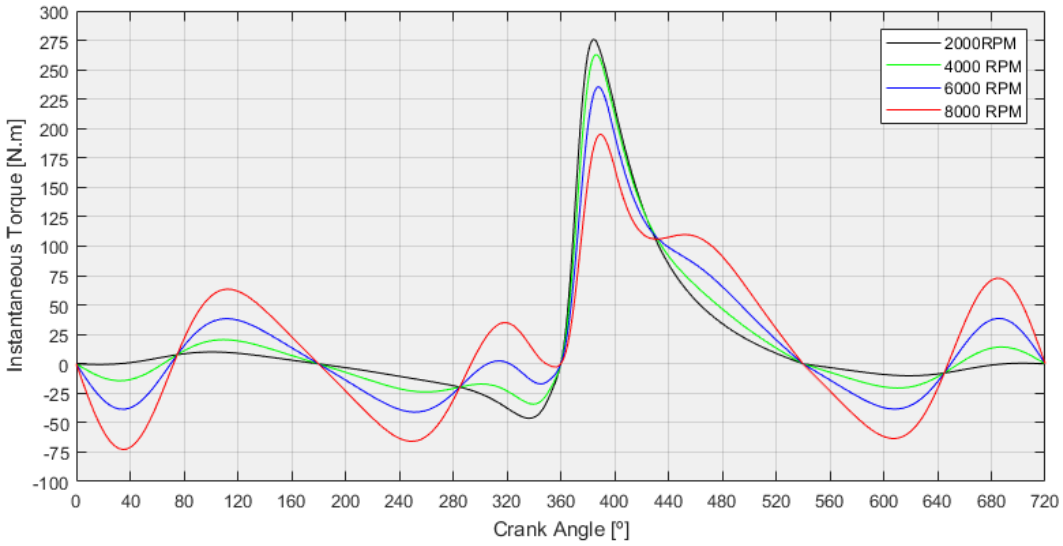

Figure 3.9. Instantaneous torque output for the OPSCE model during the cycle at various operating speeds.

3.4.3 Geared Hypocycloid Engine Dynamics

Similar to the OPSCE, the dynamics of the OPGHE were modelled as described in Chapter 2 and Sub-Chapter 3.4.1.

Figure 3.10 shows that the in-cylinder pressure for the OPGHE has similar characteristics to those of OPSCE. The maximum in-cylinder pressure is 9.604 MPa at 450 rpm. For reference, the maximum in-cylinder pressure at 2000 rpm is 9.196 MPa and 7.263 MPa at 8000 rpm.

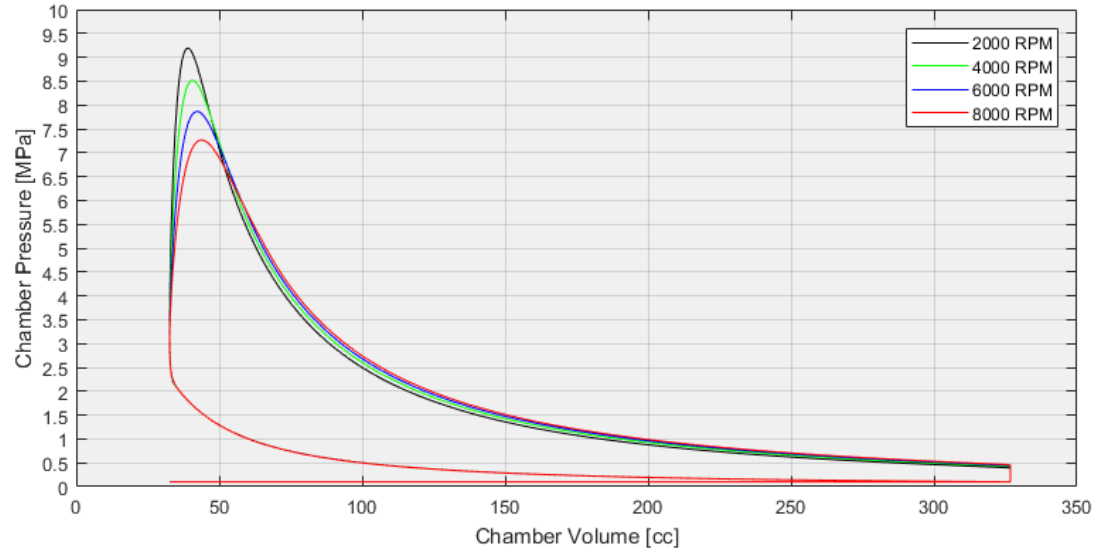

Figure 3.10. Pressure-volume diagram (p-V) for the OPGHE model at various operating speeds.

It can be seen in figure 3.11 that the forces applied to the piston of a OPGHE also have similar characteristics to those of OPSCE. The maximum force applied to the piston is 27140 N at 440 rpm. For reference, the maximum force applied to the piston at 2000 rpm is 25730 N and 16337 N at 8000 rpm.

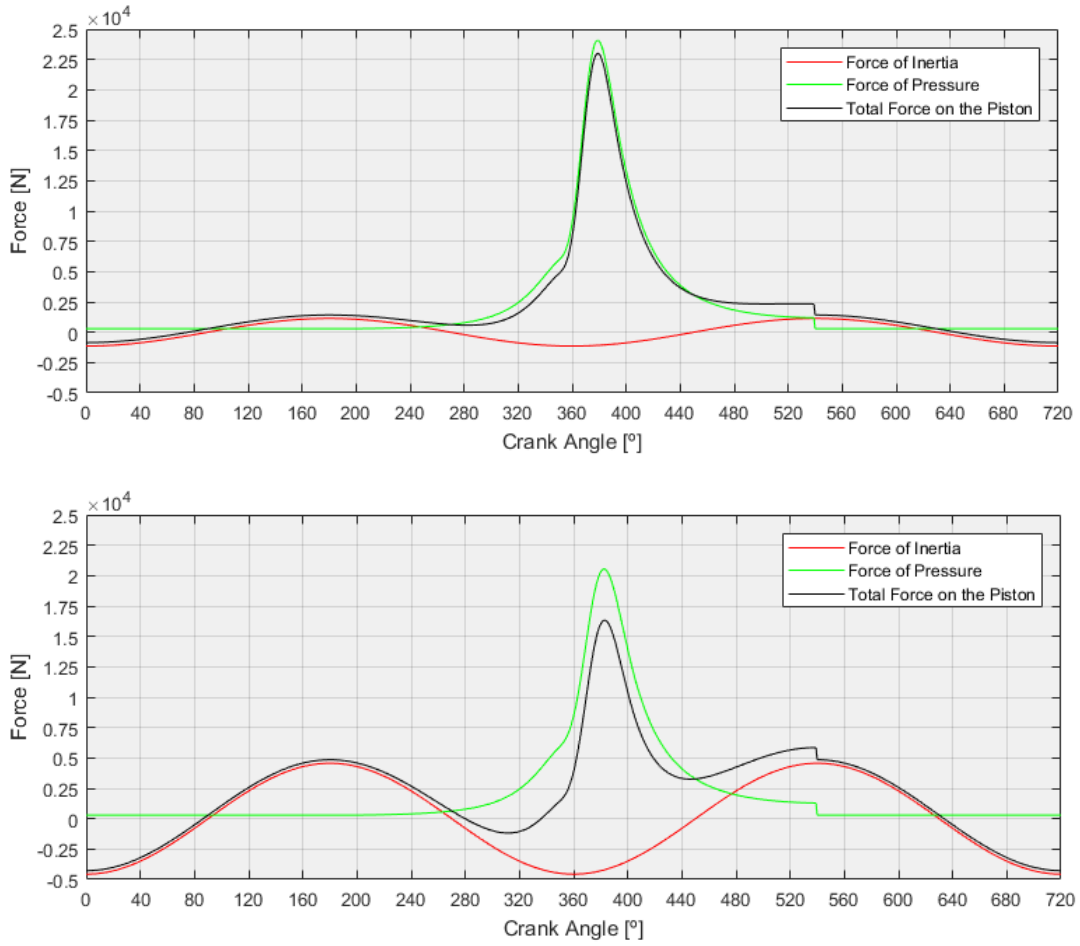

Figure 3.11. Forces applied to the piston for the OPGHE model during the cycle at 4000 rpm (top) and 8000 rpm (bottom).

It is observed in figure 3.12 that, as for the OPSCE, the maximum instantaneous torque output increases with increasing operating speed up to a certain value and then starts decreasing. The maximum torque output is 243.6 N.m at 2560 rpm with an average torque output of 36.2 N.m.

For reference, the maximum instantaneous torque output at 2000 rpm is 243.5 N.m with an average of 35.9 N.m; and 193.2 N.m with an average of 37.0 N.m at 8000 rpm. It should be noted that the maximum average torque output is 37.1 N.m at 6700 rpm, with a maximum instantaneous torque output of 212.0 N.m.

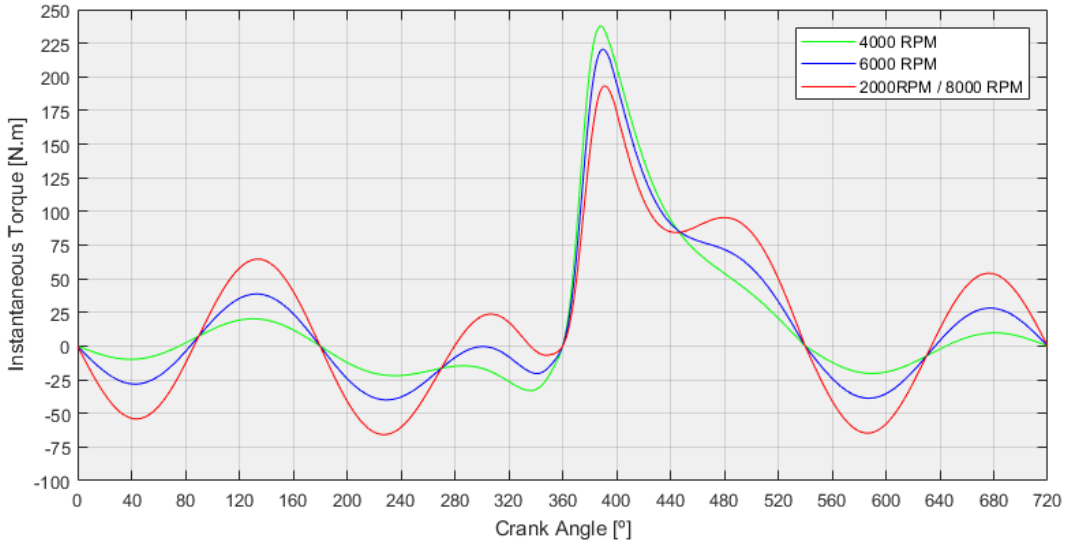

Figure 3.12. Instantaneous torque output for the OPGHE model during the cycle at various operating speeds.

Finally, the tangential gear tooth load was modelled with figure 3.13 showing that it tends to decrease with increasing operating speed. The maximum tangential gear tooth load is 9368.4 N at 2360 rpm. For reference, the maximum tangential gear tooth load at 2000 rpm is 9365.2 N and 7432.2 N at 8000 rpm.

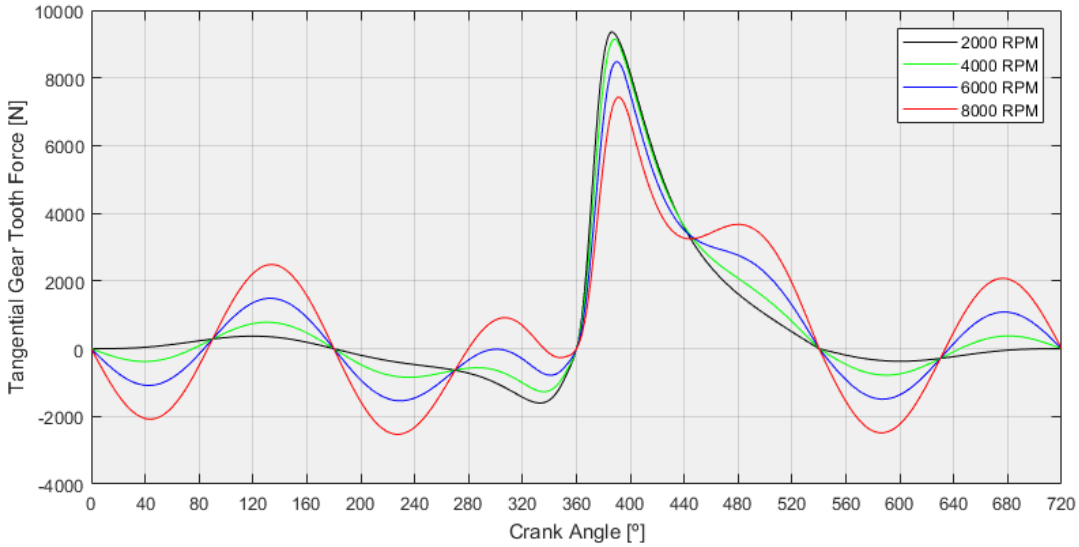

Figure 3.13. Tangential gear tooth load for the OPGHE model during the cycle at various operating speeds.

Chapter 4

Engine Design

In this chapter, some parts of the engine were designed for the OPGHE considered in this study with reference to Chapter 2 and the performance results obtained in the previous chapter. Because engine design is mostly derivative and evolutionary and little to no information is available for this type of engines, the design of the parts was mostly done with empirical correlations and manufacturers design manuals.

4.1 Materials Properties

Before starting the design of the engine parts, some materials must be considered and selected. The materials selected were three: a nitrided steel alloy known as Nitralloy N typically used for gears in high-demanding applications, an ultrahigh-strength (UHS) corrosion resistant steel alloy designated in the industry by Ferrium S53® and three aluminium alloys described as 242.0, 319.0 and A390.0 according to their casting composition.

4.1.1 Nitralloy N (AMS 6475)

Nitralloy steels contain 1% of aluminium in thesis composition which makes for very significant hardening. Nitriding is a heat treatment that hardens the surface of the gear teeth by introducing nitrogen into the surface of steel at a temperature between 500ºC and 550ºC while it is in the ferritic condition. The fact that nitriding doesn't involve heating into the austenite phase field and a subsequent quench so that martensite forms, this heat treatment can be done with minimal distortion and excellent dimensional control. Nitriding steels can be used in several gear applications where hard, wear-resistant case, good fatigue strength, low notch sensitivity and some degree of corrosion resistance are required. [Davis, 2005]

When gear teeth are heat treated with a nitriding process, a wear- and fatigue-resistant surface is produced. These gears are frequently used in applications where either are not subjected to high shock loads or the contact stress is below 1340 MPa and 1190 MPa for AGMA grade 3 and grade 2 materials, respectively. In applications where gears may operate at elevated temperatures, nitriding becomes particularly useful to maintain their surface hardness. Gears used in industrial, automotive and aerospace applications are commonly nitrided. [Davis, 2005]

A grade 2 Nitralloy N was therefore selected due to its mechanical properties and because little information regarding materials for gears operating in high-demanding applications is available. Therefore, in reference to AGMA 2101-C95, the allowable bending stress and allowable contact stress were considered. The Brinell hardness (HB) at core before nitriding is 277 and 415 after

nitriding. After nitriding, the minimum surface hardness in the Rockwell 15-N scale (HR15N) is 92.5, which is equivalent to 765 in the Brinell hardness scale. [Davis, 2005] The modulus of elasticity and Poisson's ratio were not available and were assumed to be those of low-alloy steels at 200 GPa and 0.3, respectively. [*ASM Handbook Vol. 1*, 1993]

From AGMA 2101-C95, the allowable contact stress for grade 2 Nitralloy N is 1300 MPa. It should be noted that this value is above the maximum value of 1190 MPa given by Davis for AGMA grade 2 nitrided materials. The allowable bending stress was taken from the empirical correlation for grade 2 Nitralloy: [AGMA 2101-C95]

$$\sigma_{FP} = 0.7255HB + 153.63 \tag{4.1}$$

Therefore, the allowable bending stress is 454.713 MPa.

Finally, the properties of Nitralloy N are presented in table 4.1.

Table 4.1. Mechanical properties of Nitralloy N.

Ultimate Tensile Strength	1310 MPa
Ultimate Yield Strength	1240 MPa
Allowable Bending Stress	454.713 MPa
Allowable Contact Stress	1300 MPa
Modulus of Elasticity	200 GPa
Poisson's Ratio	0.3
Density	6.675 g/cm^3

4.1.2 Ferrium S53® (AMS 5922)

The standard to which other ultrahigh-strength (UHS) steels are compared is the AISI/SAE 4340 steel. This steel is commonly used, among other applications, in crankshafts and piston rods for engines as well as landing gear and other critical structural members for aircraft. [*ASM Handbook Vol. 1*, 1993]

New UHS steels for critical structural applications need to combine high toughness and corrosion resistance without sacrificing strength. However, apart from stainless steels, all steels require a coating to be protected from corrosion damage, which is typically achieved by cadmium plating. To address these challenging requirements, a family of computationally designed UHS steels, designated Ferrium series, has recently been commercialized and inserted in service. [Sankaran & Mishra, 2017]

The first example of a such alloy is the Ferrium C61 (AMS 6517) high durability gear steel now being successfully used in off-road racing applications. However, the first alloy of this kind to reach flight qualification is the Ferrium S53 (AMS 5922) corrosion resistant landing gear steel allowing a drop-in replacement for current non-stainless landing gear steels, eliminating the need for cadmium plating. The alloy Ferrium S53 was designed to replace the 300M, 4340 and AerMet 100 alloys on an equivalent mechanical properties basis while providing the corrosion resistance required in aircraft components applications, without cadmium plating. The first flight of a Ferrium S53 landing gear occurred on December 17, 2010. [Arnold & Wong, 2010]

The properties of the Ferrium S53 alloy are given in table 4.2.

Table 4.2. Mechanical properties of Ferrium S53.

Ultimate Tensile Strength	1985 MPa
Ultimate Yield Strength	1565 MPa
Ultimate Shear Strength	1250 MPa
Density	7.98 g/cm^3

4.1.3 242.0, 319.0 and A390.0 Aluminium Alloys

Aluminium is one of the most abundant elements on earth. Its unique combination of properties makes aluminium and its alloys the most attractive metal regarding appearance, light weight, fabricability, physical properties, mechanical properties and corrosion resistance. [*ASM Handbook Vol. 2*, 1992]. In fact, aluminium alloys are second only to steels in use as structural metals. [Davis, 2001]

Aluminium has a density of only 2.7 g/cm3, about one-third that of steel. When appropriately alloyed and treated, aluminium can present excellent corrosion resistance in most environments, including atmosphere, water (including salt water), petrochemicals, and many chemical systems. Its alloys usually have a thermal conductivity of about 50 to 60% that of copper which presents as an advantage in applications such as automotive cylinder heads and radiators. [*ASM Handbook Vol. 2*, 1992]

Aluminium and its alloys may be cast or formed by virtually all known processes. Aluminium alloy castings are routinely produced by pressure-die, permanent-mould, green- and dry-sand, investment, and plaster casting. [*ASM Handbook Vol. 2*, 1992]

It is convenient to divide aluminium into two major categories: casting compositions and wrought compositions. The Aluminum Association system is the most widely recognized in the United States for identifying aluminium alloys, with cast and wrought alloy nomenclatures

having been developed. A four-digit system is used to identify wrought alloys according to their composition families. Casting compositions, on the other hand, are described by a three-digit system followed by a decimal value with the decimal .0 in all cases pertaining to casting alloy limits. Alloy families for casting compositions are the following: [Davis, 2001]

- 1xx.x Controlled unalloyed (pure) compositions, especially for rotor manufacture.
- 2xx.x Alloys in which copper is the principal alloying element, but other alloying elements may be specified.
- 3xx.x Alloys in which silicon is the principal alloying element, but other alloying elements such as copper and magnesium are specified. This series comprises nearly 90% of all shaped castings produced.
- 4xx.x Alloys in which silicon is the principal alloying element.
- 5xx.x Alloys in which magnesium is the principal alloying element.
- 6xx.x Unused.
- 7xx.x Alloys in which zinc is the principal alloying element, but other alloying elements such as copper and magnesium may be specified.
- 8xx.x Alloys in which tin is the principal alloying element.
- 9xx.x Unused.

Each digit conveys information about the alloy. The first digit indicates the alloy group which is determined by the alloying element present in the greatest mean percentage; the second and third digits identify the specific aluminium alloy or, for the aluminium 1xx.x series, its purity; and the fourth digit indicates the product form: xxx.0 indicates castings and xxx.1, for the most part, indicates ingot having limits for alloying elements the same as or very similar to those for the alloy in the form of castings. A letter before the numerical designation indicates a modification of the original alloy or an impurity limit. [Davis, 2001]

To develop and improve the properties of many alloys, thermal treatments based on phase solubilities to which such alloys respond to are used. These treatments include solution heat treatment, quenching and precipitation or age hardening. For either wrought or casting alloys, such alloys are described as heat treatable. Some casting alloys are essentially not heat treatable and are only used in as-cast or in thermally modified conditions unrelated to solution or precipitation effects. [*ASM Handbook Vol. 2*, 1992] Heat treatable casting alloys include the 2xx.x, 3xx.x and 7xx series. [Davis, 2001]

Therefore, a further designation system based on temper is used in the United States for aluminium and its alloys for all product forms, both wrought and cast, apart from ingot. The system designation considers the sequences of mechanical and/or thermal treatments used to produce the various temper. [*ASM Handbook Vol. 2*, 1992] The temper designation is always presented next to the alloy designation with a hyphen between the designation and the temper.

The first character is a capital letter which indicates the general class of heat treatment while the digits that follow indicate the specific combination of basic operations. [Kaufman, 2000]

The different designations for the general class of heat treatment are F (as treated), O (annealed), H (strain hardened), W (solution heat treated) and T (thermally treated to produce stable tempers other than F, O or H) with the last being the only heat treatment considered relevant for this study. For cast alloys, there are four commercially used subdivisions of the basic T temper which are the following: [Kaufman, 2000]

- T4, solution heat treated and naturally aged to a substantially stable condition.
- T5, cooled from an elevated temperature shaping process, then artificially aged.
- T6, solution treated, then artificially aged.
- T7, solution heat treated and overaged/stabilized.

Additional digits are sometimes used with these T5, T6 and T7 temper designations although to indicate a variation in treatment that significantly alters the product characteristics that are or would be obtained using the basic treatment. Among these, the relevant designation considered is T571 which means that the casting has been cooled from the casting process and then artificially aged (i.e., in a furnace), as per the basic temper T5. However, a special chill was added as the casting cooled to ensure higher strengths. Unfortunately, because many of these tempers have been used for many years and have not gone through a rigorous rationalization process, there is no clear resource to document the exact nature and degree of consistency of these variations. [Kaufman, 2000]

Aluminium and its alloys are widely used due to their high strength-to-density ratio, corrosion resistance and weight efficiency in practically all segments of the aircraft, missile and spacecraft industry. *[ASM Handbook Vol. 2*, 1992]

Alloys 242 and A242 are extensively used for applications that require strength and hardness at high temperatures. Applications of such alloys include, among others, heavy-duty pistons, motorcycle, diesel and aircraft pistons or air-cooled cylinder heads. [*ASM Handbook Vol. 2*, 1992 & *Casting Source Directory 2017*]

The properties of sand-cast 242.0-T571 aluminium alloy are presented in table 4.3. [*ASM Handbook Vol. 2*, 1992]

Table 4.3. Mechanical properties of sand-cast 242.0-T571 aluminium alloy.

Ultimate Tensile Strength	220 MPa
Ultimate Tensile Strength (at 260 ºC)	90 MPa
Ultimate Yield Strength	207 MPa
Fatigue Strength	75 MPa (at $5x10^8$ cycles; R. R. Moore type test)
Thermal Conductivity	134 W/(m.K)
Modulus of Elasticity	71 GPa (Tension) 26.5 GPa (Shear)
Poisson's Ratio	0.33
Density	2.823 g/cm^3

Alloys 319 and A319 present good castability, weldability, pressure tightness, moderate strength and are stable alloys which means that variations in their impurity content don't affect their casting and mechanical properties. Applications for sand casting of these alloys include internal combustion engine crankcases and gasoline and oil tanks. [*ASM Handbook Vol. 2*, 1992 & *Casting Source Directory 2017*)

The properties of sand-cast 319.0-T6 aluminium alloy are presented in table 4.4. [*ASM Handbook Vol. 2*, 1992]

Table 4.4. Mechanical properties of sand-cast 319.0-T6 aluminium alloy.

Ultimate Tensile Strength	250 MPa
Ultimate Yield Strength	165 MPa
Fatigue Strength	75 MPa (at $5x10^8$ cycles; R. R. Moore type test)
Thermal Conductivity	109 W/(m.K)
Modulus of Elasticity	74 GPa (Tension) 28 GPa (Shear)
Poisson's Ratio	0.33
Density	2.79 g/cm^3

The use of aluminium in place of cast iron in engine components became highly desirable to reduce fuel consumption which can be directly related to vehicle weight. Thus, in the late 1950s, cylinder blocks were manufactured from die cast aluminium-silicon alloys for the automotive industry to take advantage of the light weight and good thermal conductivity offered by hypoeutectic alloys. However, these alloys only had moderate wear resistance which required cast-in steel cylinder liners to be used in early engine blocks. However, the use of die cast aluminium engine blocks with a cast iron cylinder liner proved to be too costly in production which promoted the development of hypereutectic aluminium-silicon alloys with greater wear resistance that could be used without liners. [*ASM Casting Design and Performance*, 2009]

One such alloy developed specifically for its high wear resistance is the hypereutectic aluminium-silicon A390 (A390.0) which has been used in engine blocks without a liner. An electrochemical surface treatment is used to etch away some of the matrix aluminium, exposing the eutectic and primary silicon particles that provide the bearing surface and resulting in improved resistance. Another application for such alloy that has been explored is the manufacture of cylinder liners to be inserted into the engine block produced from conventional aluminium-base alloys. (ASM Casting Design and Performance)

The hypereutectic alloys are likely to dominate because of their wear resistance, high hardness, low coefficient of thermal expansion and fluidity properties, which allow the manufacture of thinner wall castings. Applications typical for the A390.0 alloy are internal combustion engine pistons and blocks, four cycle air-cooled engines, and cylinder bodies for compressors, pumps and brakes. [*ASM Handbook VOL 2*, 1992, *ASM Casting Design and Performance,* 2009 & *Casting Source Directory 2017*)

The properties of sand-cast A390.0-T6 aluminium alloy are presented in table 4.5. [*ASM Handbook Vol. 2*, 1992]

Table 4.5. Mechanical properties of sand-cast A390.0-T6 aluminium alloy.

Ultimate Tensile Strength	275 MPa
Ultimate Yield Strength	275 MPa
Fatigue Strength	105 MPa (at $5x10^8$ cycles; R. R. Moore type test)
Thermal Conductivity	134 W/(m.K)
Modulus of Elasticity	81.2 GPa (Tension) 82.8 GPa(Compression)
Density	2.73 g/cm^3

4.2 Piston and Rod Design

The piston can be seen as a disk reciprocating within the cylinder that transmits the energy from the expanding gas within the cylinder due to combustion to the crankshaft through the connecting rod. The piston rings ensure a tight seal between the piston and cylinder and can be of two types: compression rings and oil control rings. The first type makes a tight seal with the cylinder to keep the pressure within and also transfer heat from the piston to the cylinder liner while the second provide proper lubrication to the liner by allowing some oil to flow with the piston motion. [Gupta & Khurmi, 2005]

It should be noted that no piston skirt was considered since there's no side thrust. In reference to figure 4.1, the thickness of piston head (t_H), diameter of piston rod (d_r), radial (t_1) and axial (t_2) thickness of piston rings, piston groove depth (b_{groove}), width of top land (b_1), width of other lands (b_2), maximum (t_3) and minimum (t_4) piston barrel thickness, height of the piston head (L_{piston}) and height of piston rod (L_{rod}) were calculated.

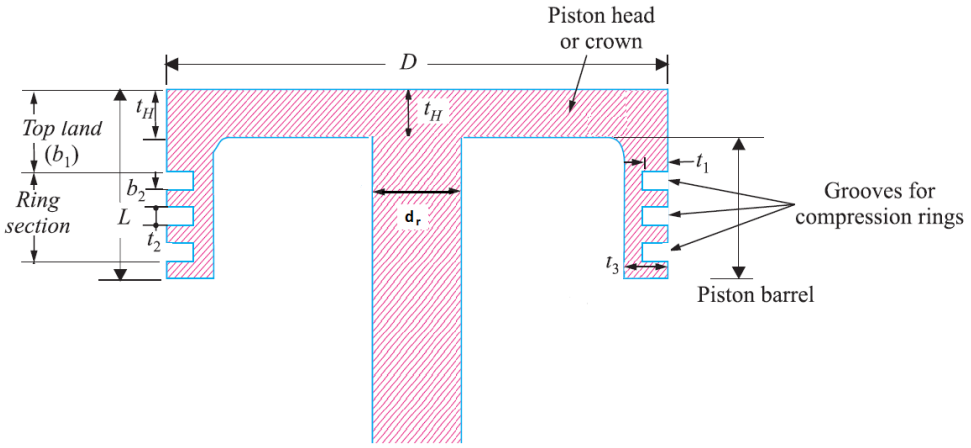

Figure 4.1. Piston and rod geometry. (Adapted from Khurmi and Gupta)

The material chosen for the piston was the 242.0 aluminium alloy. The thickness of the piston head (t_H) is calculated taking into consideration that it should have adequate strength to withstand the forces applied to it due to the in-cylinder pressure and that it should dissipate the heat from the combustion. Therefore, it can be calculated for the first case, according to Grashoff's formula, by: [Gupta & Khurmi, 2005]

$$t_H = \sqrt{\frac{3pB^2}{16\,\sigma_t}} \tag{4.2}$$

Where σt is the permissible bending (tensile) strength for the material of the piston. According to the literature, the temperature on the piston head can be assumed to be 260 ºC to 290 ºC at the centre and 185 ºC to 215 ºC at the edges [Gupta & Khurmi, 2005]. Considering a tensile strength of 90 MPa at 260 ºC for the 242.0-T571 aluminium alloy and a safety factor of 1.5, the permissible bending stress is assumed to be 60 MPa. According to the literature, it may be taken as 50 to 90 MPa [Gupta & Khurmi, 2005], with the value obtained falling within the range. Thus, the maximum thickness of the piston head due to the in-cylinder pressure calculated from Eq. 4.2 is 10.39 mm.

Taking into consideration the heat transfer, the thickness of the piston head can be calculated by: [Gupta & Khurmi, 2005]

$$t_H = \frac{H}{12.56k\ (T_C - T_E)} \tag{4.3}$$

Where H is the heat flowing through the piston head, k is the thermal conductivity coefficient for the material and T_C and T_E is the piston temperature at the centre and edge of the piston head, respectively. The difference between T_C and T_E can be assumed to be 75 ºC for aluminium. [Gupta & Khurmi, 2005]

The heat flowing through the piston head can be calculated by:

$$H = C_{heat}.QHV.\dot{m}_{fuel} \tag{4.4}$$

Where C_{heat} represents the portion of heat released during combustion that flows through the piston head and is assumed to be equal to 0.05. [Gupta & Khurmi, 2005]

The maximum thickness of the piston head due to heat transfer calculated from Eq. 4.3 is 13.74 mm.

Therefore, the thickness of the piston head was taken as 13.75 mm.

The diameter of the piston rod (d_r) can be calculated by: [Gupta & Khurmi, 2005]

$$d_r = \sqrt{\frac{4F_t}{\pi\ \sigma_f}} \tag{4.5}$$

Where F_t is the maximum force applied to the piston and σ_f is the allowable tensile strength for the material considered. The material considered for the piston rod is the 242.0 aluminium alloy with the piston head and rod being designed as a single piece. Because the piston rod suffers cyclic loads, the allowable tensile strength was assumed to be equal to the fatigue

strength with a safety factor of 1.5. Therefore, the allowable tensile strength is taken as 60 MPa. The piston rod diameter calculated from Eq. 4.5 is then 26.29 mm. For this study, the diameter of the piston rod was taken as 26.5 mm.

The radial thickness of the ring (t_1) can be calculated by: [Gupta & Khurmi, 2005]

$$t_1 = B\sqrt{\frac{3p_w}{\sigma_t}} \tag{4.6}$$

Where p_w is the pressure of gas on the cylinder wall, ranging from 0.025 MPa to 0.042 MPa, and σ_t is the allowable bending (tensile) stress, which ranges from 85 MPa to 110 MPa for cast iron rings. [Gupta & Khurmi, 2005] Therefore, the radial thickness of the ring ranges from 1.57 mm to 2.31 mm, and was taken as 2 mm.

The axial thickness of the piston ring (t_2) can be obtained empirically from: [Gupta & Khurmi, 2005]

$$t_2 = \frac{B}{10n_{rings}} \tag{4.7}$$

Where n_{rings} is the number of rings, which was taken as 3. Therefore, the axial thickness of the piston ring is 2 mm.

The groove depth (b_{groove}) is given empirically by: [Gupta & Khurmi, 2005]

$$b_{groove} = t_1 + 0.4 \tag{4.8}$$

Thus, the groove depth is equal to 2.4 mm, which was the value considered in this study.

The width of the top land (b_1) is considered empirically to range from t_H to 1.2 t_H [Gupta & Khurmi, 2005], i.e., between 13.75 mm and 16.5 mm. For this study, it was taken as 13.75 mm. The width of the other lands (b_2) is considered empirically to range from $0.75t_2$ to [Gupta & Khurmi, 2005], i.e., between 1.5 mm and 2 mm. For this study, it was taken as 1.5 mm.

The maximum thickness of the piston barrel (t_3) can be calculated by: [Gupta & Khurmi, 2005]

$$t_3 = 0.03B + t_1 + 4.9 \tag{4.9}$$

From Eq. 4.9, the maximum thickness of the piston barrel is 8.7 mm, being the value considered for this study. Because there is no piston skirt, the minimum thickness of the piston barrel was taken as constant.

The height of the piston head (L_{piston}) is then given by:

$$L_{piston} = b_1 + n_{rings}t_2 + n_{rings}b_2 \tag{4.10}$$

From Eq. 4.10, the height of the piston head is 24.3 mm.

Knowing the volume of the piston (V_{piston}) is 104.379 cm^3, the mass of the piston was calculated by:

$$m_{piston} = V_{piston} * \rho \tag{4.11}$$

From Eq. 4.11, the mass of the piston is equal to 294.7 g, which is close to the mass considered in the model.

The piston rod cap was calculated according to the bearings selected later in this chapter. Knowing the distance between the axis of rotation of the crankshaft and the plane of symmetry of the engine is 145 mm, the length of the piston rod (L_{rod}) was calculated as follows:

$$L_{rod} = 145 - \frac{S}{4} - \frac{d_{TDC}}{2} - t_H - \frac{ID_{cap}}{2} \tag{4.12}$$

Where d_{TDC} is the distance between both piston heads at TDC which is calculated in the next sub-chapter, and ID_{cap} is the internal diameter of the piston rod cap that is equal to the outer diameter of the bearings considered (32 mm). The result is 88.6 mm.

The dimensions of the piston and rod considered for this study are presented in table 4.6 and two CAD views of the final assembly are presented in figure 4.2.

Table 4.6. Dimensions of the piston and rod.

Thickness of Piston Head	13.8 mm
Diameter of Piston Rod	26.5 mm
Radial Thickness of Piston Ring	2 mm
Axial Thickness of Piston Ring	2 mm
Groove Depth of Piston Ring	2.4 mm
Width of Top Land	13.8 mm
Width of Other Lands	1.5 mm
Maximum Thickness of Piston Barrel	8.7 mm
Minimum Thickness of Piston Barrel	8.7 mm
Height of Piston Head	24.3 mm
Mass of Piston	294.7 g

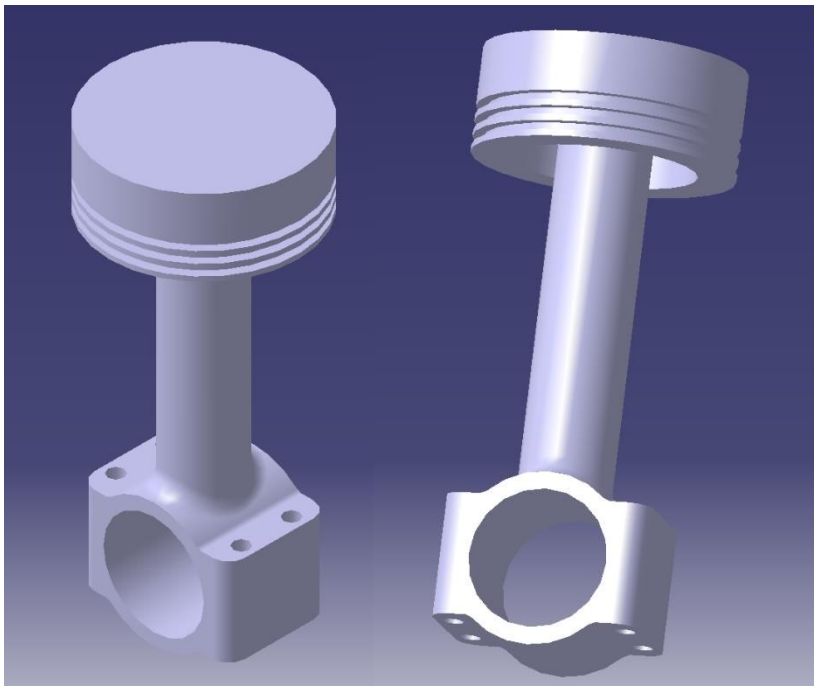

Figure 4.2. Two views of the piston design.

4.3 Cylinder Design

The cylinder of an engine retains the working fluid and guides the piston. Due to the high temperature from the fuel burn, it has to be cooled with single cylinder engines being usually air-cooled. It is beyond the scope of this study to account for the cooling. [Gupta & Khurmi, 2005]

For the cylinder design, some parameters were calculated such as cylinder wall thickness, minimum number of studs and its diameter, and thickness of the cylinder flange. The cylinder was considered as a single piece to avoid using a gasket and increase its strength. The material chosen for the cylinder was the A390.0 aluminium alloy.

Firstly, the permissible hoop stress (σ_c), which is the maximum allowable stress for the cylinder material exerted due to internal pressure, must be considered. Because values for the permissible hoop stress are not available for the material chosen, the fatigue strength and a safety factor were considered to take as the permissible hoop stress. Therefore, for a safety factor of 2 and a fatigue strength of 105 MPa, the permissible hoop stress is taken as 52.5 MPa. The permissible hoop stresses are considered to range from 35 MPa to 100 MPa, depending on the material. [Gupta & Khurmi, 2005] Therefore, this value falls within the range.

The thickness of the cylinder wall (t_{cw}) can be calculated by: [Gupta & Khurmi, 2005]

$$t_{cw} = \frac{p\,B}{2\,\sigma_c} + C_{reboring} \tag{4.13}$$

Where $C_{reboring}$ is the allowance for reboring.

The cylinder was designed without a liner. However, to prolong the life of the engine, the possibility of installing a dry liner was considered. The thickness of a dry liner (t_{liner}) was then assumed to be the allowance for reboring and calculated empirically by: [Gupta & Khurmi, 2005]

$$t_{liner} = 0.03B \; to \; 0.035B \tag{4.14}$$

For a bore of 60 mm, the thickness of the dry liner ranged between 1.8 mm and 2.1 mm, and thus it was assumed to be 2 mm.

As seen before, the maximum in-cylinder pressure for the OPGHE is 9.604 MPa at 450 rpm. The thickness of the cylinder wall, from Eq. 4.13, is equal to 7.49 mm. Thus, it was assumed to be 7.5 mm.

The cylinders are cast integral with the upper half of the crankcase or attached to the crankcase with a flange and studs or bolts and should be thicker than the cylinder wall. The thickness of the flange (t_f) can be assumed empirically to be 1.2 to 1.4 times thicker than the cylinder wall [Gupta & Khurmi, 2005], in this case, between 9 mm and 10.5 mm. It was assumed to be 10mm.

The minimum length of the cylinder ($L_{cylinder}$) was calculated accounting for the height of the piston head (L_{piston}) and the distance between each piston head at TDC (d_{TDC}) and BDC (d_{BDC}). The distance between each piston head at TDC and BDC is give, respectively, by:

$$d_{TDC} = \frac{V_C}{A_{piston}} \tag{4.15}$$

$$d_{BDC} = d_{TDC} + S \tag{4.16}$$

From table 3.2, d_{TDC} is 1.2 mm and d_{BDC} is 105.2 mm.

Considering the height of the piston head is equal to 24.3 mm, at BDC, the distance between bottom of the both pistons is then the sum of d_{BDC} and the height of each piston, and thus, is equal to 153.8 mm. Taking a clearance of 15% the stroke of each piston on both sides of the cylinder (Khurmi and Gupta), the minimum length of the cylinder is then given by:

$$L_{cylinder} = d_{BDC} + 2\left(L_{piston} + 0.15\frac{S}{2}\right) = \frac{V_C}{A_{piston}} + 2L_{piston} + 2.3\frac{S}{2} \tag{4.17}$$

Which is then equal to 169.4 mm. For this study, is was taken as 170 mm.

The diameter of the bolts (d_{bolt}) can be calculated by: [Gupta & Khurmi, 2005]

$$d_{bolt} = \sqrt{\frac{B^2\, p}{n_{bolt}\sigma_{bolt}}} \tag{4.18}$$

Where σ_{bolt} is the allowable tensile stress for the material of bolts in MPa which can be taken as 35 MPa to 70 MPa and n_{bolt} is the number of bolts which can be taken as 0.01B+4 to 0.02B+4 [Gupta & Khurmi, 2005], i.e., 4.6 to 5.2. In this study, it taken as 5.

The diameter of the bolts calculated from Eq. 4.18 ranges from 9.94 mm to 14.06 mm. Another empirical correlation assumes the diameter of the bolts to range between $0.75t_f$ and t_f [Gupta & Khurmi, 2005], i.e., 9 and 10.5 mm. Therefore, comparing the results, the diameter of the bolts was taken as 10 mm.

The results are then presented in table 4.7 and two CAD views of the cylinder with and without cooling fins are presented in figure 4.3.

Table 4.7. Dimensions of the cylinder.

Cylinder Wall Thickness	7.5 mm
Cylinder Flange Thickness	10 mm
Cylinder Length	170 mm
Number of Bolts	5
Diameter of Bolts	10 mm
Mass of the Cylinder (with fins)	1902.4 g

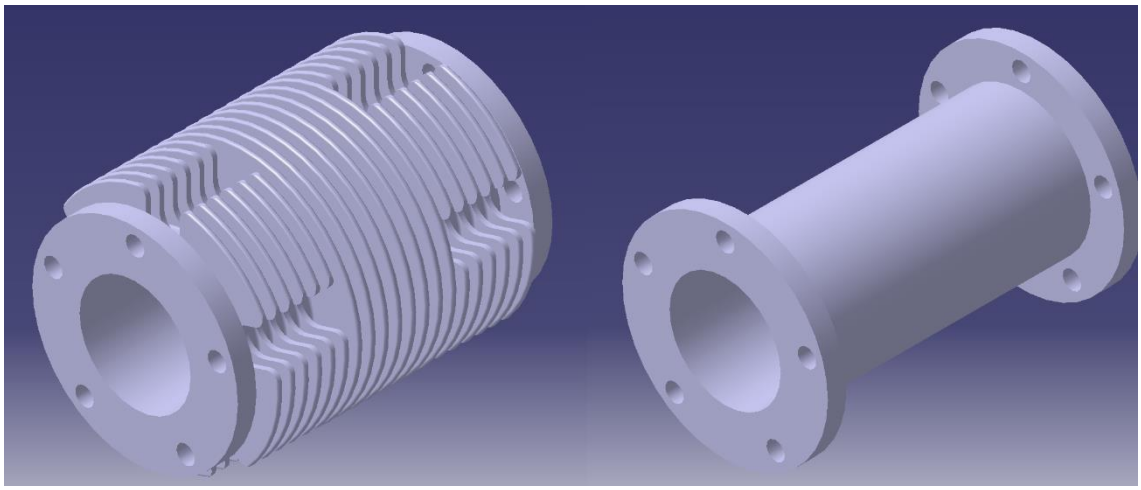

Figure 4.3. Two views of the cylinder design with (left) and without (right) cooling fins.

4.4 Geared Hypocycloid Mechanism Design

4.4.1 Geometric Parameters

Referring to Chapters 2, 3 and 4, the geared hypocycloidal mechanism was designed. To define some initial parameters regarding the gear design, some considerations were made.

Spur gears typically have pressure angles of 14.5º, 20º and 25º. Lower pressure angles have the advantage of smoother and quieter action because of the large profile contact ratio. On the other hand, higher pressure angles have the advantage of better load-carrying capacity as far as both strength and durability are concerned, as well as lower sliding velocities and consequent better scoring and wear performance characteristics. Some cases have used very high pressure angles such as 28º or 30º or, as high as 45º. Most designers usually prefer a 20º pressure angle for spur gears for being considered a good compromise and 25º as an alternative high-strength design. Because the geared hypocycloidal mechanism will be subjected to high loads and noise is not a constraint, a pressure angle of 25º was chosen.

The next step to design the geared hypocycloidal mechanism was to choose the addendum, dedendum, whole depth, backlash and fillet radius. To design gears and calculate the bending and contact stresses it is necessary the pitting resistance and bending strength geometry factors (I and J, respectively). These were obtained from AGMA 908-B89 which describes the geometry factors for determining the pitting resistance and bending strength of spur, helical and herringbone gear teeth. This information sheet also includes tables of I and J values generated for a specific tool form defined by whole depth factor, normal pressure (profile) and tool edge (tip) radius. Therefore, considering that the maximum bending stress occurs at the highest point of single tooth contact (HPSTC), three tables with values of I and J were considered and compared. Common to all were a pressure angle of 25º, a whole depth factor of 2.350, a tool edge radius of 0.270 and a tooth thinning for backlash of 0.024. However, the first applies to gears with no addendum modification, the second to a 0.25 addendum modification and the third to a 0.50 addendum modification, i.e., the first considers the gears with equal addendum, a 25% percent long addendum pinion and 25% short addendum gear for the second, and a 50% long addendum pinion and 50% short addendum gear for the third. The tables are included in Annex. The addendum modification is done to prevent undercut or balance scoring, specific sliding and tooth strength between the gear and the pinion. [Radzevich, 2012]

It should be noted that the aforementioned tables apply to external gears only with an analytical method for determining the Bending Strength Geometry Factor for internal gears not available. In addition, interpolation between the values of these tables is not recommended. [AGMA 908-B89] However, as stated before, internal gears are inherently stronger than equivalent external gears therefore, and in lack of available analytical methods for determining

such geometry factors, the internal gear was considered an external spur gear and interpolation was used to obtain the values for both geometry factors presented in table 4.8.

Gears can be made to any desired module as long as the cutting tools are available for the tooth size chosen. However, some modules are commonly used and recommended as a start for gear design such as 25, 20, 15, 12, 10, 8, 6, 5, 4, 3, 2.5, 2, 1.5, 1, 0.8 and 0.5. [Radzevich, 2012] Thus, considering the stroke of the engine is 52 mm, the pitch diameter of the gear is equal to the stroke of each piston and the pitch diameter of the pinion needs to be half that of the gear to keep the gear ratio of 2:1 and be a hypocycloidal mechanism, and the number of teeth has to be a whole number, module values of 1 and 2 were considered. When the internal gear has at least 10 teeth more than the pinion, there is sufficient clearance between the tips of both the pinion and gear no fouling interference occurs. [AGMA 917-B97] Finally, the problem of undercut almost ceases to exist with 25° teeth [Radzevich, 2012], and are identified in the tables available from AGMA 908-B89.

Therefore, in reference to A.2 to A.4 in annex, the following values of I and J were obtained:

Table 4.8. Geometry factors interpolated from AGMA 908-B89 tables.

Pressure Angle = 25°	Tooth Thinning for Backlash = 0.024
Tool Edge Radius = 0.270	Loaded at Highest Point of Single
Whole Depth Factor = 2.350	Tooth Contact (HPSTC)

Addendum Modification Factor (x)	Number of teeth	Pitting Resistance Geometry Factor (I)		Bending Strength Geometry Factor (J)	
		Pinion	Gear	Pinion	Gear
$x_{pinion} = 0$ $x_{gear} = 0$	Pinion=26 Gear=52	0.1168		0.4385	0.4855
	Pinion=52 Gear=104	0.1190		0.5153	0.5382
$x_{pinion} = 0.25$ $x_{gear} = -0.25$	Pinion=26 Gear=52	0.1233		0.4900	0.4440
	Pinion=52 Gear=104	0.1222		0.5516	0.5043
$x_{pinion} = 0.50$ $x_{gear} = -0.50$	Pinion=26 Gear=52	0.1278		0.5385	0.4010
	Pinion=52 Gear=104	0.1246		0.5770	0.4704

Therefore, some initial common parameters were defined:

Table 4.9. Initial geometric parameters for the pinion and gear.

Parameters	Pinion	Gear
Gear Ratio	2:1	
Pitch Diameter	26 mm	52 mm
Centre Distance	26 mm	
Pressure Angle	25°	
Whole Depth	2.35m mm	
Working Depth	2m mm	
Backlash	0.024m mm	
Fillet Radius	0.270m mm	

4.2.2 Correction Factors for Bending and Contact Stress

The overload factor (K_O) is intended to take into consideration externally applied loads that exceed the nominal tangential load. For an overload of unity, this rating includes the capacity to sustain a limited number of up to 200% momentary overload cycles (typically less than four starts in 8 hours, with a peak not exceeding one second duration). [AGMA 2001-D04] In this study, the design of the gears is done considering a constant maximum tangential load of 9368.4 N at 2360 rpm with the engine rarely operating at such speed, and therefore, a lower tangential load being applied to the gears. Therefore, the overload factor was taken as 1.

When the rim thickness is not sufficient to provide full support for the tooth root, bending fatigue may occur through the gear rim instead of at the tooth fillet and, for such cases, a rim thickness factor (K_B) should be considered. When the rim thickness is 1.2 times greater than the whole depth, it can be taken as 1, [AGMA 2001-D04] which is the case for this study.

The size factor (K_S) accounts for a non-uniformity of material properties and depends mainly on tooth size, diameter of gears, ratio of tooth size to diameter of gear, face width, area of stress pattern, ratio of case depth to tooth size and hardenability and heat treatment of materials. The size factor can be taken as 1 when a proper choice of steel is made for the size of the gear and its heat treatment and hardening process [AGMA 2001-D04], which is the case for this study.

The load distribution factor (K_m) considers a non-uniform distribution of the load along the lines of contact which can be influenced by a manufacturing variation of gears, assembly variations of installed gears, deflections due to applied loads and distortions due to thermal and centrifugal effects. This factor is dependent on two factors - C_{mf} which is the load distribution

factor and C_{mt} which is the transverse load distribution factor; and so is defined as: [AGMA 2001-D04]

$$K_m = f(C_{mf}, C_{mt}) \tag{4.19}$$

For spur gears, where instantaneous contact lines are parallel to the axes, C_{mf} is affected mainly by lead and parallelism and C_{mt} is affected by the transverse contact ratio. Standard procedures to evaluate the influence of C_{mt} have not been established and can assumed to be unity, and so Eq. 4.19 can be modified to: [AGMA 2001-D04]

$$K_m = C_{mf} \tag{4.20}$$

For relatively stiff gear designs, the following approximate method may be used: [AGMA 2001-D04]

$$C_{mf} = 1.0 + C_{mc}(C_{pf}C_{pm} + C_{ma}C_e) \tag{4.21}$$

Where C_{mc} is the lead correction factor, C_{pf} is the pinion proportion factor, C_{pm} is the pinion proportion modifier, C_{ma} is the mesh alignment factor and C_e is the mesh alignment correction factor. It should be noted that this empirical method is recommended for gear designs where the face width-to-pitch diameter ratio isn't more than 2, the gear elements are mounted between bearings (not overhung), the face width doesn't exceed 1020 mm and contact across full face of narrowest member when loaded is considered. [AGMA 2101-C95]

The lead correction factor is 1 for gears with unmodified leads, which is the case considered in this study. The pinion proportion factor is given by: [AGMA 2101-C95]

$$C_{pf} = \frac{FW}{10\ d_{pitch}} - 0.025, \qquad FW \leq 25\ mm \tag{4.22}$$

$$C_{pf} = \frac{FW}{10\ d_{pitch}} - 0.0375 + 0.000492\ FW, \qquad 25mm < FW \leq 432mm \tag{4.23}$$

With the FW in this study to be considered the maximum possible face width of the gear, i.e., 25 mm for FW≤25 mm and 52 mm for both pinion and gear for 25 mm<FW≤52 mm to keep the face width-to-pitch diameter ratio below or equal to 2.

The pinion proportion modifier is assumed to be 1 for the internal gear and 1.1 for the pinion. [AGMA 2101-C95]

Considering an extra precision enclosed gear unit, the mesh alignment factor is defined empirically by: [AGMA 2101-C95]

$$C_{ma} = 0.380x10^{-1} + 0.402\text{x}10^{-3}FW - 1.27\text{x}10^{-7}\,FW^2 \tag{4.24}$$

With the FW in this study to be considered, again, the maximum possible face width of the gear, i.e., 25 mm for FW≤25 mm and 52 mm for both pinion and gear for 25 mm<FW≤52 mm to keep the face width-to-pitch diameter ratio below or equal to 2.

The mesh alignment correction factor is 0.8 when gearing is adjusted at assembly [AGMA 2101-C95], which is the case considered in this study. Finally, the load distribution factor can be calculated.

The dynamic factor (K_V) considers the transmission accuracy level (A_V) which ranges between 12 and 6 with lower values relating to higher accurate gearing, and can be calculated by: [AGMA 2001-D04 & AGMA 2101-C95]

$$K_V = \left(\frac{C_{kv} + \sqrt{200v_t}}{C_{kv}}\right)^B \tag{4.25}$$

Where v_t is the pitch line velocity in m/s. The pitch line velocity, B and C are given by: [AGMA 2001-D04 & AGMA 2101-C95]

$$v_t = \frac{\pi d_{pitch} N}{60} \tag{4.26}$$

$$B_{kv} = 0.25(A_V - 5)^{0.667}, \qquad for\ 6 \le A_V \le 12 \tag{4.27}$$

$$C_{kv} = 50 + 56(1 - B_{kv}) \tag{4.28}$$

With an accuracy level of 6 considered for this study. The maximum pitch line velocity (v_{tmax}) is given by: [AGMA 2001-D04 & AGMA 2101-C95]

$$v_{tmax} = \frac{[C_{kv} + (14 - A_V)]^2}{200} \tag{4.29}$$

The life factor (Y_N and Z_N) is 1 for 10^7 number of load cycles. The temperature factor (K_T) is 1 when gears operate with temperatures not above 120ºC. The reliability factor (K_R) is taken as 1 when fewer than 1 failure occurs in 100 applications. The safety factor (SH and SF) in this study was taken as 1. The surface condition factor (C_f) is 1 provided appropriate surface condition is achieved, which is the case in this study. The hardness ratio factor (C_H) is taken as

1 for both gear and pinion. Finally, the elastic coefficient (Z_E) is given by: [AGMA 2001-D04 & AGMA 2101-C95]

$$Z_E = \sqrt{\frac{1}{\pi\left[\left(\frac{1-\nu_{pinion}{}^2}{E_{pinion}}\right)+\left(\frac{1-\nu_{gear}{}^2}{E_{gear}}\right)\right]}} \tag{4.30}$$

Finally, the correction factors are as presented in table 4.10:

Table 4.10. Correction factors.

	Pinion	Gear
Overload Factor (KO)	1	
Rim Thickness Factor (KB)	1	
Size Factor (KS)	1	
Load Distribution Factor (Km)	1.2537	1.1349
Dynamic Factor (KV)	Min: 1.0044 (10 rpm) Max: 1.1073 (8000 rpm)	Min: 1.0062 (10 rpm) Max: 1.1438 (8000 rpm)
Life Factor (YN=ZN)	1	
Temperature Factor (KT)	1	
Reliability Factor (KR)	1	
Safety Factor (SF=SH)	1	
Surface Condition Factor (C_f)	1	
Hardness Ratio Factor (C_H)	1	
Elastic Coefficient (Z_E)	1.8703×10^5 $(N/mm^2)^{0.5}$	

4.4.3 Face Width for Pinion and Gear from Bending and Contact Stresses

The material chosen for the gears was Nitralloy N. From Eqs. 2.77 and 2.79, and considering the properties of Nitralloy N, the working bending and contact stresses were calculated as 454.713 MPa and 1300 MPa, respectively.

Then, from Eqs. 2.76 and 2.78, the face width for both pinion and gear was calculated across the entire operating range (0 – 8000 rpm) for all combinations of pinion and gear teeth and addendum modification factor. The maximum face width calculated in each combination is presented in table 4.11:

Table 4.11 Face width for a single gearset considering various addendum modification factors and number of teeth.

Addendum Modification Factor (x)	Number of teeth	Face Width due to Bending Stress		Face Width due to Contact Stress	
		Pinion	Gear	Pinion	Gear
$x_{pinion} = 0$ $x_{gear} = 0$	Pinion=26 Gear=52	62.68 mm	52.45 mm	85.18 mm	39.46 mm
	Pinion=52 Gear=104	106.68 mm	94.62 mm	83.61 mm	38.73 mm
$x_{pinion} = 0.25$ $x_{gear} = - 0.25$	Pinion=26 Gear=52	56.09 mm	57.35 mm	80.69 mm	37.38 mm
	Pinion=52 Gear=104	99.66 mm	100.98 mm	81.42 mm	37.71 mm
$x_{pinion} = 0.50$ $x_{gear} = - 0.50$	Pinion=26 Gear=52	51.04 mm	63.50 mm	77.85 mm	36.06 mm
	Pinion=52 Gear=104	95.27 mm	108.26 mm	79.85 mm	36.99 mm

As said before, the face width-to-pitch diameter can't be over 2, i.e., the facewidth of the pinion, and consequently of the gear, can't be over 52 mm. Therefore, it was decided to make a geared hypocycloidal mechanism with two gears as illustrated in figure 4.12, to reduce the gear tooth tangential load in half by considering a twin gearset. Therefore, the face width was calculated for each gearset as presented in table 4.12:

Table 4.12. Face width for a twin gearset considering various addendum modification factors and number of teeth.

Addendum Modification Factor (x)	Number of teeth	Face Width due to Bending Stress		Face Width due to Contact Stress	
		Pinion	Gear	Pinion	Gear
$x_{pinion} = 0$ $x_{gear} = 0$	Pinion=26 Gear=52	31.34 mm	26.22 mm	42.59mm	19.50 mm
	Pinion=52 Gear=104	53.34 mm	47.31 mm	41.80 mm	19.14 mm
$x_{pinion} = 0.25$ $x_{gear} = - 0.25$	Pinion=26 Gear=52	28.05 mm	28.67 mm	40.34 mm	18.47 mm
	Pinion=52 Gear=104	49.83 mm	50.49 mm	40.71 mm	18.64 mm
$x_{pinion} = 0.50$ $x_{gear} = - 0.50$	Pinion=26 Gear=52	25.52 mm	31.75 mm	38.92 mm	17.82 mm
	Pinion=52 Gear=104	47.64 mm	54.13 mm	39.92 mm	18.28 mm

From table 4.12, the twin gearset with the lowest face width (38.92 mm for each gearset) is composed by a pinion with 26 teeth and an addendum modification factor of 0.50 and by a gear with 52 teeth and an addendum modification factor of -0.50. Therefore, this was the selected gearset for the geared hypocycloidal engine with facewidth of the pinion to be taken as 39 mm and the facewidth of the gear to be taken as 40 mm to account for any axial movement of the pinion. The outside diameter of the internal gear was taken as 62 mm, ensuring a rim thickness of more than 1.2 times the whole depth. The pinion has a hole of 15 mm for the crankshaft to go through. It should be noted that in internal gears, the inside circle should not extend below the base circle. [Radzevich, 2012]

Finally, the gearset dimensions were chosen as presented in table 4.13 and figure 4.4 is a CAD view of the internal gear and pinion.

Table 4.13. Dimensions for the geared hypocycloid mechanism.

Parameters	Pinion	Gear
Gear Ratio	2:1	
Pitch Diameter	26 mm	52 mm
Centre Distance	26 mm	
Number of Teeth	26	52
Module	1 mm	
Pressure Angle	25°	
Addendum	1.5 mm	0.5 mm
Dedendum	0.5 mm	1.5 mm
Whole Depth	2.350 mm	
Working Depth	2.000 mm	
Backlash	0.024 mm	
Fillet Radius	0.270 mm	
Face Width	39 mm	40 mm
Mass	95.3 g	230.3 g

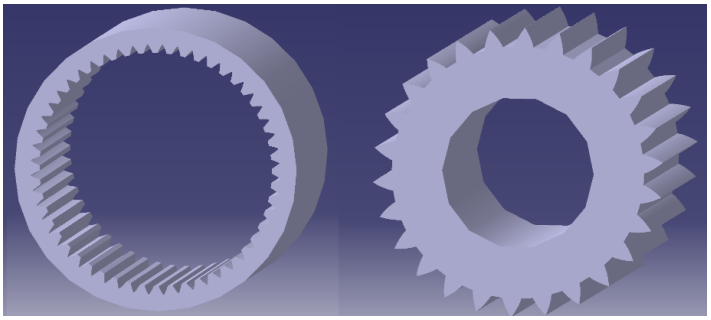

Figure 4.4. View of the internal gear (left) and pinion (right).

4.5 Crankshaft Design

A crankshaft converts the reciprocating motion of the piston into rotary motion. In this study, a single throw centre crankshaft was considered, as represented in figure 5. [Gupta & Khurmi, 2005]

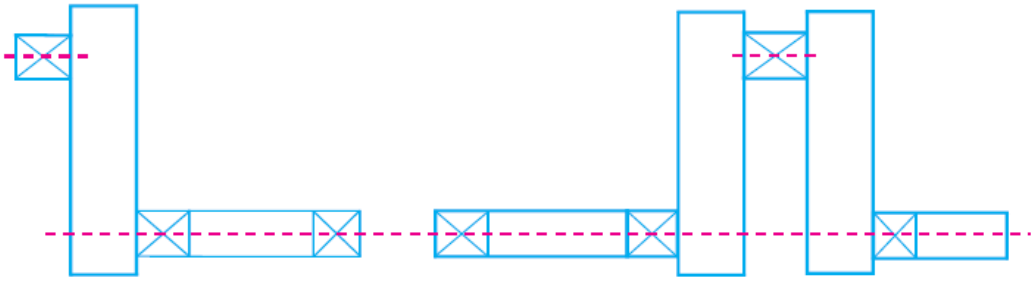

Figure 4.5. Side crankshaft (left) and centre crankshaft (right). [Gupta & Khurmi, 2005]

The material considered for the crankshaft is the Nitralloy N alloy, the same used for the gears.

Considering the bearings selected in the sub-chapter 4.7, the distance between the centre of the bearings ($d_{bearing}$) is taken as 86 mm, and the distance between the centre of the bearing and the force applied at the crankshaft (d_{force}) is taken as 43 mm. The maximum force applied at the centre of the crankpin from the piston rod (F_t) is 27410 N at 440 rpm. The maximum force applied at the main bearing ($F_{bearing}$) is given by: [Gupta & Khurmi, 2005]

$$F_{bearing} = \frac{F_t \, d_{force}}{d_{bearing}} \tag{4.31}$$

From Eq. 4.31, the maximum force applied at the main bearing is 13705 N.

The diameter of the crankpin ($d_{crankpin}$) is given by: [Gupta & Khurmi, 2005]

$$d_{crankpin} = \sqrt[3]{\frac{32 \, F_{bearing} d_{force}}{\pi \sigma_b}} \tag{4.32}$$

Where σ_b is the allowable bending stress for the crankpin, which is equal to 454.713 MPa. Thus, the diameter of the crankpin is equal to 23.63 mm. In this study, the diameter of the crankpin was taken as 25 mm. Due to bearings selected in subchapter 4.7, the length of the crankpin ($l_{crankpin}$) is taken as 34 mm.

The thickness of the crank web ($t_{crankweb}$) can be taken empirically as ranging from 0.22D to 0.32D [Gupta & Khurmi, 2005], i.e., between 13.2 mm and 19.2 mm. For this study, the thickness of the crankweb was taken as 15 mm.

The width of the crankweb ($w_{crankweb}$) is given empirically by: (Khurmi and Gupta)

$$w_{crankweb} = 1.125 d_{crankpin} + 12.7 \tag{4.33}$$

From Eq. 4.33, the width of the crankweb is equal to 40.82 mm. Due to the unique configuration of the geared hypocycloidal engine, the crankweb is circular with a diameter of 65 mm, which is more than the width calculated and should pose no issue.

The total stress on the crank web ($\sigma_{crankweb}$) is given by: [Gupta & Khurmi, 2005]

$$\sigma_{crankweb} = \frac{6F_{bearing}\left(d_{force} - \frac{l_{crankpin}}{2} - \frac{t_{crankweb}}{2}\right)}{w_{crankweb} \cdot {t_{crankweb}}^2} + \frac{F_{bearing}}{w_{crankweb} \cdot t_{crankweb}} \tag{4.34}$$

The total stress on the crank web is then equal to 118.074 MPa, which is less than the allowable bending stress of 454.713 MPa, and therefore, is within the limits.

For this study, the diameter of the shaft was taken as 15mm.

To account for the width of the bearings and the face width of the gears, the length of the shaft is taken as 77 mm.

Therefore, the dimensions of the crankshaft are presented in table 4.14 and a CAD view can be seen in figure 4.6.

Table 4.14. Dimensions of the crankshaft.

Diameter of Crankpin	25 mm
Length of Crankpin	34 mm
Thickness of Crankweb	15 mm
Diameter of Crankweb	65 mm
Diameter of Shaft	15 mm
Length of Shaft	77 mm
Mass	415.9 g

It should be noted that the design of the crankshaft was done considering that the crank shaft is at TDC, which is when is subjected to bending moments only. (Khurmi and Gupta)

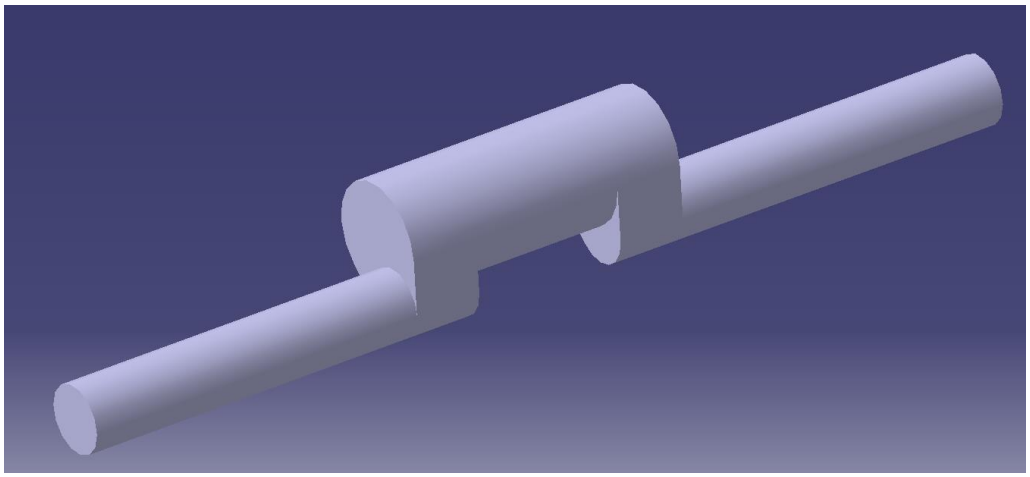

Figure 4.6. View of the crankshaft.

4.6 Output Shaft and Support Shaft Sets Design

The output shaft set in this study converts the rotary motion of the pinion to a rotary motion of a shaft. From now on, unless stated otherwise, both the output shaft set and support set shaft will not be distinguished since they are similar with the only difference being the length of the output shaft, as seen in figure 4.7.

The output shaft set was designed considering the bearings selected and only the diameter of the output shaft was calculated considering the maximum torque output (Tq_{max}), by: [Gupta & Khurmi, 2005]

$$d_{shaft} = \sqrt[3]{\frac{Tq_{max} * 16}{\pi \, \sigma_S}} \tag{4.35}$$

Where σ_S is the allowable shear stress for the material selected. Considering a safety factor of 1.5 and the shear strength of 1250 MPa for the Ferrium S53 alloy, which was the material selected, the diameter of the output shaft equals 7.82 mm. For this study, is was taken as 8 mm.

4.6.1 Balancing

The output shaft set is also designed to balance the entire mechanism. It should be noted that because of the opposed piston configuration, no balance due to the piston motion at the cylinder axis was required because the forces cancel each other. Therefore, only the rotary motion was balanced. Because the centre of mass of both crank pin and crank web are coincident with the cylinder axis, only the rotary motion of the shaft next to the crank web

was considered. It should be noted that the symmetry in reference to the centre of the crankpin was considered. Thus, the mass of each part that contributes to the imbalance of the mechanism and respective distance from their centre of mass to the axis of rotation of the output shaft were calculated and are given in table 4.15.

Table 4.15. Mass and distance of centre of mass considering symmetry in reference to the plane intersecting the centre of the crankpin and cylinder axis.

Part	Mass	Distance of Centre of Mass
Shaft Next to the Crank Web	90.8 g	13 mm
1ST HN 1516	14.0 g	13 mm
2ND HN 1516	14.0 g	13 mm
Pinion	95.3 g	13 mm
Output Shaft Set	729.8 g	-3.81 mm
Support Shaft Set	685.4 g	-4.06 mm

Considering the momentum as the force times the distance, and force as the mass times acceleration, then the following correlation can be considered:

$$M_{balance} = F.b = m.a.b \tag{4.36}$$

Where $M_{balance}$ is the momentum due to the rotary motion of each part. Because all parts have the same acceleration, in this case, angular acceleration, Eq. 4.36 can be simplified to:

$$M_{balance} = m.b \tag{4.37}$$

From Eq. 4.37, and referring to table 4.13, the total momentum of imbalance from all parts except the output shaft set is equal to 2783 g.mm/s^2. To achieve balance, the output shaft set needs to imprint a momentum of approximately -2783 g.mm/s^2. Therefore, the output shaft set was designed iteratively achieving a momentum of -2781 g.mm/s^2 for the values given in table 4.15, which is close to 2783 g.mm/s^2 and was considered adequate.

It should be noted that for this study, although the output shaft set which acts only as support has a shorter output shaft length, its balancing is similar to the output shaft set. In fact, from table 4.15, the momentum calculated is 2783 g.mm/s^2, which correlates with the previous statement.

A CAD view is presented in figure 4.7.

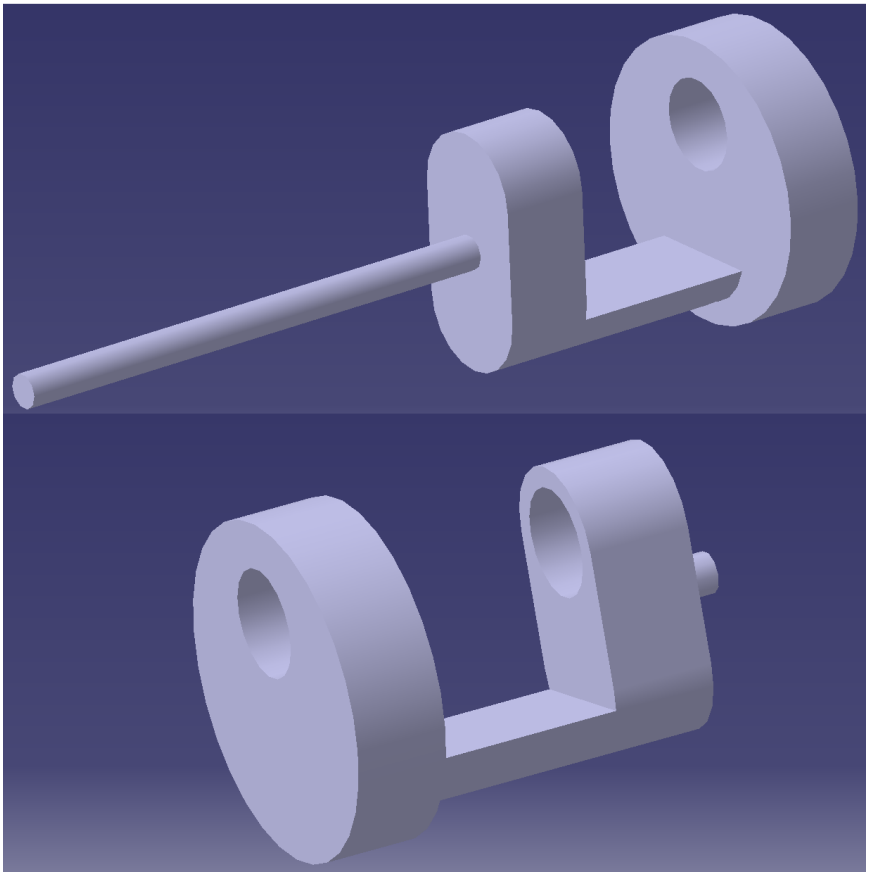

Figure 4.7. View of the output shaft set (top) and support shaft set (bottom).

4.7 Belt Drive Design

To ensure the synchronization of both pistons motion and, therefore, the engine operation, a timing belt is required to transfer the torque output from one shaft to the other. The deciding factors for choosing a belt system as opposed to a geared system were reduction of weight, no need for lubrication and reduced complexity. No study was done regarding the appropriate belt. Nonetheless, in the assembly design, a belt was considered.

4.8 Bearing Selection

A bearing is a machine element that permits a relative motion between the contact surfaces of two machine elements, while carrying the load. There are two main types of bearings depending on the nature of contact: sliding contact bearings and rolling contact bearings, as exemplified in figure 4.8. [Gupta & Khurmi, 2005] In sliding contact bearings, the sliding occurs between the surfaces of contact of both moving and fixed element whereas in rolling contact bearings steel balls or rolls are interposed between the moving and fixed elements. The advantages of rolling bearings over sliding contact bearings are low starting and running friction

except at very high speeds, ability to withstand momentary shock loads, accuracy of shaft alignment, low cost of maintenance due to lack of lubrication required, small overall dimensions, reliability of service, easy to mount and erect and cleanliness. However, the disadvantages are more noise at very high speeds, low resistance to shock loading, more initial cost and complicated design of bearing housing. (Khurmi and Gupta) For this study, all bearings were taken as rolling bearings.

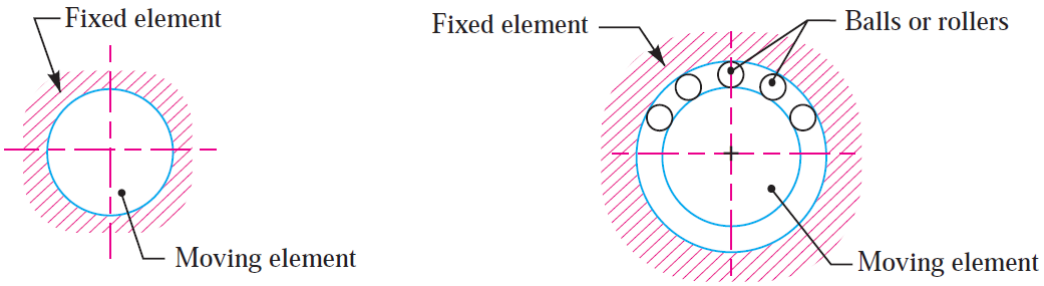

Figure 4.8. Sliding (left) and rolling (left) contact bearings. (Khurmi and Gupta)

For the relative motion between the piston rod and crankpin, a set of two drawn cup needle roller HK 2516 bearings from SKF was selected. Considering the maximum load transmitted is 27140 N at 440 rpm, and each bearing has a dynamic and static load rating of 15.1 kN and 24 kN, the set has a dynamic load rating of 30.2 kN which is more than the maximum load transmitted.

For the relative motion between each output/support shaft set and crankcase, two deep groove ball bearings, the 6013 M and 628-2RS1 models from SKF, were selected (see figure 4.9). Considering a force applied to the 6013 M bearing of half that of the maximum load transmitted of 27140 N, the bearing load is taken as 13570 N. Also, the bore of the bearing was required to be above the stroke of the engine (52 mm) and the outer diameter to be enough for the piston rod to have clearance inside the crankcase. The 628-2RS1 was selected based on the diameter of the output shaft (8 mm) and chosen for sealing the steel balls, and conversely, the inside of the crankcase.

For the relative motion between the output shaft set and the crankshaft, a set of two drawn cup needle HN 1516 bearings from SKF was selected. These were selected based purely on the shaft diameter of 15 mm and assuming a maximum load of no more than the load applied to the 6013 M.

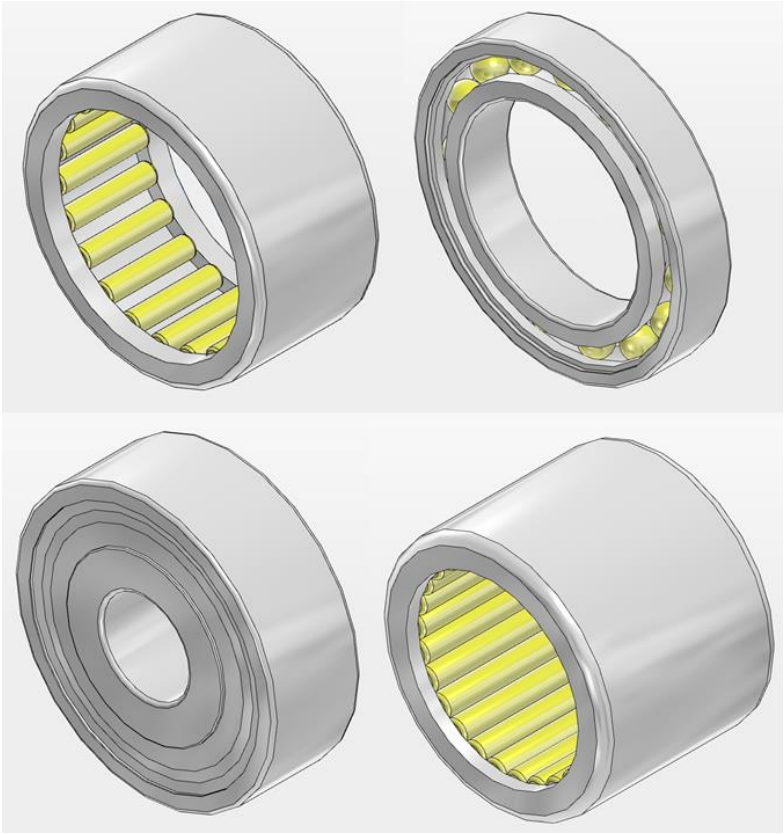

Figure 4.9. Render of HK 2516 (top left), 6013 M (top right), 628-2RS1 (bottom left) and HN 1516 (bottom right) SKF bearings. [SKF]

The properties of the selected SKF bearings are presented in table 4.16.

Table 4.16. Properties of SKF bearings.

SKF Bearing Designation	HK 2516	6013 M	628-2RS1	HN 1516
Bore	25 mm	65 mm	8 mm	15 mm
Outside Diameter	32 mm	100 mm	24 mm	21 mm
Width	16 mm	18 mm	8 mm	16 mm
Basic Dynamic Load Rating	15.1 kN	31.9 kN	3.9 kN	15.1 kN
Basic Static Load Rating	24 kN	25 kN	1.66 kN	24 kN
Reference Speed	9500 rpm	14000 rpm	-	12000 rpm
Limiting Speed	11000 rpm	12000 rpm	19000 rpm	15000 rpm
Mass of Bearing	25 g	440 g	17 g	14 g

4.9 Crankcase Design

The crankcase houses the crankshaft and should be designed to be both light and strong. The material chosen for the crankcase was the 319.0 aluminium alloy. It should be noted that the all crankcases were designing without considering any calculations regarding the stresses they are subjected to.

From figure 4.10, the front and back crankcases are joined to the central crankcase with six bolts with a diameter of 5 mm. It can also be seen that a protuberance was designed to hold the 6013 M bearing in place.

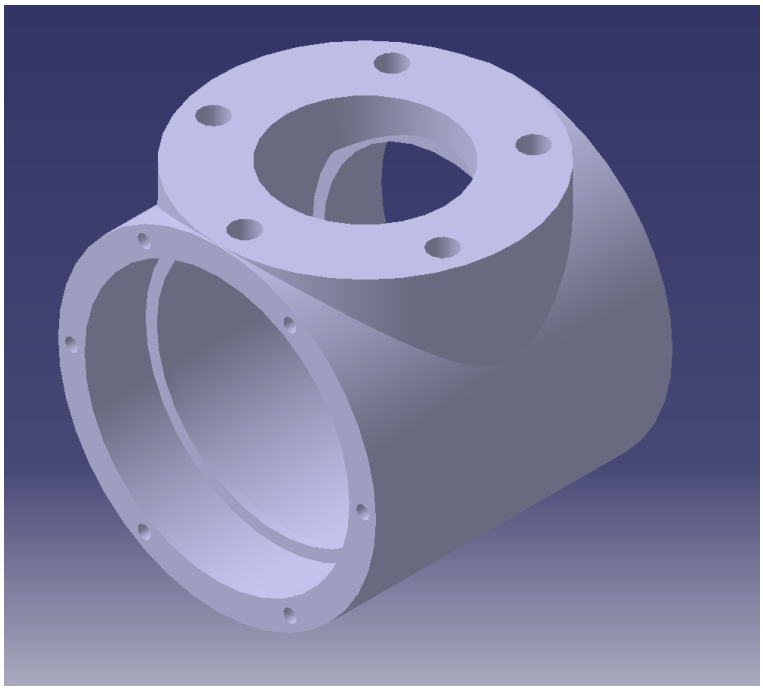

Figure 4.10. View of the central crankcase.

In reference to figure 4.11, it is clear the front and back crankcases have the same geometry, with the only difference being the hole for the output shaft in the front crankcase, which does not exist for the back crankcase. However, the back crankcase may be modified in conjunction with the support shaft set to install a camshaft by extending the support shaft. It can also be seen that similarly to the central crankcase, a protuberance was designed to keep the 6013 M bearing in place.

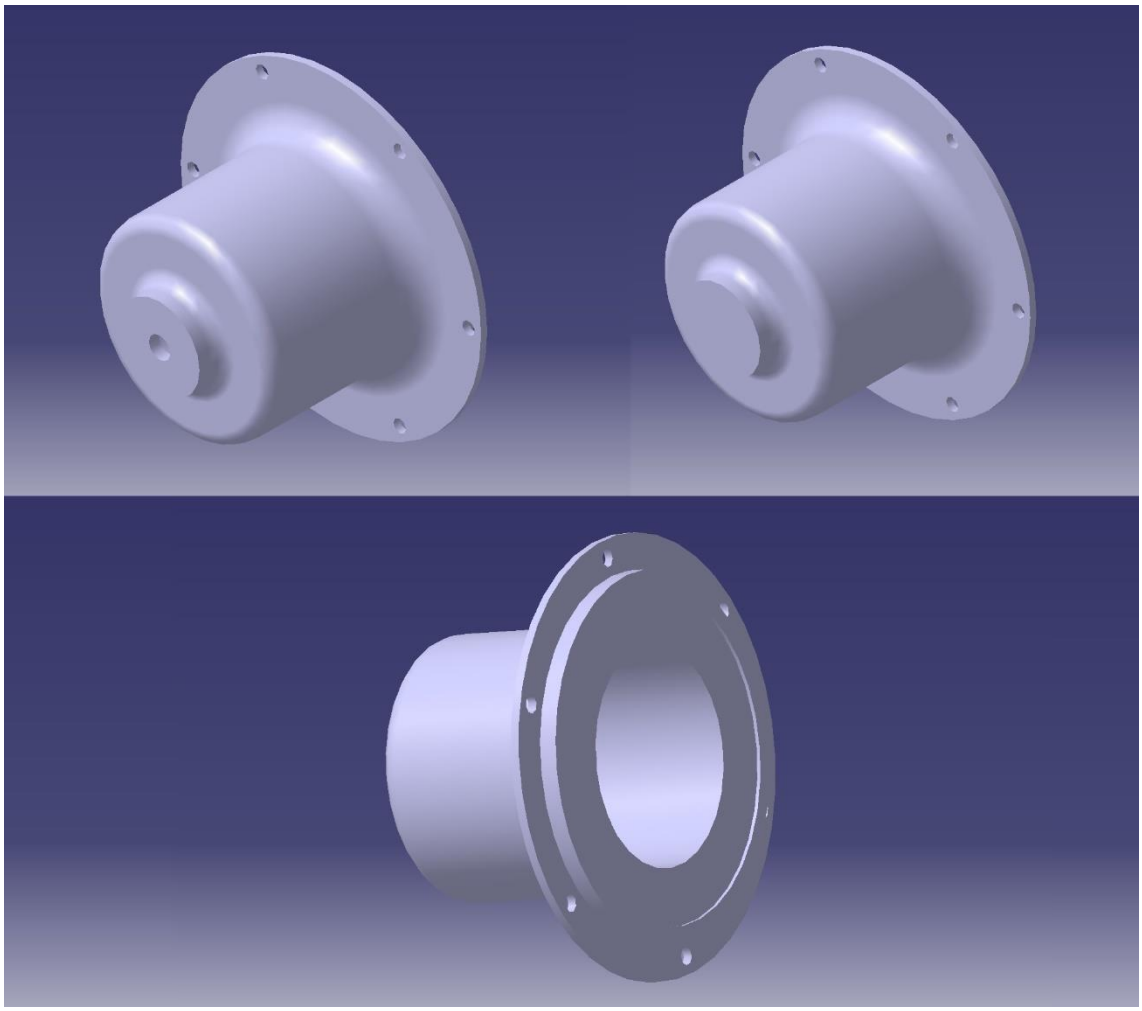

Figure 4.11. View of the front crankcase (top left and bottom) and back crankcase (top right and bottom).

The mass of each crankcase is presented in table 4.16.

Table 4.17. Mass of central, front and back crankcases.

	Central Crankcase	Front Crankcase	Back Crankcase
Mass	1188.8 g	367.0 g	399.3 g

4.10 Final Design

Assembling all the parts designed, the final design of the OPGHE considered in this study is presented in figures 4.12 and 4.13.

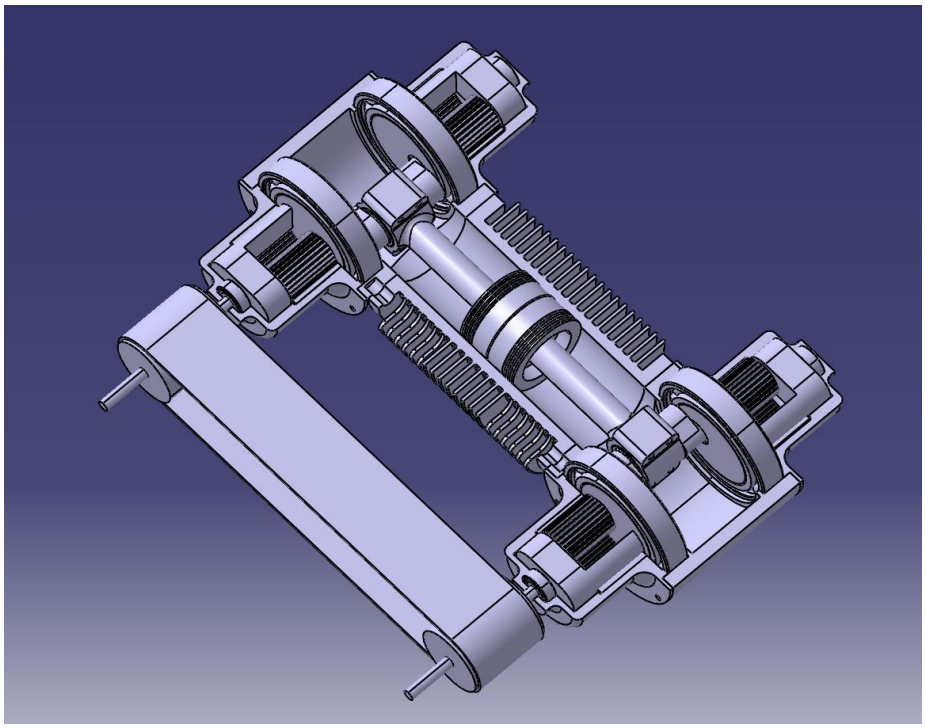

Figure 4.12. Cross-section view of the designed OPGHE.

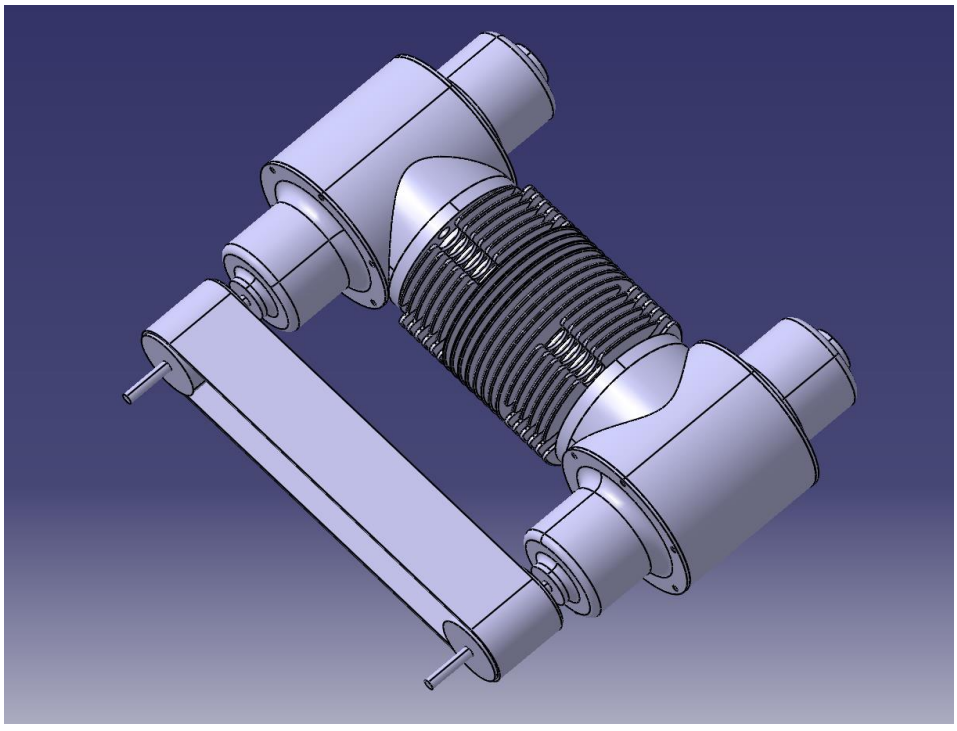

Figure 4.13. External view of the designed OPGHE.

Chapter 5

Results

In this chapter, the results from the MATLAB model developed, in reference to chapters 2 and 3, are presented and compared to analyse the performance advantages and disadvantages of the OPGHE in comparison to the OPSCE. Therefore, the average torque, power, specific fuel consumption, efficiency, mean effective pressure and power-to-weight ratio for both engines are presented.

5.1 Engine Performance

5.1.1 Opposed Piston Slider Crank Engine

From Eq. 2.66, the average torque output by the OPSCE engine, not considering any mechanical losses, was calculated at Wide-Open-Throttle (WOT) for the entire operating speed range with the results presented in figure 5.1. It can be seen the average torque output increases abruptly at low speeds from about 15 N.m until around 500 rpm where it has a value of 33.4 N.m. It reaches a maximum average torque output of 37.1 N.m at 5400 rpm and starts decreasing slightly to a value of 36.9 N.m at 8000 rpm.

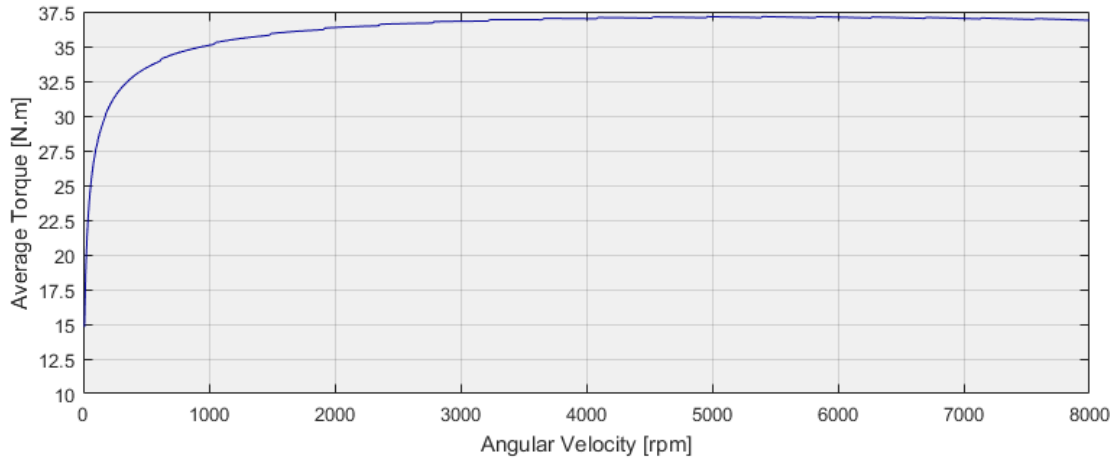

Figure 5.1. Average torque output for the OPSCE model.

From Eq. 2.46, the power output by the OPSCE for the entire operating speed range at WOT was calculated and presented in figure 5.2. It can be seen the power output varies linearly to from an initial value of 0 kW to a maximum of 30.9 kW (41.4 HP).

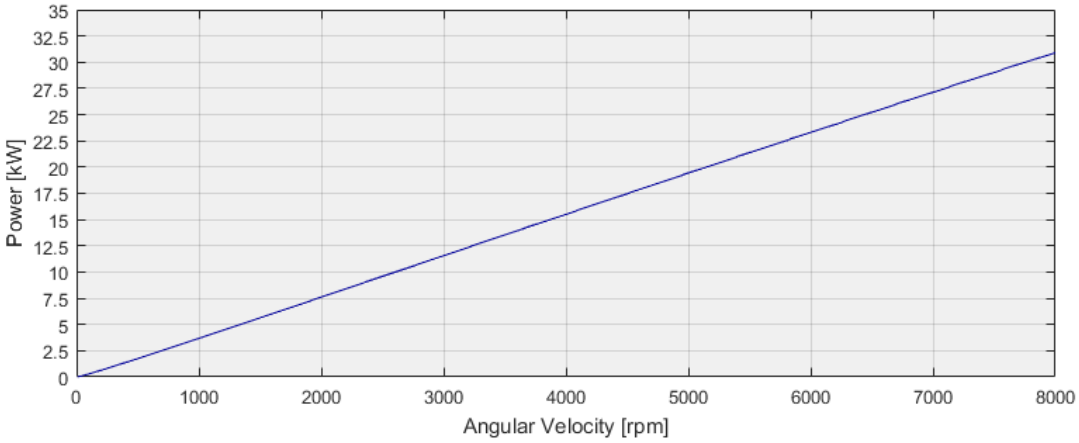

Figure 5.2. Power output for the OPSCE model.

The specific fuel consumption was calculated as in Eq. 2.52 and represented in figure 5.3. It can be seen it decreases abruptly at low speeds from an initial value of about 475 g/(kW.h) to around 250 rpm where it has a value of 218.5 g/(kW.h). It reaches a minimum value of 184.5 g/(kW.h) at 5400 rpm and starts increasing to a value of 185.8 g/(kW.h) at 8000 rpm.

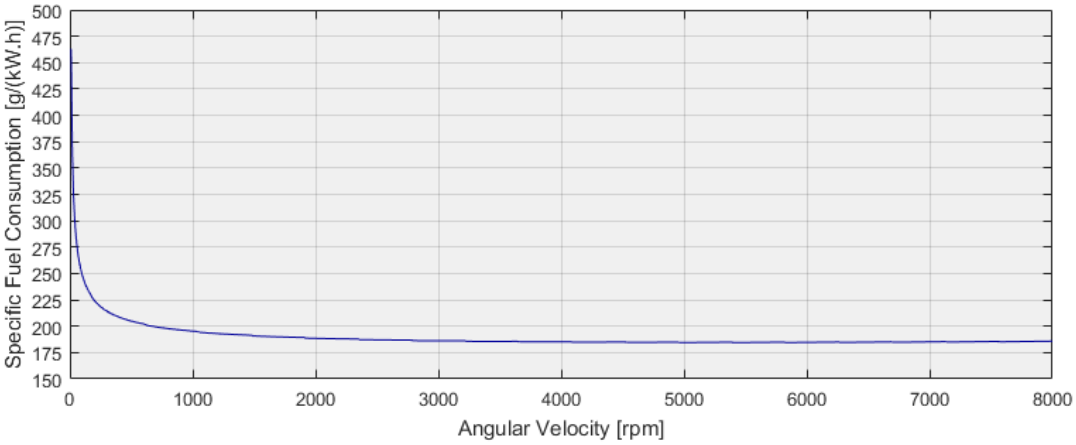

Figure 5.3. Specific fuel consumption for the OPSCE model.

The mean effective pressure was calculated as in Eq. 2.51 and represented in figure 5.4. It can be seen it increases abruptly at low speeds from an initial value of about 600 kPa to around 500 rpm where it has a value of 1428.8 kPa. It reaches a maximum value of 1586.8 kPa at 5400 rpm and starts decreasing to a value of 1575.3 kPa at 8000 rpm.

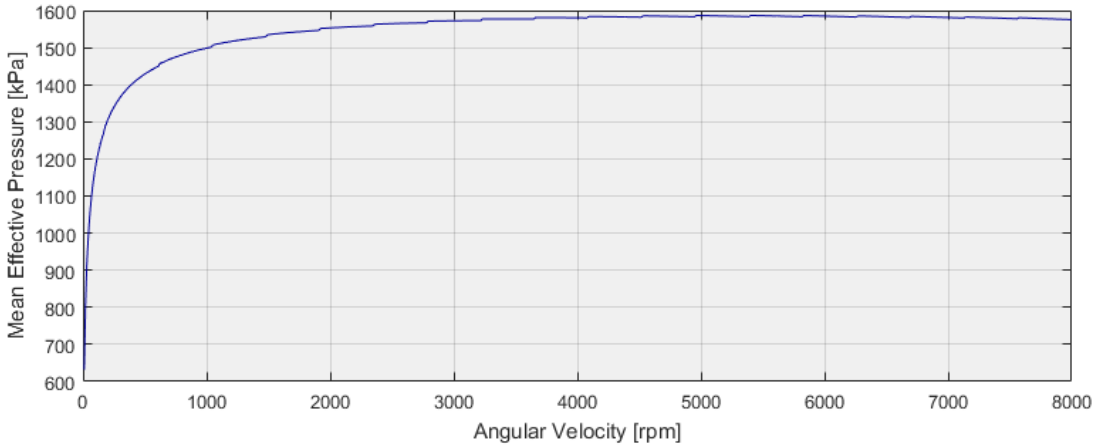

Figure 5.4. Mean effective pressure for the OPSCE model.

The fraction of fuel energy lost to heat, work, exhaust and unburnt fuel were calculated and presented in figure 5.5. It can be seen the total heat loss decreases abruptly from an initial value of about 0.65 until around 500 rpm where it has a value of 0.278 and keeps decreasing to a minimum value of 0.130 at 8000 rpm. For reference, it has a value of 0.192, 0.158 and 0.142 at 2000 rpm, 4000 rpm and 6000 rpm, respectively.

It can also be seen the work increases abruptly from an initial value of about 0.15 until around 500 rpm where it has a value of 0.403 and keeps increasing to a maximum value of 0.449 at 5400 rpm. For reference, it has a value of 0.434, 0.447 and 0.449 at 2000 rpm, 4000 rpm and 6000 rpm, respectively.

Similarly, it can be seen the fraction of fuel energy lost to the exhaust increases abruptly from an initial value of about 0 until around 500 rpm where it has a value of 0.176 and keeps increasing to a maximum value of 0.281 at 8000 rpm. For reference, it has a value of 0.228, 0.252 and 0.268 at 2000 rpm, 4000 rpm and 6000 rpm, respectively.

Finally, the fraction of fuel energy lost to unburnt fuel decreases with a linear tendency, although it is not linear, from an initial value of around 0.144 to a minimum of about 0.141. In fact, the maximum value is 0.144 at 170 rpm and the minimum value is 0.141 at 7570 rpm.

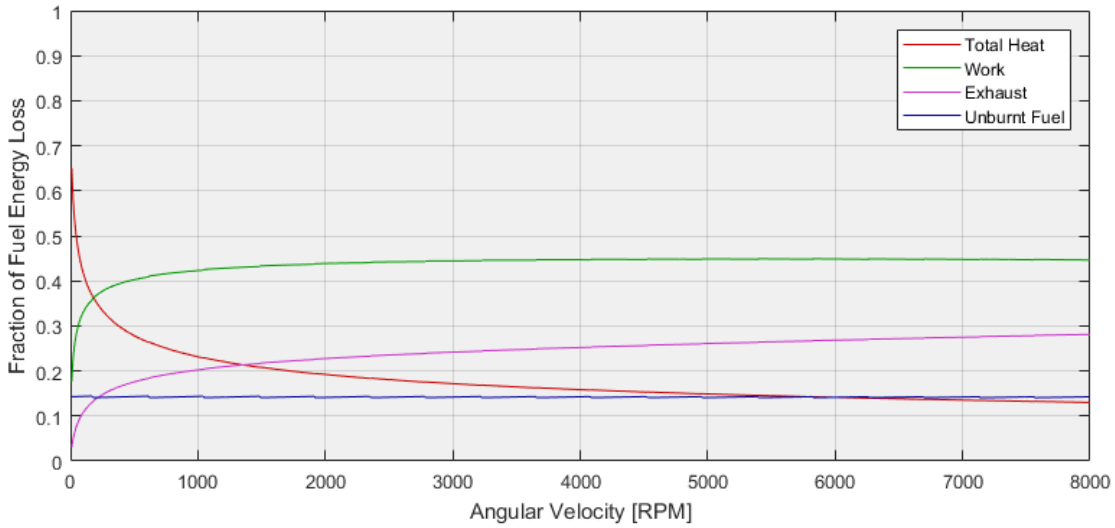

Figure 5.5. Fraction of fuel energy loss for the OPSCE model.

The maximum theoretical thermal efficiency according to the ideal Otto cycle was calculated from Eq. 2.3, with a result of 60.2 % for a compression ratio of 10. The thermal efficiency was calculated as in Eq. 2.53 and represented in figure 5.6. It can be seen it increases abruptly at low speeds from an initial value of about 15 % to around 500 rpm where it has a value of 40.4 %. It reaches a maximum value of 44.9 % at 5400 rpm and starts decreasing to a value of 44.5 % at 8000 rpm.

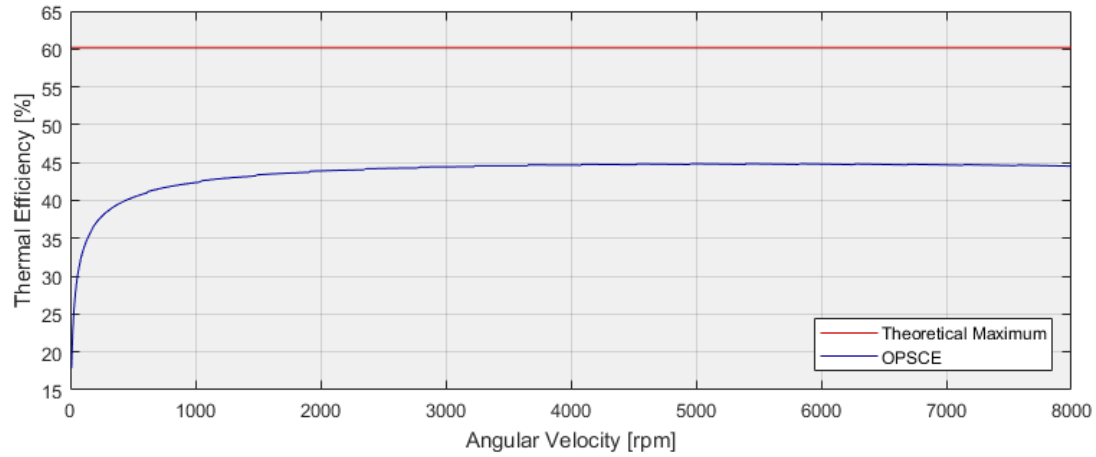

Figure 5.6. Thermal efficiency for the OPSCE model.

5.1.2 Opposed Piston Geared Hypocycloid Engine

From Eq. 2.74, the average torque output by the OPGHE engine, not considering any mechanical losses, was calculated at Wide-Open-Throttle (WOT) for the entire operating speed range with the results presented in figure 5.7. It can be seen the average torque output increases abruptly at low speeds from about 12.5 N.m until around 500 rpm where it has a value of 32.6 N.m. It reaches a maximum average torque output of 37.1 N.m at 6700 rpm and starts decreasing slightly to a value of 37.0 N.m at 8000 rpm.

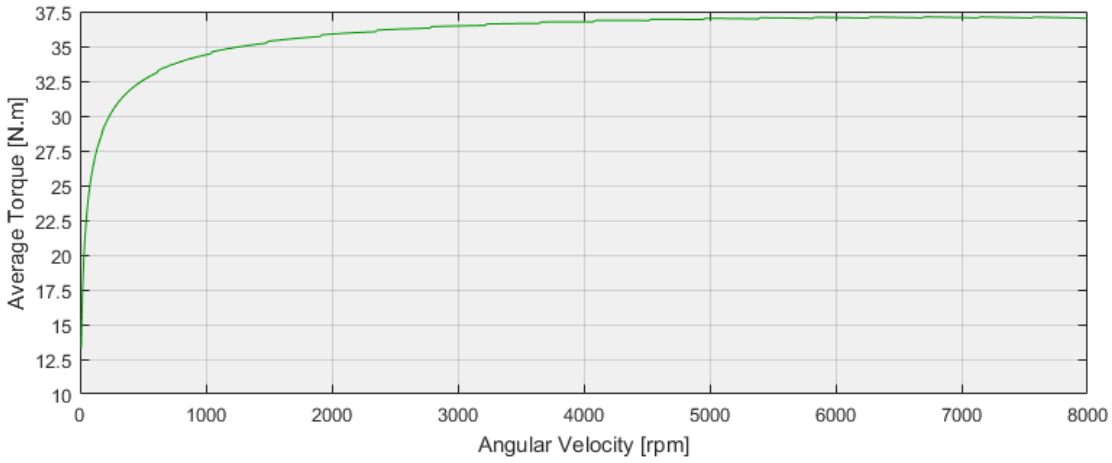

Figure 5.7. Average torque output for the OPGHE model.

Similar to the OPSCE, from Eq. 2.46, the power output by the OPGHE for the entire operating speed range at WOT was calculated and presented in figure 5.8. It can be seen the power output varies linearly to from an initial value of 0 kW to a maximum of 31.0 kW (41.6 HP).

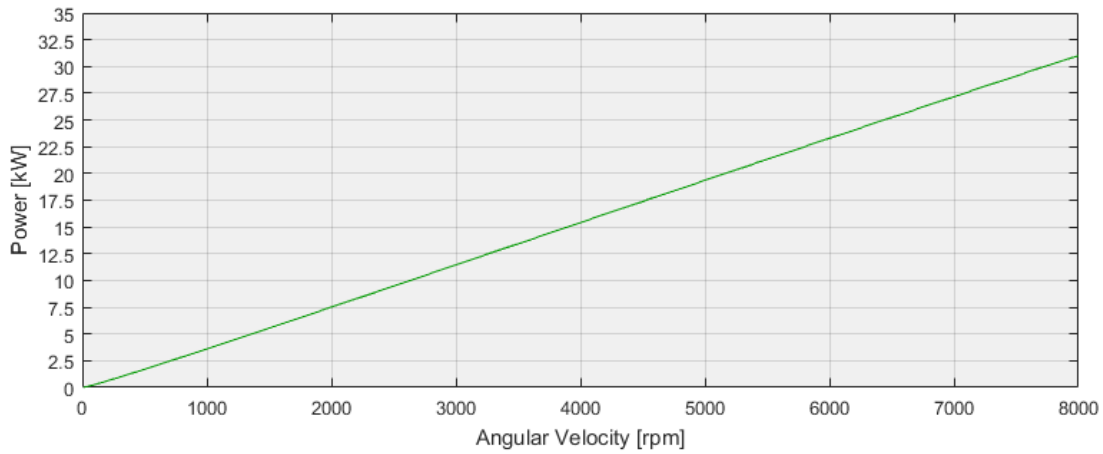

Figure 5.8. Power output for the OPGHE model.

The specific fuel consumption was also calculated as in Eq. 2.52 and represented in figure 5.9. It can be seen it decreases abruptly at low speeds from an initial value of about 525 g/(kW.h) to around 250 rpm where it has a value of 226.6 g/(kW.h). It reaches a minimum value of 184.7 g/(kW.h) at 6700 rpm and starts increasing to a value of 185.2 g/(kW.h) at 8000 rpm.

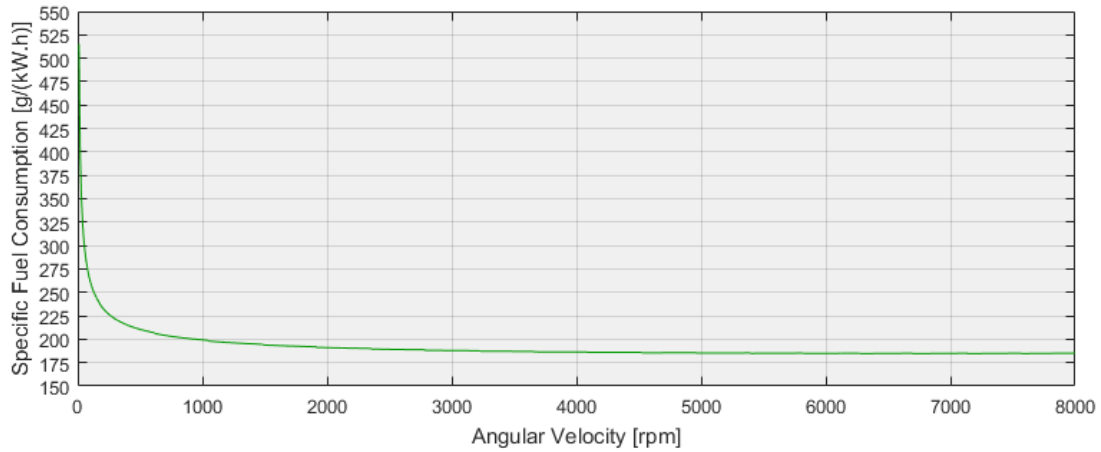

Figure 5.9. Specific fuel consumption for the OPGHE model.

The mean effective pressure was also calculated as in Eq. 2.51 and represented in figure 5.10. It can be seen it increases abruptly at low speeds from an initial value of about 550 kPa to around 500 rpm where it has a value of 1390.3 kPa. It reaches a maximum value of 1585.3 kPa at 6700 rpm and starts decreasing to a value of 1581.0 kPa at 8000 rpm.

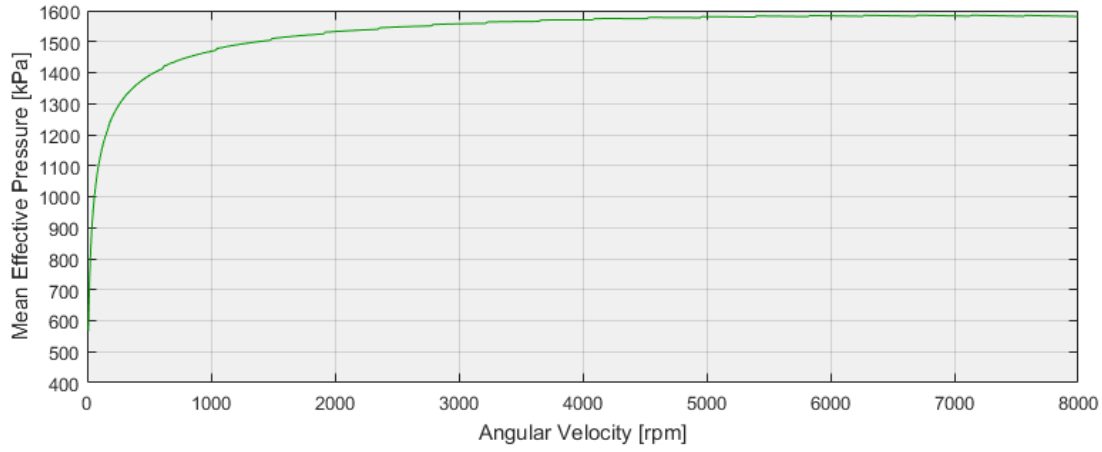

Figure 5.10. Mean effective pressure for the OPGHE model.

The fraction of fuel energy lost to heat, work, exhaust and unburnt fuel were calculated and presented in figure 5.11. It can be seen the total heat loss decreases abruptly from an initial value of about 0.65 until around 500 rpm where it has a value of 0.292 and keeps decreasing to a minimum value of 0.135 at 8000 rpm. For reference, it has a value of 0.202, 0.166 and 0.148 at 2000 rpm, 4000 rpm and 6000 rpm, respectively.

It can also be seen the work increases abruptly from an initial value of about 0.15 until around 500 rpm where it has a value of 0.394 and keeps increasing to a maximum value of 0.449 at 6700 rpm. For reference, it has a value of 0.434, 0.444 and 0.448 at 2000 rpm, 4000 rpm and 6000 rpm, respectively.

Similarly, it can be seen the fraction of fuel energy lost to the exhaust increases abruptly from an initial value of about 0 until around 500 rpm where it has a value of 0.172 and keeps increasing to a maximum value of 0.274 at 8000 rpm. For reference, it has a value of 0.224, 0.247 and 0.263 at 2000 rpm, 4000 rpm and 6000 rpm, respectively.

Finally, the fraction of fuel energy lost to unburnt fuel is the same as for the OPSCE.

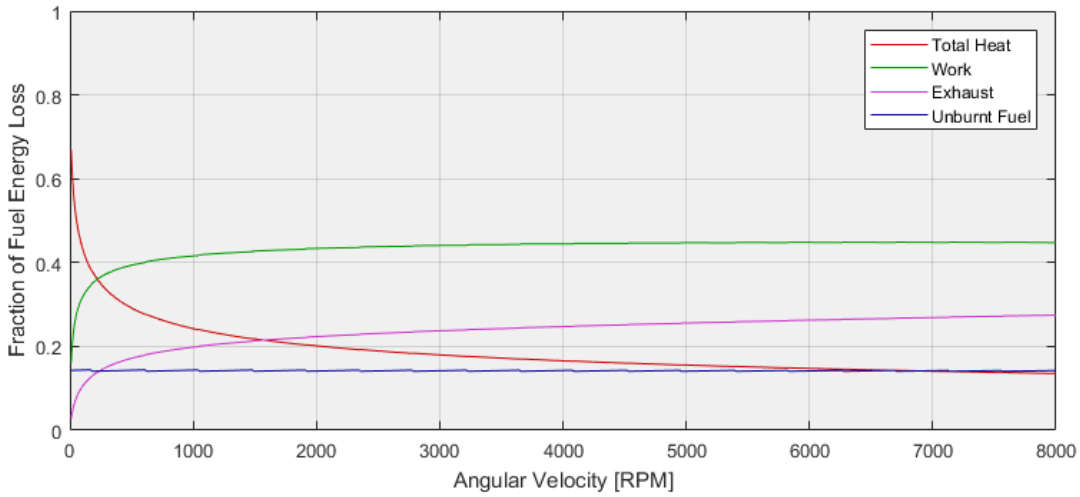

Figure 5.11. Fraction of fuel energy loss for the OPGHE model.

The maximum theoretical thermal efficiency according to the ideal Otto cycle is the same as for the OPSCE, i.e., 60.19 %. The thermal efficiency was calculated as in Eq. 2.53 and represented in figure 5.12. It can be seen it increases abruptly at low speeds from an initial value of about 15 % to around 500 rpm where it has a value of 39.31 %. It reaches a maximum value of 44.82 % at 6700 rpm and starts decreasing to a value of 44.70 % at 8000 rpm.

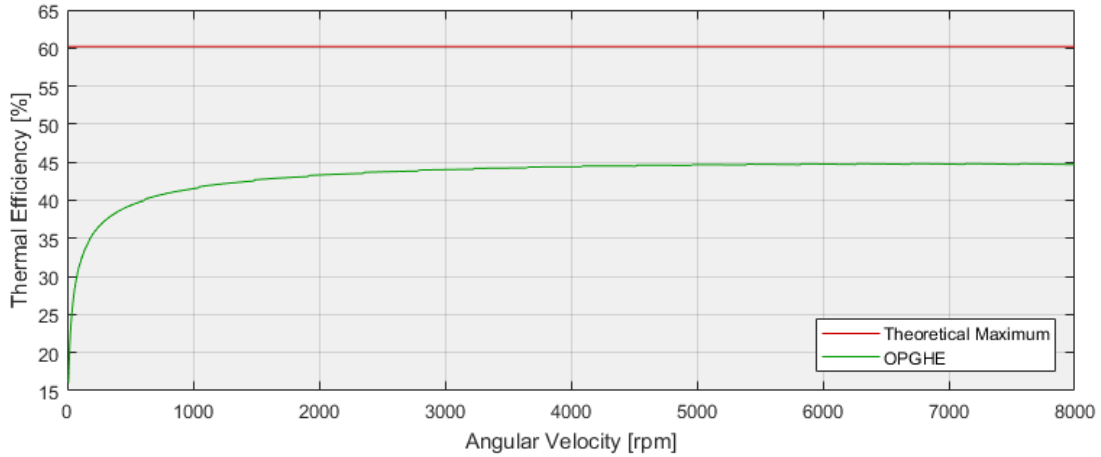

Figure 5.12. Thermal efficiency for the OPGHE model.

Finally, the power-to-weight ratio was calculated for the OPGHE. Considering a total mass for the engine, excluding the belt drive, of 13406.6 g (approximately 13.407 kg), the power-to-weight ratio was then calculated by dividing the power output at WOT by the mass of the engine across the entire operating speed range and is represented in figure 5.13. It can be seen it varies linearly from an initial value of 0 kW/kg to a value of 2.313 kW/kg.

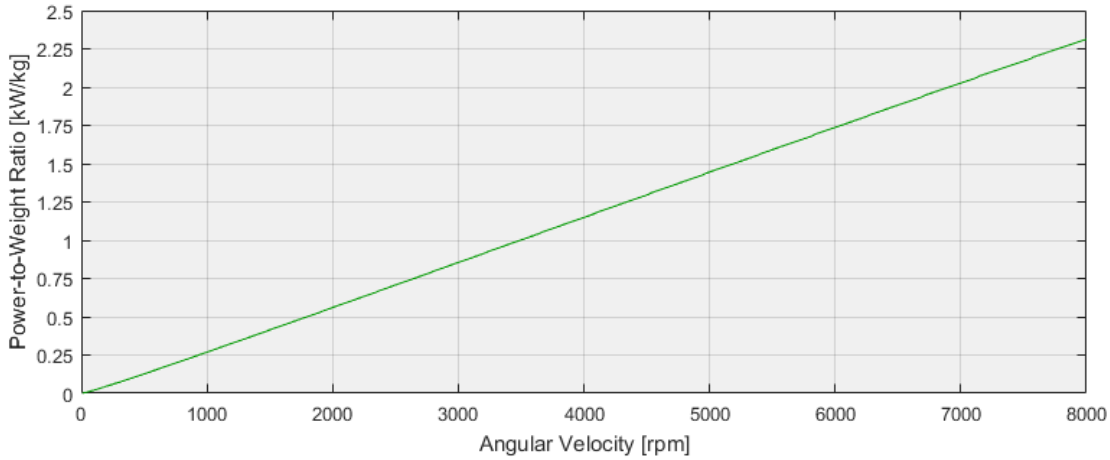

Figure 5.13. Power-to-weight ratio for the OPGHE model.

5.2 Engine Comparison

In this chapter, both the OPSCE and OPGHE are compared.

From figure 5.14, it can be seen the OPSCE has an increased average torque output until 6436 rpm where both have an average torque output of 37.1 N.m. From then on, the OPGHE has an increased average torque output.

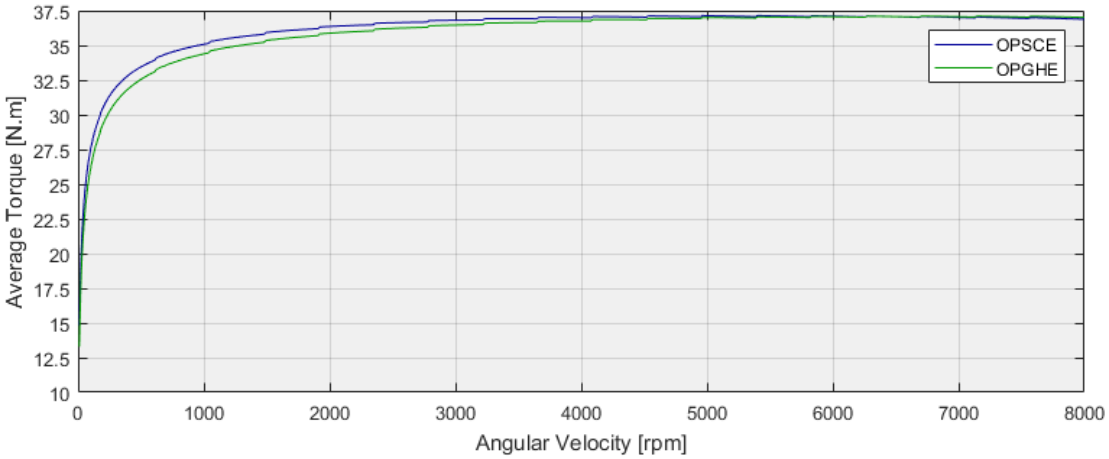

Figure 5.14. Average torque output comparison between the OPSCE and OPGHE models.

From figure 5.15, and as expected because of the average torque output, it can be seen the OPSCE has an increased power output until 6436 rpm where both have a power output of 25.0 kW. From then on, the OPGHE has an increased power output.

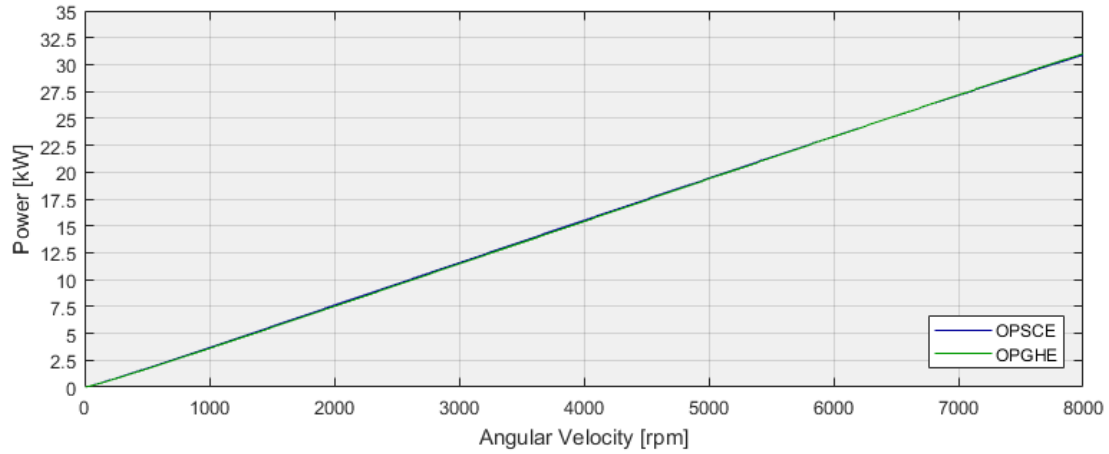

Figure 5.15. Power output comparison between the OPSCE and OPGHE models.

From figure 5.16, and as expected because of the power output and equal mass of fuel flow for both engines, it can be seen the OPSCE has a decreased specific fuel consumption until 6436 rpm where both have a specific fuel consumption of 184.8 g/(kW.h). From then on, the OPGHE has a decreased specific fuel consumption.

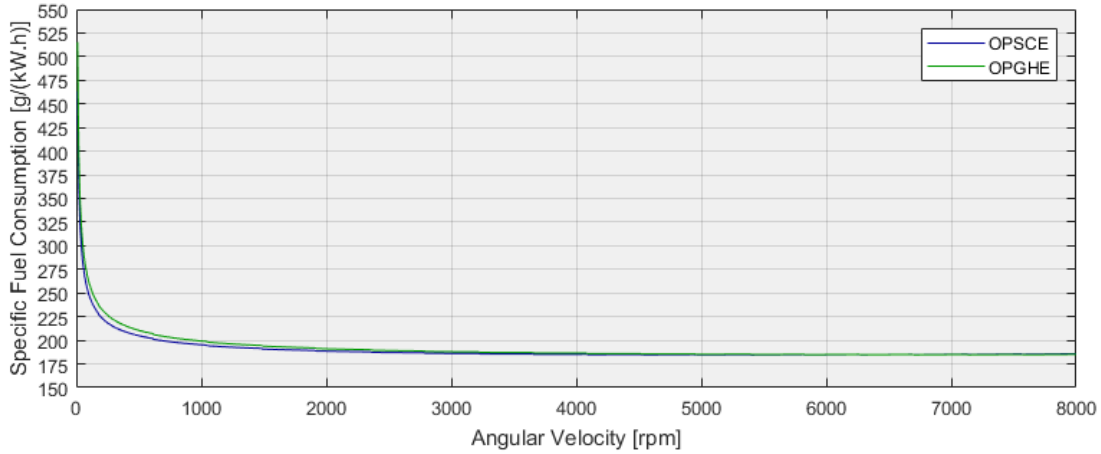

Figure 5.16. Specific fuel consumption comparison between the OPSCE and OPGHE models.

From figure 5.17, it can be seen the OPSCE has an increased mean effective pressure until 6436 rpm where both have a mean effective pressure of 1583.9 kPa. From then on, the OPGHE has an increased mean effective pressure.

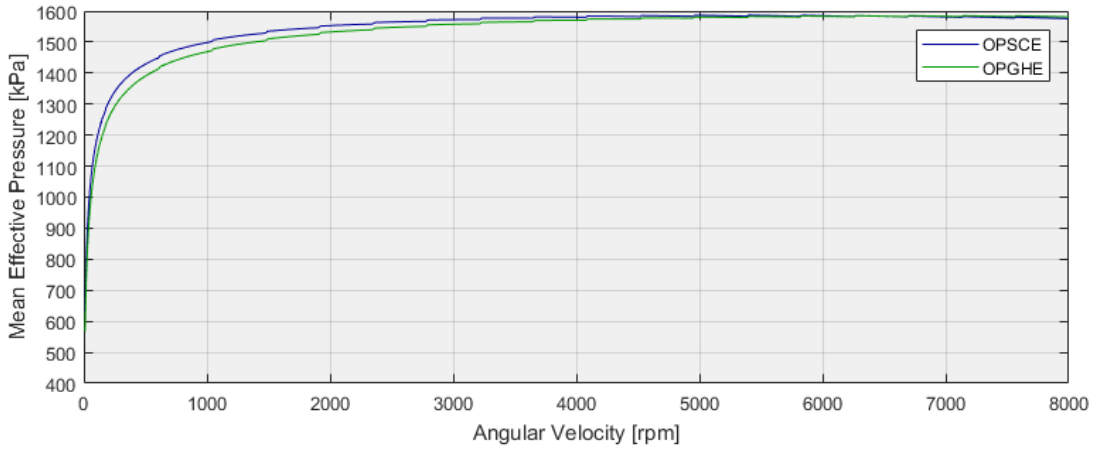

Figure 5.17. Mean effective pressure comparison between the OPSCE and OPGHE models.

The fraction of fuel energy lost to heat, work, exhaust and unburnt fuel were compared and presented in figure 5.18.

The OPGHE has increased total heat loss during the entire operating speed range, with 2.03 % more initially, increasing to a maximum difference of 4.79% at 1040 rpm, decreasing then to a difference of 4.04 % at 8000 rpm.

The OPGHE has less work done with 8.61 % less work done initially until 6500 rpm where both engines produce the same work. Above 6500 rpm, the OPGHE starts producing more work than the OPSCE increasing to a difference of 2.9 % at 8000 rpm.

The OPGHE has less fuel energy lost to the exhaust gases during the entire operating speed range, with 8.78 % less initially, decreasing to a minimum difference of 1.84 % at 2730 rpm, increasing again to a difference of 2.33 % at 8000 rpm.

Finally, as seen before, the fraction of fuel energy lost to unburnt fuel is similar between both OPSCE and OPGHE. There is also a variation of about 2,5 % between the values, which was considered negligible.

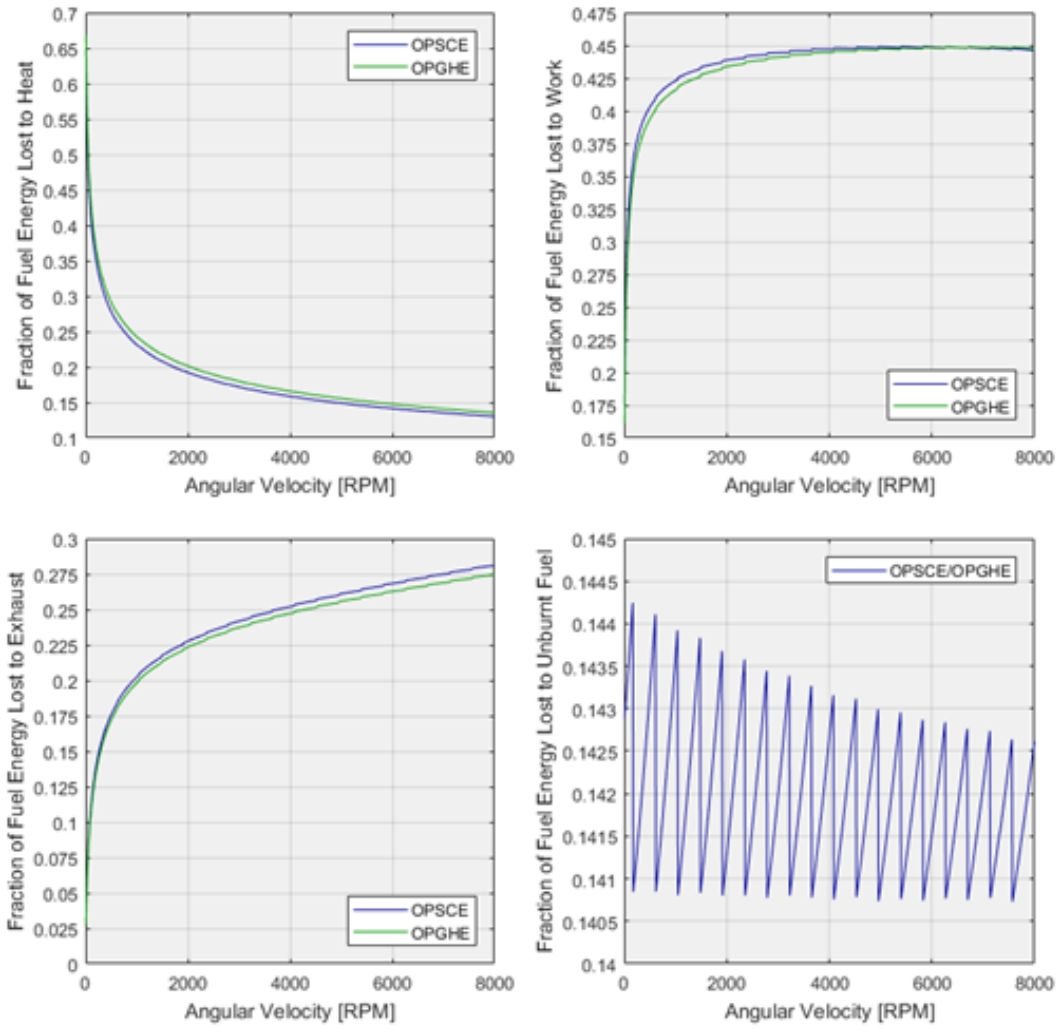

Figure 5.18. Fraction of fuel energy loss comparison between the OPSCE and OPGHE models.

Finally, from figure 5.19, and as expected due to the previous comparison, it can be seen the OPSCE has an increased efficiency until 6436 rpm where both have an efficiency of 44.78 %. From then on, the OPGHE has an increased mean effective pressure. As seen before, the maximum theoretical thermal efficiency according to the ideal Otto cycle for a compression of 10 is 60.19 %.

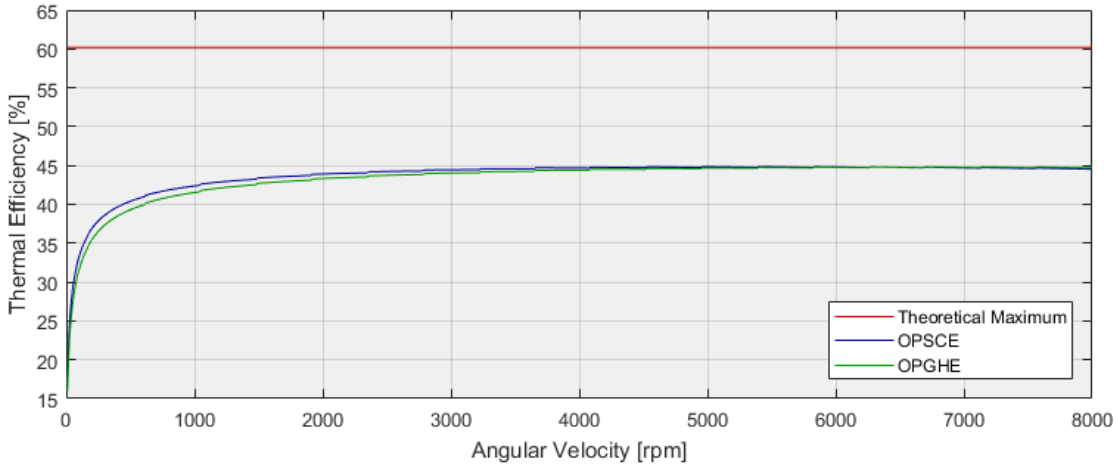

Figure 5.19. Thermal efficiency comparison between the OPSCE and OPGHE models.

Chapter 6

Conclusions

The slider crank conventional engine has been, by far, the most successful commercially with very few alternative engine configurations having seen widespread application, especially in the aviation industry. The OPGHE presents itself as a promising alternative for the coming years with its performance not falling behind that of the slider crank engine, even in opposed piston configuration, and excluding the mechanical losses which have the potential of being significantly reduced in an OPGHE. Furthermore, this configuration avoids the issues that have been common among the early opposed piston engines, such as oil consumption and high emissions, by working in a four-stroke cycle, therefore having the potential for achieving much higher efficiencies. Also of note is the balance of the engine achieved due to the reciprocating and sinusoidal motion of both pistons, which is a huge advantage for aircraft applications where vibrations are a great concern. Also, the possibility of having longer piston rods which don't affect the geometric characteristics of the piston, and therefore its kinematics, may present as an advantage for some applications. As seen before, the study of heat dissipation via the heat fins, the valve system and consequent intake and exhaust processes were beyond the scope of this study. Several steps in this study during the design of the OPGHE were iterative and multidisciplinary which made the overall design of the engine to be constantly reviewed. The values of efficiency, power and torque output, and power-to-weight ratio achieved are very promising, although it must be considered that several simplifications were taken.

Finally, the objective of this study is considered to have been successfully achieved with a comparison between both OPSCE and OPGHE performance having been made as well as the design of the engine components relevant to this study.

6.1 Alternative Materials and Possible Improvements

During this study, some possible improvements were contemplated but not considered, mainly due to the lack of information regarding such improvements. One of the design steps that has the most impact on the engine performance is the geared hypocycloid mechanism, for which very little information is available, probably due to very little research having been done in this field. Also, the design of gears is mostly done from experience and tests, with few methods for predicting the performance of a gearset accurately being available, specially for internal gears.

When designing the geared hypocycloid mechanism, a material had to be chosen and, due to the high-stress both the gear and pinion are subjected to, not any material could be used, with the Nitralloy N steel alloy being chosen for its very high strength characteristics. However, for a OPGHE, it proved to not be enough with a twin gearset for each piston having to be considered. This may be minimized by a more accurate modelling of the engine performance characteristics which will probably reduce the gear tooth load, by a more accurate method for predicting the stresses the gearset is subjected to or by subjecting the geared hypocycloid mechanism to the expected loads during the engine operation and study its behaviour.

Another alternative was the use of materials possibly even stronger than Nitralloy N, such as the Maraging Steels. These steels have been developed in the last decades and used in aerospace applications successfully. They are hardened by a metallurgical reaction without carbon, contrary to conventional steels and are designed to provide tensile yield strengths from 1030 MPa to 2420 MPa, with some having tensile yield strengths as high as 3450 MPa. [Davis, 2005] The allowable bending and contact stresses may be taken, by rule of thumb when no further information is available [Davis, 2005], as 0.3 times the Ultimate Tensile Strength for the first, and approximately equal to the Ultimate Tensile Strength for the second. Therefore, for Maraging 350 with an Ultimate Tensile Strength of 2340 MPa (342 ksi) [Service Steel Aerospace Corp., 2016], the allowable bending and contact stresses would be 702 MPa and 2340 MPa, which is an increase of about 54.4 % and 80 %, respectively. The face width, and therefore, the overall dimensions of the geared hypocycloid mechanism, could be reduced in at least half making for a lighter and more compact engine and possibly reduce the mechanical losses even further. Some alternative materials for the cylinder, piston or crankcase may also be considered and its impact on performance analysed, such as cylinders cast from compressed compacted graphite iron which are becoming promising even when compared to cylinders made from aluminium alloys.

One other improvement for the geared hypocycloid engine is the decrease of the bore/stroke ratio, which would reduce the tangential gear tooth load, thus reducing the overall dimensions of the gearset as well. However, the impact on the engine performance would have to be considered. The possibility of operating on higher compressions ratios can also be considered to further increase efficiency. Finally, a turbocharging system to maintain the pressure ratio of 1 with increasing altitude, or even increase the pressure ratio therefore increase the torque and power output of the engine, can be considered.

6.2 Future Work

Seeing this as a first stage of engine design, more work must be done to successfully design and build the entire engine in view of commercial applications.

Firstly, more accurate models must be developed to predict the performance of the geared hypocycloid mechanism in conjunction with testing the materials to be used to more closely find the mechanical properties of such material. Secondly, the intake and exhaust processes need to be modelled to more accurately predict the engine performance as well as design the entire intake and exhaust system followed by a computational fluid dynamics analysis. The mechanical losses must also be analysed since this is one of the greatest advantages of the geared hypocycloid engine. The use of finite-element analysis should be carried out to ensure the structural integrity of all components. Since the engine is to operate on a four-stroke cycle, the valve system also needs to be studied and designed in conjunction with a camshaft. In addition, the belt system must be designed considering a timing belt to ensure synchronous operation between both pistons and valve system. Furthermore, both the fuel and ignition systems would have to be chosen and designed, with fuel injection and electronic controlled ignition being recommended for better performance. Finally, the use of a flywheel should be considered or, for aircraft applications, an adequate propeller.

The final stage is build the engine as designed and test it to improve its characteristics and make the necessary changes.

Bibliography

American National Standard ANSI/AGMA 2001-D04, *Fundamental Rating Factors and Calculation Methods for Involute Spur and Helical Gear Teeth,* American Gear Manufacturers Association, 2004

American National Standard ANSI/AGMA 2101-C95, *Fundamental Rating Factors and Calculation Methods for Involute Spur and Helical Gear Teeth,* American Gear Manufacturers Association, 1995

Arnold, S. M. & Wong, T. T. *Models, Databases, and Simulation Tools Needed for the Realization of Integrated Computational Materials Engineering,* Proceedings of the Symposium Held at Materials Science & Technology 2010, Houston, Texas, ASM International, 2010

ASM International, *Casting Design and Performance,* ASM International, 2009

ASM International Handbook Committee, *ASM Handbook. Volume 1, Properties and Selection: Irons, Steels and High Performance Alloys, 10th Edition, Second Printing,* ASM International, 1993

ASM International Handbook Committee, *ASM Handbook. Volume 2, Properties and Selection: Nonferrous Alloys and Special-Purpose Materials, 10th Edition Metals Handbook, Second Printing,* ASM International, 1992

Aziz, E. S. & Chassapis, C. *Enhanced Hypocycloid Gear Mechanism for Internal Combustion Engine Applications*, Journal of Mechanical Design, Vol. 138, December 2016.

Blair, G. P. *Design and Simulation of Four-Stroke Engines,* Society of Automotive Engineers, Inc., 1999.

Budynas, R. G. & Nisbett, J. K. *Shigley's Mechanical Engineering Design, Tenth Edition*, Mc-Graw-Hill Education, 2015.

Caton, J. A. *An Introduction to Thermodynamic Cycle Simulations for Internal Combustion Engines,* John Wiley & Sons, Ltd., 2016

Colbourne, J. R. *The Geometry of Involute Gears,* Springer-Verlag New York Inc., 1987

Conner, T. *Critical Evaluation and Optimization of a Hypocycloid Wiseman Engine,* Thesis Presented in Partial Fulfilment of the requirements for the Degree Master of Technology, Arizona State University, December 2011.

Cuddihy, J. L. *A User-Friendly, Two-Zone Heat Release Model for Predicting Spark-Ignition Engine Performance and Emissions,* Thesis Presented in Partial Fulfilment of the Requirements for the Degree of Master of Science with a Major in Mechanical Engineering in the College of Graduate Studies, University of Idaho, May 2014

Data Sheet, *Ferrium S53, Corrosion Resistant Ultrahigh-Strength Steel for Aerospace Structural Applications*, QuesTek Innovations LLC 2010

Data Sheet, *Maraging,* Service Steel Aerospace Corp., 2016

Davis, J. R. *Alloying, Understanding the Basics,* ASM International, 2001

Davis, J. R. *Gear Materials, Properties, and Manufacture,* ASM International, 2005

Gregório, J. M. P. *Desenvolvimento de um Motor Alternativo de Combustão Interna de Pistões Opostos*, Thesis for the degree of Doctor in Aeronautical Engineering, Universidade da Beira Interior, March 2017.

Gupta, H. N. *Fundamentals of Internal Combustion Engines, Second Printing,* PHI Learning Private Limited, New Delhi, 2006

Gupta, J.K. & Khurmi, R.S. *A Textbook of Machine Design, First Multicolour Edition*, Eurasia Publishing House Limited, 2005.

Hall, A. M. & Slunder, C. J. *The Metallurgy, Behavior, and Application of the 18-Percent Nickel Maraging Steels,* Technology Utilization Division, National Aeronautics and Space Administration, 1968

Herold, R. E., Wahl, M. H., Regner, G., Lemke, J. U. & Foster, D. E. *Thermodynamic Benefits of Opposed-Piston Two-Stroke Engines,* SAE International, 2011

Heywood, J. B. *Internal Combustion Engine Fundamentals,* Mc-Graw-Hill, Inc., 1988

Ianneli, A. A. *Processing of 18% Ni Maraging Steel (350 Grade),* Army Materials and Mechanics Research Center, 1972

Information Sheet AGMA 908-B89, *Geometry Factors for Determining the Pitting Resistance and Bending Strength of Spur, Helical and Herringbone Gear Teeth,* American Gear Manufacturers Association, 1989

Information Sheet AGMA 911-A94, *Design Guidelines for Aerospace Gearing,* American Gear Manufacturers Association, 1994

Information Sheet AGMA 917-B97, *Design Manual for Parallel Shaft Fine-Pitch Gearing,* American Gear Manufacturers Association, 1997

Jones, L., *Sectioned Drawings of Piston Aero Engines,* Rolls-Royce Heritage Trust, 1995

Karhula, J. *Cardan Gear Mechanism versus Slider Crank Mechanism in Pumps and Engines,* Thesis for the degree of Doctor of Science (Technology), Lappeenranta University of Technology, February 2008.

Kaufman, J. G. *Introduction to Aluminium Alloys and Tempers, ASM International, 2000*

Kuo, P. S. *Cylinder Pressure in a Spark-Ignition Engine: A Computational Model,* Journal of Undergraduate Sciences 3: 141-145, 1996

Maitra, G. M. *Handbook of Gear Design, Second Edition, Fifth Reprint,* Tata McGraw-Hill Publishing Company Limited, 2001

McGuire, M. *Stainless Steels for Design Engineers,* ASM International, 2008

Metal Casting Design & Purchasing, *Casting Source Directory 2017,* American Foundry Society, 2017

Pirault, J. & Flint, M., *Opposed Piston Engines: Evolution, Use and Future Applications,* SAE International, 2010

Qin, X., Ntone, F., Leon, L. & Lyford-Pike, E. *The Effect of Stroke-to-Bore Ratio on Combustion Performance of a Lean Burn Heavy-Duty Gaseous SI Engine,* ASME 2010 Internal Combustion Engine Division Fall Technical Conference ICEF2010, San Antonio, Texas, USA, September 12-15, 2010

Radzevich, S. P. *Dudley's Handbook of Pratical Gear Design and Manufacture, Second Edition,* CRC Press, 2012

Ray, P. *Performance and Scaling Analysis of a Hypocycloid Wiseman Engine,* Thesis Presented in Partial Fulfilment of the requirements for the Degree Master of Technology, Arizona State University, May 2014.

Rittenhouse, J. A., B.S. Captain, USAF, *Thermal Loss Determination for a Small Internal Combustion Engine,* Thesis Presented in Partial Fulfilment of the Requirements for the Degree of Master of Science in Aeronautical Engineering, Department of the Air Force Air University, Air Force Institute of Technology, Wright-Patterson Air Force Base, Ohio, March 2014

Safety Data Sheet, *CarTech Nitralloy N,* Carpenter Technology Corp, 2015

Salazar, F. *Internal Combustion Engines,* Department of Aerospace and Mechanical Engineering, University of Notre Dame, 1998

Sankaran, K. K. & Mishra, R. S. *Metallurgy and Design of Alloys with Hierarchical Microstructures,* Elsevier Inc., 2017

Savage, M. & Coe, H. H. *Bending Strength Model for Internal Spur Gear Teeth, NASA Technical Memorandum 107012, Prepared for the 31st Joint Propulsion Conference and Exhibit, July 10-12, 1995*

Spitsov, O. *Heat Transfer Inside Internal Combustion Engine: Modelling and Comparison with Experimental Data,* Master's Thesis for Degree Programme in Energy Technology, Lappeenranta University of Technology, 2013

Srivastava, R. K. *Proceedings of All India Seminar on Advances in Product Development (APD-2006),* New Age International, 2006

Stone, R. *Introduction to Internal Combustion Engines, Third Edition,* Macmillan Press Ltd., 1999

Taylor, C. F. *The Internal Combustion Engine in Theory and Practice, Volume II: Combustions, Fuels, Materials, Designed, Revised Edition,* The M.I.T. Press, 1985

Xue, Y., Du, Q., Zhao, F. & Zhu, J. *Dynamic Analysis of a Hypocycloid Mechanism with Planetary Gears for Internal Combustion Engine,* 7th Intl. Conf. on Sys. Simulation and Scientific Computing, 2008 Asia Simulation Conference.

http://www.skf.com/group/products/bearings-units-housings/ball-bearings/deep-groove-ball-bearings/deep-groove-ball-bearings/index.html?designation=6013%20M
(As accessed on 23/09/2017)

http://www.skf.com/ph/products/bearings-units-housings/ball-bearings/deep-groove-ball-bearings/deep-groove-ball-bearings/index.html?designation=628-2RS1
(As accessed on 23/09/2017)

http://www.skf.com/group/products/bearings-units-housings/roller-bearings/needle-roller-bearings/drawn-cup-needle-roller-bearings/drawn-cup-pt/index.html?designation=HK%202516
(As accessed on 23/09/2017)

http://www.skf.com/group/products/bearings-units-housings/roller-bearings/needle-roller-bearings/drawn-cup-needle-roller-bearings/drawn-cup-pt/index.html?designation=HN%201516
(As accessed on 23/09/2017)

Annex

A.1. Engine database considered for the parametric review.

Brand	Model	Bore (mm)	Stroke (mm)	# Cylinders	Displacement (cc)	Disp. per cylinder (cc)	Power (HP)	@rpm	cc/HP Ratio	Bore/Stroke Ratio	Compression Ratio	NOTES
Aeroconversions	Aerovee 2.1	92	82	4	2180,416	545,104	80	3400	27,255	1,122	7:1	4-stroke gasoline
Aeroconversions	Aerovee Turbo	92	82	4	2180,416	545,104	80	3400	27,255	1,122	7:1	4-stroke gasoline, turbocharged
Rotax	912 ULS /S	84	61	4	1352,192	338,048	100	5800	13,522	1,377	10.4:1	4-stroke gasoline
Rotax	914 UL/F	79,5	61	4	1211,195	302,799	115	5800	10,532	1,303	9:1	4-stroke gasoline
Austro	E4	83	92	4	1991,104	497,776	168	-	11,852	0,902	-	4-stroke diesel
Lycoming	O-145	92	89	4	2366,549	591,637	75	3200	31,554	1,034	6.5:1	4-stroke gasoline
Continental	200	103,2	98,4	4	3292,338	823,084	100	2750	32,923	1,049	7:1	4-stroke gasoline
HKS	700E	85	60	2	680,940	340,470	60	6200	11,349	1,417	11.3:1	4-stroke gasoline
HKS	700T	85	62,5	2	709,313	354,656	80	5300	8,866	1,360	8.8:1	4-stroke gasoline, turbocharged
Revmaster	R-2300	94	84	4	2331,765	582,941	80	3000	29,147	1,119	8:1	4-stroke gasoline
Jabiru	2200	97,5	74	4	2209,993	552,498	80	3300	27,625	1,318	8:1	4-stroke gasoline
ULPower Aero Engines	UL260i	105,6	74	4	2592,444	648,111	97	3300	26,726	1,427	8.16:1	4-stroke gasoline
Robin	EY15	63	46	1	143,393	143,393	3,5	4000	40,970	1,370	6.3:1	4-stroke gasoline
Wiseman	-	36,5	28,6	1	29,926	29,926	0,5	5000	59,851	1,276		2-stroke gasoline
Limbach	L275E	66	40	2	273,696	136,848	20	7200	13,685	1,650	-	2-stroke gasoline
Sauer	S625V	76	69	2	626,031	313,016	50	5500	12,521	1,101	-	2-stroke gasoline
Simonini	Mini 4	61	54	1	157,813	157,813	23	7400	6,861	1,130	10:1	2-stroke gasoline
Simonini	Mini 2 Plus	66	58	1	198,429	198,429	26	7500	7,632	1,138	10.5:1	2-stroke gasoline
Simonini	Mini 2 EVO	70	60	1	230,907	230,907	33	8000	6,997	1,167	10:1	2-stroke gasoline
Simonini	Mini 3	72,8	65	1	270,561	270,561	36	7500	7,516	1,120	10.5:1	2-stroke gasoline
Zanzottera Engines	498H	75	56	2	494,801	247,400	44	6500	11,245	1,339	10.6:1	2-stroke gasoline, Boxer
Zanzottera Engines	305H	65	47	2	311,921	155,960	26	7000	11,997	1,383	10.7:1	2-stroke gasoline, Boxer
Hirth Engines	F 36	70	54	1	207,816	207,816	14,9	6000	13,947	1,296	-	2-stroke gasoline
Hirth Engines	F 33 ES	76	69	1	313,016	313,016	28	6200	11,179	1,101	-	2-stroke gasoline
Hirth Engines	2702 V	72	64	2	521,153	260,576	40	5500	13,029	1,125	-	2-stroke gasoline
Hirth Engines	3202 E+V	76	69	2	626,031	313,016	55	5500	11,382	1,101	-	2-stroke gasoline
Hirth Engines	F23 LW	72	64	2	521,153	260,576	50	6500	10,423	1,125	-	2-stroke gasoline, Boxter
Hirth Engines	H32E	76	69	2	626,031	313,016	65	6400	9,631	1,101	-	2-stroke gasoline
Hummel	28HP	88	69	2	839,333	419,667	28	-	29,976	1,275	-	
Hummel	32HP	92	69	2	917,370	458,685	32	-	28,668	1,333	-	
Hummel	37HP	92	78	2	1037,027	518,514	37	-	28,028	1,179	-	

A.2. Geometry Factors for external spur gear and pinion meshing with addendum modification factor of 0. (AGMA 908-B89)

***I* AND *J* FACTORS FOR:**[1]

25.0 DEG. PRESSURE ANGLE
0.0 DEG. HELIX ANGLE
0.270 TOOL EDGE RADIUS
EQUAL ADDENDUM ($x_1 = x_2 = 0$)

2.350 WHOLE DEPTH FACTOR
0.024 TOOTH THINNING FOR BACKLASH
LOADED AT HIGHEST POINT OF SINGLE TOOTH CONTACT

		PINION TEETH																	
GEAR		12		14		17		21		26		35		55		135			
TEETH		P	G	P	G	P	G	P	G	P	G	P	G	P	G	P	G		
12	I																		
	J	U	U																
14	I			0.086															
	J	U	U	0.33	0.33														
17	I			0.091		0.090													
	J	U	U	0.33	0.36	0.36	0.36												
21	I			0.095		0.096		0.092											
	J	U	U	0.33	0.39	0.36	0.39	0.39	0.39										
26	I			0.100		0.101		0.099		0.094									
	J	U	U	0.33	0.41	0.37	0.42	0.40	0.42	0.43	0.43								
35	I			0.106		0.109		0.108		0.104		0.095							
	J	U	U	0.34	0.44	0.37	0.45	0.40	0.45	0.43	0.46	0.46	0.46						
55	I			0.113		0.119		0.121		0.119		0.112		0.095					
	J	U	U	0.34	0.47	0.38	0.48	0.41	0.49	0.44	0.49	0.47	0.50	0.51	0.51				
135	I			0.123		0.132		0.139		0.142		0.141		0.131		0.096			
	J	U	U	0.35	0.51	0.38	0.52	0.42	0.53	0.45	0.53	0.48	0.54	0.53	0.56	0.57	0.57		

1 The letter "U" indicates a gear tooth combination which produces an undercut tooth form in one or both components and should be avoided. See Section 7 and Fig 7-1.

A.3. Geometry Factors for external spur gear and pinion meshing with addendum modification factor of 0.25. (AGMA 908-B89)

***I* AND *J* FACTORS FOR:**

25.0 DEG. PRESSURE ANGLE
0.0 DEG. HELIX ANGLE
0.270 TOOL EDGE RADIUS
25 PERCENT LONG ADDENDUM PINION ($x_1 = 0.25$)
25 PERCENT SHORT ADDENDUM GEAR ($x_2 = -0.25$)

2.350 WHOLE DEPTH FACTOR
0.024 TOOTH THINNING FOR BACKLASH
LOADED AT HIGHEST POINT OF SINGLE TOOTH CONTACT

		PINION TEETH																	
GEAR		12		14		17		21		26		35		55		135			
TEETH		P	G	P	G	P	G	P	G	P	G	P	G	P	G	P	G		
12	I		0.091																
	J	0.38	0.22																
14	I		0.095		0.093														
	J	0.38	0.25	0.40	0.25														
17	I		0.100		0.099		0.094												
	J	0.38	0.29	0.40	0.29	0.43	0.29												
21	I		0.106		0.106		0.102		0.095										
	J	0.38	0.32	0.41	0.32	0.43	0.33	0.46	0.33										
26	I		0.111		0.112		0.109		0.103		0.095								
	J	0.39	0.35	0.41	0.35	0.44	0.36	0.46	0.36	0.48	0.37								
35	I		0.118		0.120		0.119		0.115		0.108		0.096						
	J	0.39	0.38	0.41	0.39	0.44	0.39	0.47	0.40	0.49	0.41	0.51	0.41						
55	I		0.127		0.131		0.133		0.131		0.126		0.116		0.096				
	J	0.39	0.42	0.42	0.43	0.44	0.44	0.47	0.44	0.49	0.45	0.52	0.46	0.55	0.47				
135	I		0.138		0.145		0.151		0.153		0.153		0.148		0.135		0.096		
	J	0.40	0.47	0.42	0.48	0.45	0.49	0.48	0.49	0.50	0.50	0.53	0.51	0.56	0.53	0.59	0.55		

A.4. Geometry Factors for external spur gear and pinion meshing with addendum modification factor of 0.5. (AGMA 908-B89)

***I* AND *J* FACTORS FOR:**[1]

25.0 DEG. PRESSURE ANGLE
0.0 DEG. HELIX ANGLE
0.270 TOOL EDGE RADIUS
2.350 WHOLE DEPTH FACTOR
0.024 TOOTH THINNING FOR BACKLASH
LOADED AT HIGHEST POINT OF SINGLE TOOTH CONTACT
50 PERCENT LONG ADDENDUM PINION ($x_1 = 0.50$)
50 PERCENT SHORT ADDENDUM GEAR ($x_2 = -0.50$)

		PINION TEETH															
GEAR		12		14		17		21		26		35		55		135	
TEETH		P	G	P	G	P	G	P	G	P	G	P	G	P	G	P	G
12	I																
	J	T	T														
14	I																
	J	T	T	T	T												
17	I																
	J	T	T	T	T	T	T										
21	I							0.096									
	J	T	T	T	T	T	T	0.52	0.27								
26	I							0.106		0.096							
	J	T	T	T	T	T	T	0.52	0.30	0.53	0.31						
35	I							0.120		0.110		0.096					
	J	T	T	T	T	T	T	0.52	0.35	0.53	0.35	0.55	0.36				
55	I							0.139		0.131		0.118		0.096			
	J	T	T	T	T	T	T	0.52	0.40	0.54	0.41	0.56	0.42	0.58	0.43		
135	I							0.167		0.163		0.155		0.138		0.096	
	J	T	T	T	T	T	T	0.53	0.46	0.54	0.47	0.56	0.48	0.58	0.50	0.60	0.53

1 The letter "T" indicates a gear tooth combination which produces pointed teeth with a top land less than $0.3/P_{nd}$ in one or both components and should be avoided. See Section 7.

A.5. Technical Drawing of the Piston and Rod.

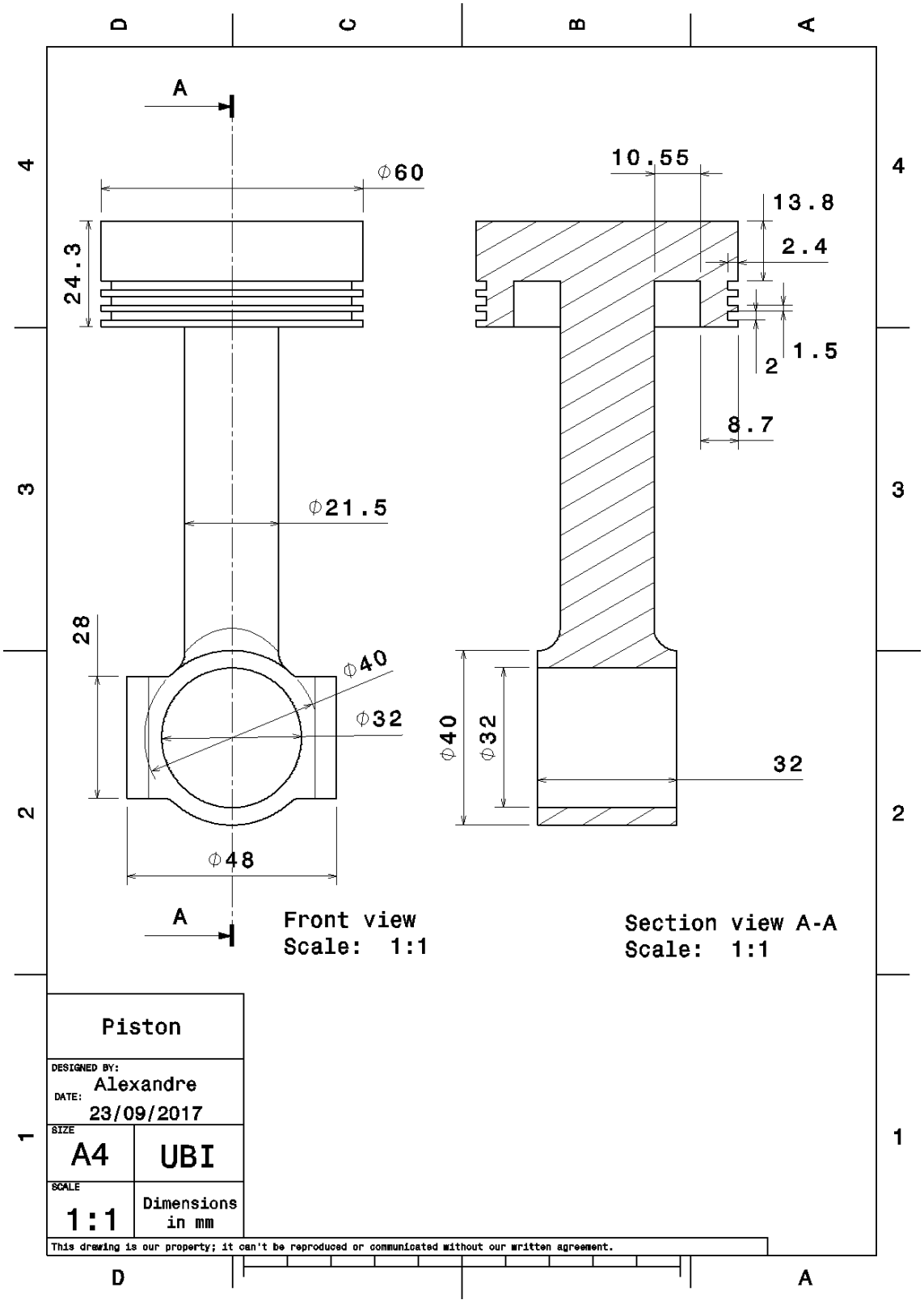

A.6. Technical Drawing of the Cylinder.

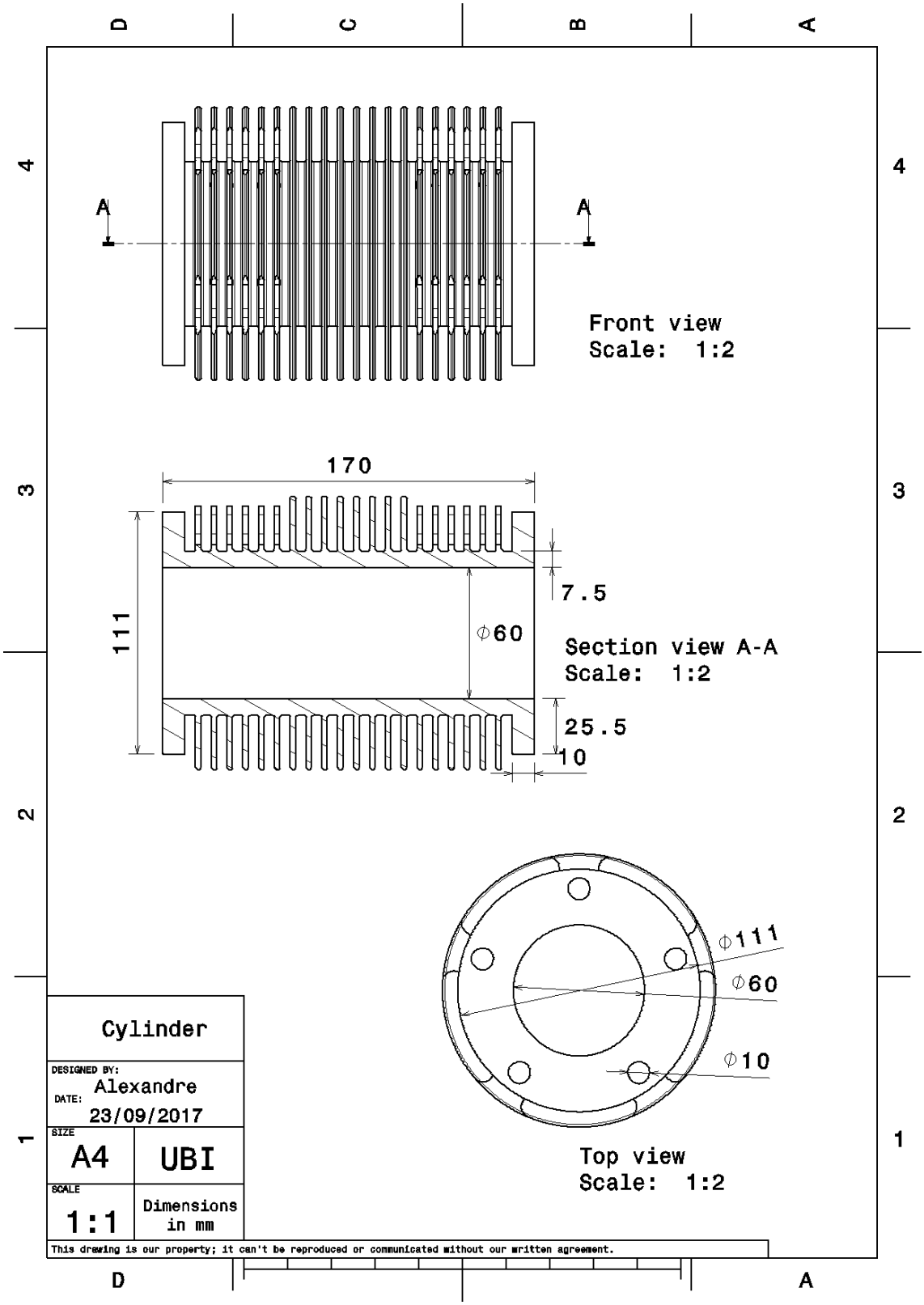

A.7. Technical Drawing of the Internal Gear.

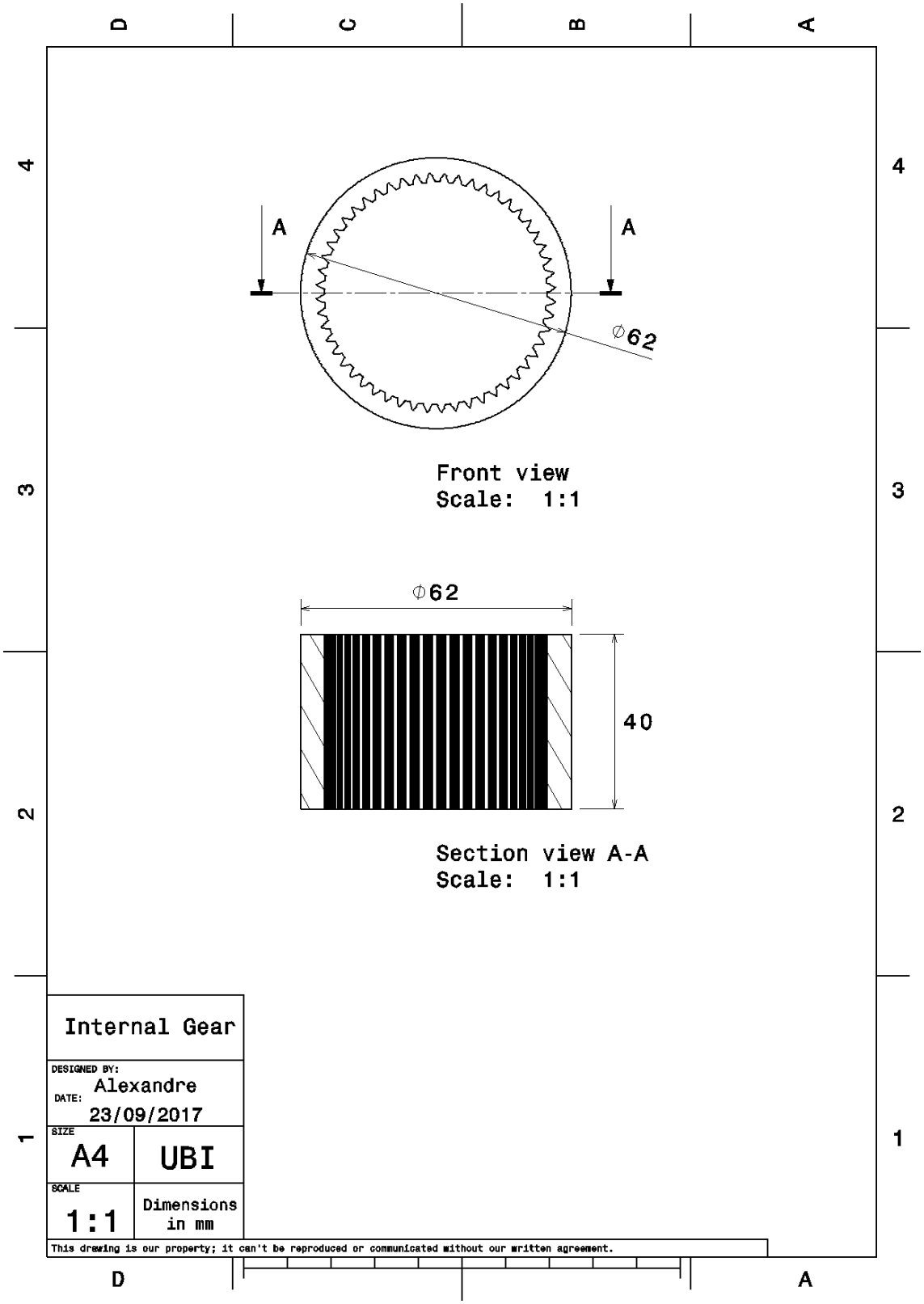

A.8. Technical Drawing of the Pinion.

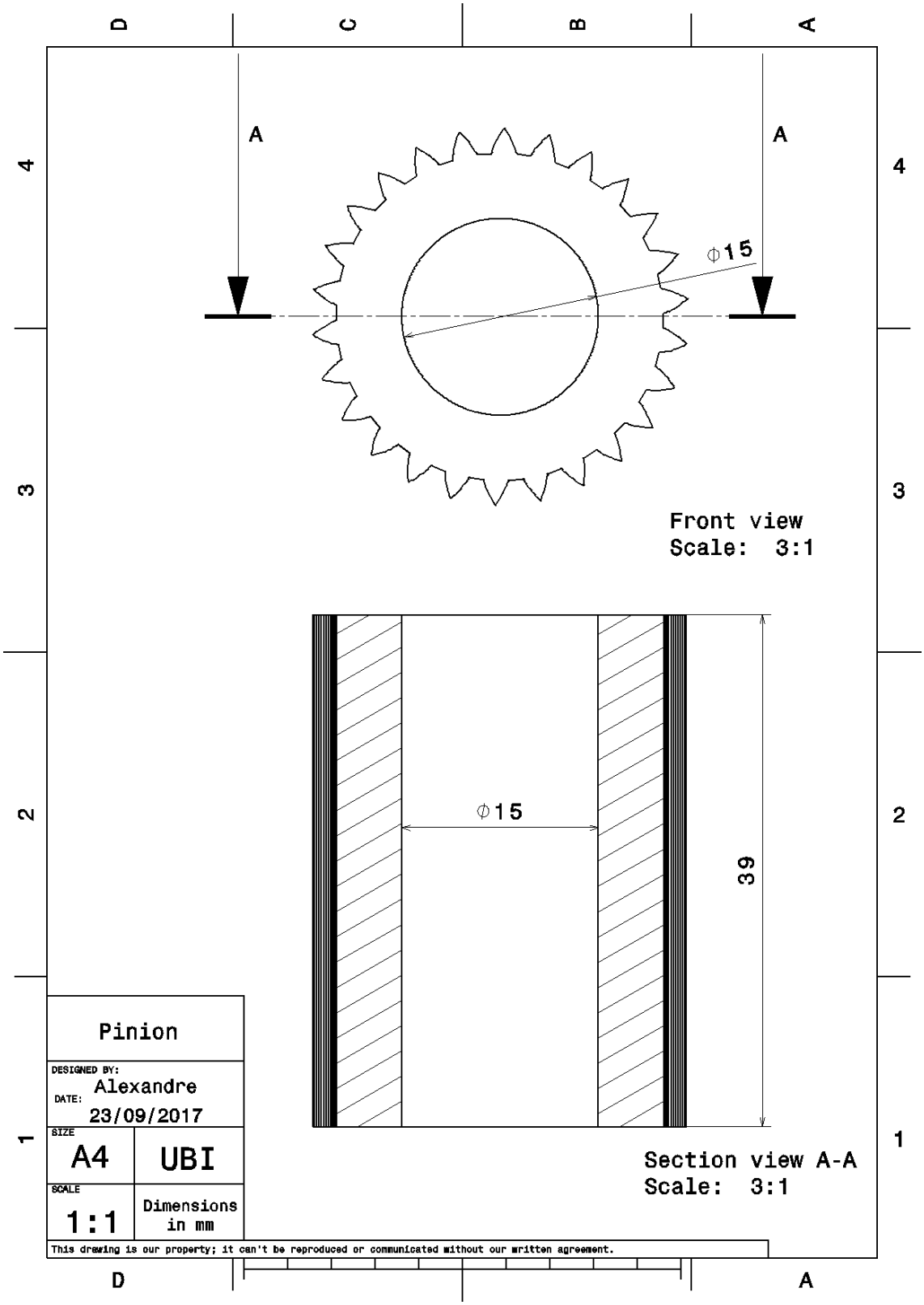

A.9. Technical Drawing of the Crankshaft.

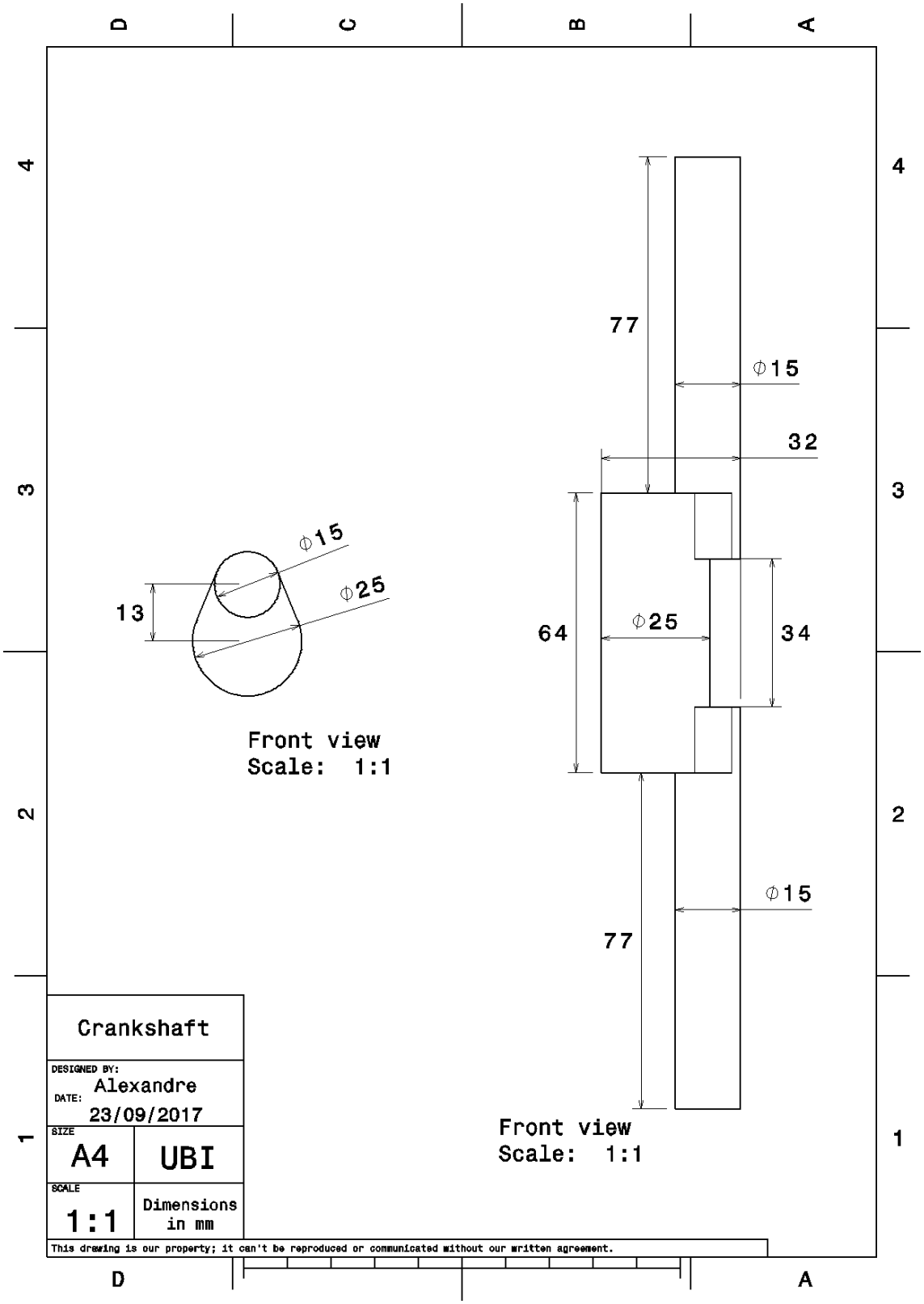

A.10. Technical Drawing of the Output Shaft.

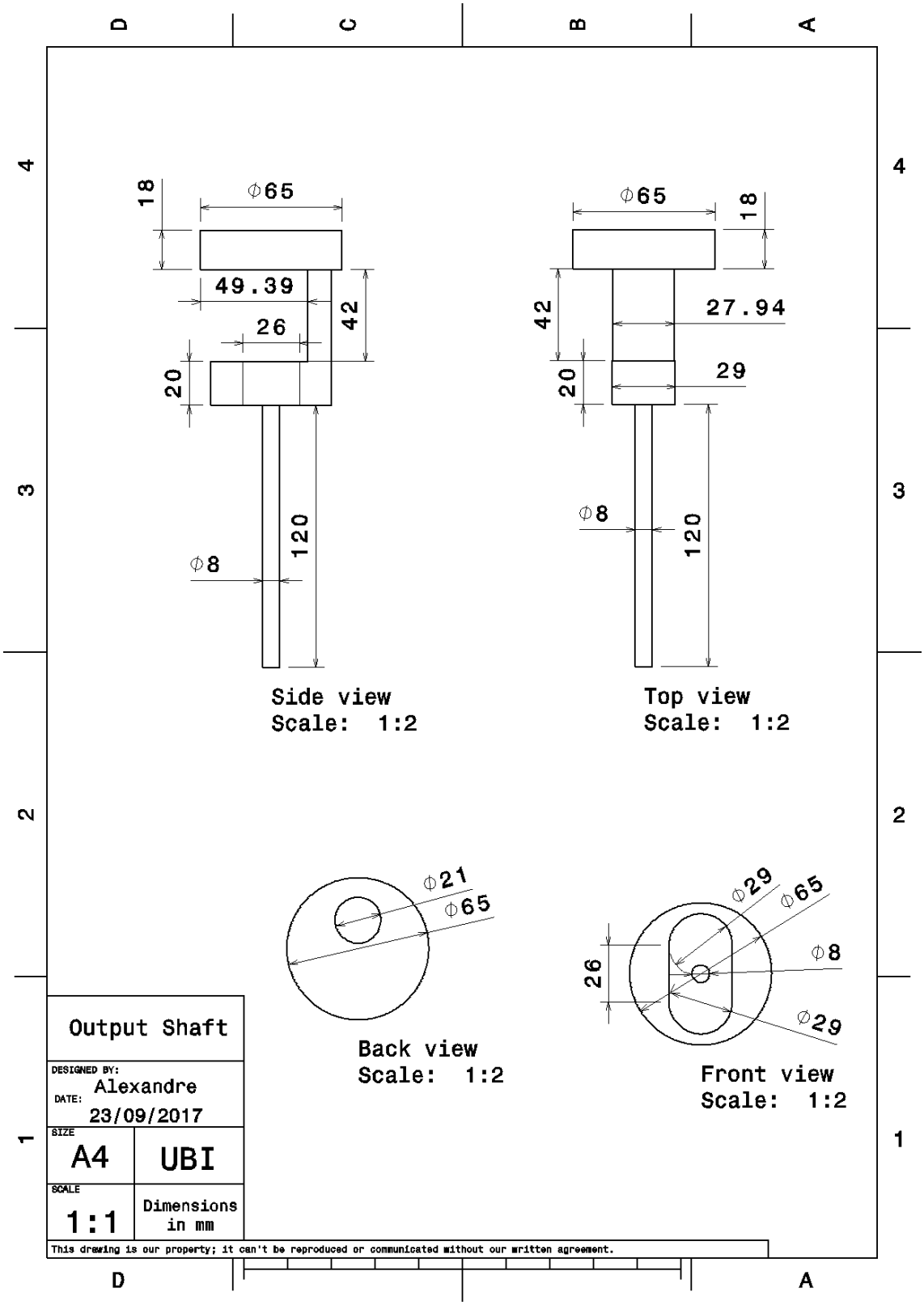

A.11. Technical Drawing of the Support Shaft.

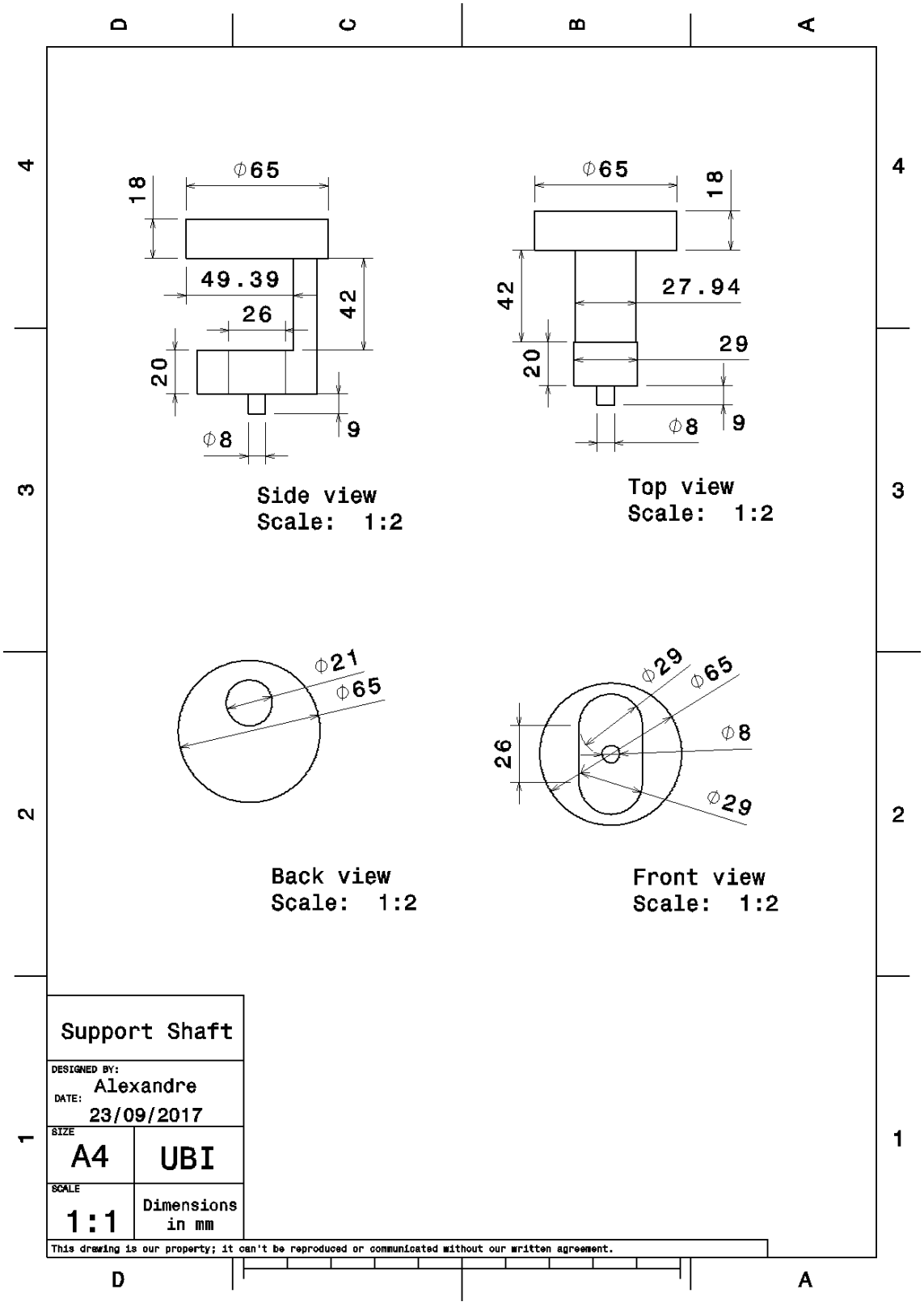

A.12. Technical Drawing of the Central Crankcase.

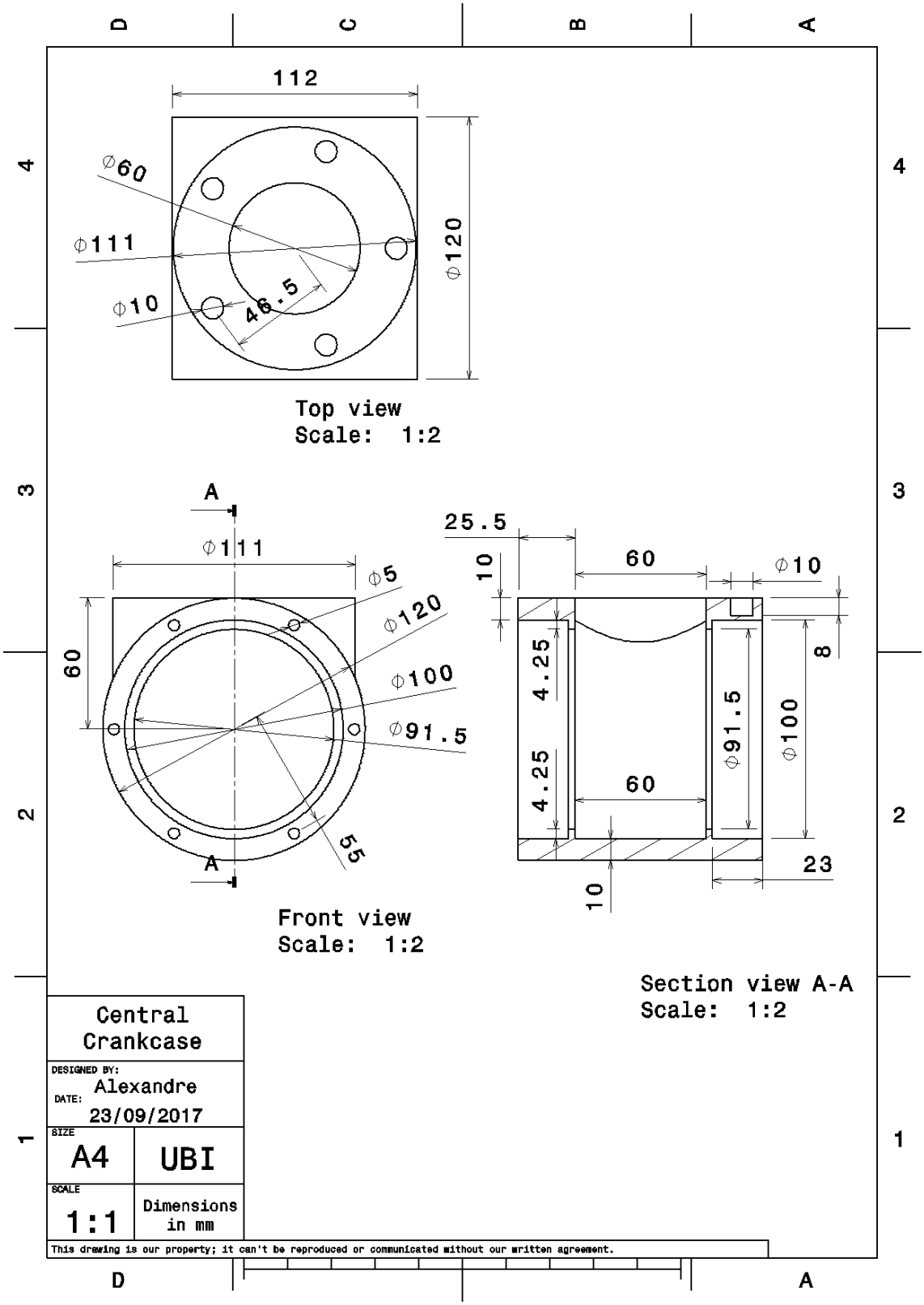

A.13. Technical Drawing of the Front Crankcase.

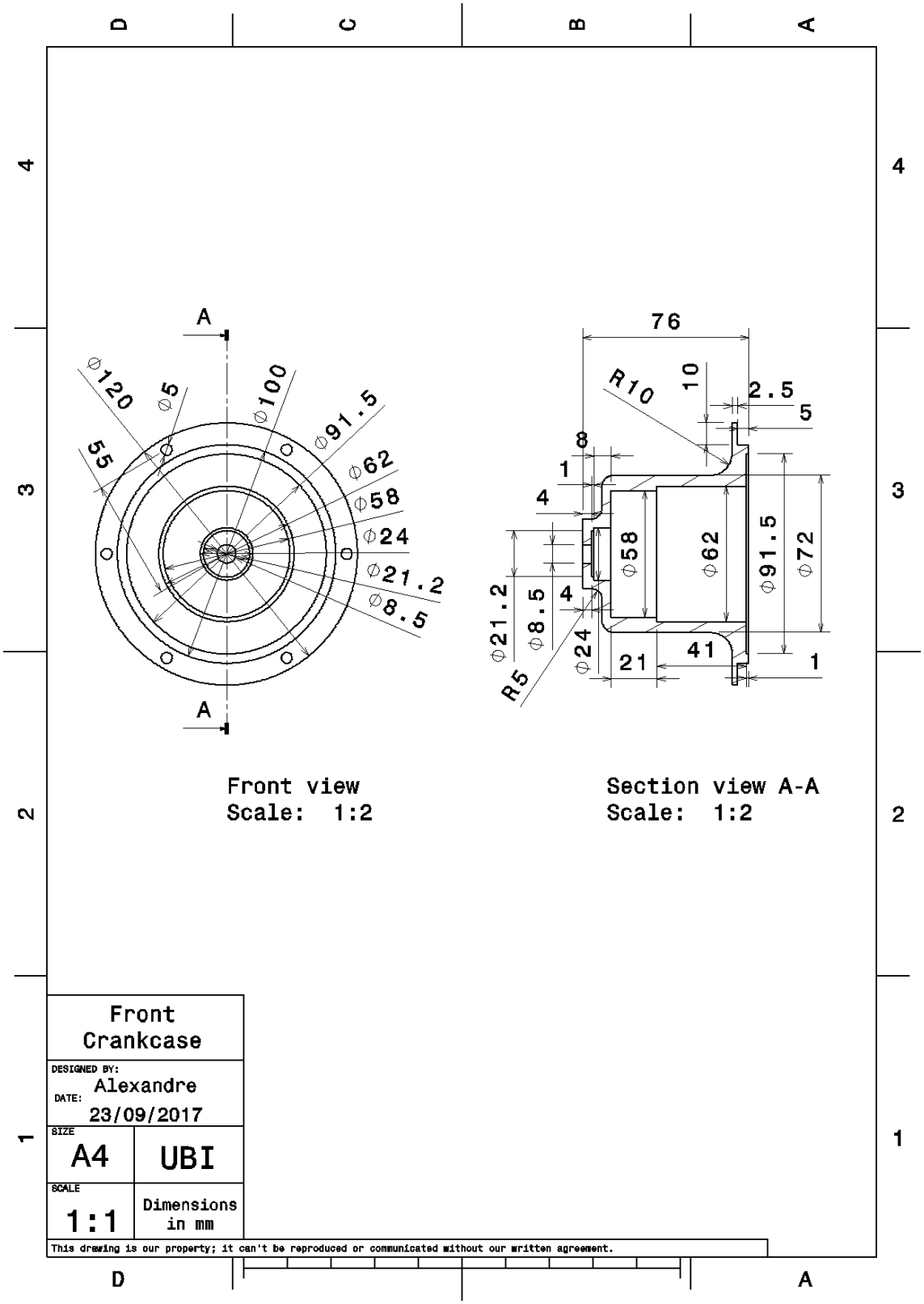

A.14. Technical Drawing of the Back Crankcase.